QUANTITATIVE ANALYSIS OF ELASTIC NEAR FIELDS IN A HALF-SPACE

by

T. K. Chao

ProQuest LLC.
789 East Eisenhower Parkway
P.O. Box 1346
Ann Arbor, MI 48106 – 1346

T 1277

A Thesis submitted to the Faculty and the Board of Trustees of the Colorado School of Mines in partial fulfillment of the requirements for the degree of Doctor of Science in Geophysical Engineering.

Signed: Tsu Ko Chao
Tsu Ko Chao

Golden, Colorado
Date: 17 Dec., 1969

Approved: Frank Hadsell
Frank A. Hadsell
Thesis Advisor

John C. Hollister
Head of Department

Golden, Colorado
Date: 17 Dec., 1969

ABSTRACT

This thesis is meant to provide a quantitative analysis of the non-classical ray fields in a half-space. The central purpose is to separate those components of the near field that are to make up the classical ray fields and those whose geometric attenuation precludes their observation in the far field. This analysis is done in the frequency domain as well as the time domain. The time domain is used so that the waveforms of the displacements of the four components of the body waves, the Rayleigh wave, and the second surface wave can be computed separately. The frequency domain is used in order that comparisons among the amplitudes of the vertical displacements of these wave components can be made and the amplitude variations at the free surface of the half-space can be examined in terms of spectral component. As a result of the amplitude comparisons, portions of the half-space where certain wave components dominate can be defined in terms of frequency and some specific levels of amplitude comparisons.

CONTENTS

ILLUSTRATIONS

INDEX OF SYMBOLS

Symbol	Definition	Eq.	Page
$A(r,z,t)$	Green's function solution - transmission factor for compressional wave	10	12
A_n	Compressional transmission factors for all wave components, $n = 1,2,3$	15	20
a	$a = (U^2 + S^2)^{1/2}$		13
$B(r,z,t)$	Green's function solution - transmission factor for shear wave	11	13
B_n	Shear transmission factor for all wave components, $n = 1,2,3$	16	20
b	$b = (U^2 + s^2)^{1/2}$		13
C	Amplification factor in Leitinger's computations		23
E	Fixed branch		14
$F(t)$	Source function		11
$f(u)$	$f(u) = \frac{bu^2}{(u^2+\frac{s^2}{2})^2-abu^2}$		13
g	Velocity ratio V_p/V_S		29
h	Source depth		7
I, I', I_1 I_2	Angles of incidence and reflection		7
$j(u)$	$j(u) = \frac{u^2+s^2/2}{(u^2+s^2/2)-abu^2}$		13

Symbol	Definition	Eq.	Page
l_r	Radial component of particle displacement	6	11
l_z	Vertical component of particle displacement	7	11
m	Velocity ratio V_p/V_R		29
M(r,z)	Position of the receiver		7
P(t)	Pressure in the source	8,9	11
R	Radius vector from source $R^2=r^2 + (z-h)^2$		13
r	Horizontal distance, source to distance		7
R_o	Radius of the source		7
R'	Length of raypath for reflection $R'^2=r^2+(z+h)^2$		13
R_1, R_2	Raypath distances for reflection		7
S	Compressional slowness $S = 1/V_p$		13
s	Shear slowness		13
$\mathcal{s}$	Laplace transform variable		9
t	Time		
t_R	Classical Rayleigh wave arrival time		29
U(r,z,t)	Shear wave potential	9	11
u	A complex variable		12
V_p, V_S	Compressional and shear velocity		10
$\overline{W}(\mathcal{s})$	Transformed impulse response of the source		10

Symbol	Definition	Eq.	Page
$W(t)$	Impulse response of the source	5	10
$W'(t)$	Derivative of $W(t)$ with respect to t, $W'(t) = d/dt\ W(t)$		9
$W^{-1}(t)$	$W^{-1}(t) = \int_0^\infty W(t)dt$		33
$W^{-2}(t)$	$W^{-2}(t) = \int_0^\infty W^{-1}(t)dt$		34
ω	Angular frequency		37
ω_o	$2V_s/R_o$		10
z	Vertical distance; receiver to boundary		7
γ	$\omega_o\{1 - \zeta^2\}^{1/2}$		10
$\delta(t)$, $\delta'(t)$	Singlet and Doublet generalized functions		10,11
ζ	V_s/V_p		10
λ_p	For compressional wave		58
ρ	Density of the solid medium		10
τ	Time variable		10
$\phi(r,z,t)$	Dilatational wave potential		11
$\psi(R_o,\tau)$	Dilatational wave potential at the source boundary		8

ACKNOWLEDGMENTS

The author wishes to express his sincere gratitude to Professor Frank A. Hadsell of the Colorado School of Mines, who acted as advisor on this research project. A series of lectures on Cagniard's theory delivered by Professor Hadsell was the inducement for doing my doctoral thesis research. His devotion, patience, understanding, and many valuable discussions are deeply acknowledged.

I should like to express my deepest appreciation to the American Petroleum Institute and its Executive Committee on Exploration and Production Research for the generous grant which provides fellowships for the past two and half years. Only this support made this research in spherical wave propagation possible.

I am grateful to Professor John C. Hollister for inducing me to do graduate work in Geophysics Dept. at the Colorado School of Mines and for serving on my doctoral thesis committee. I am also grateful to Professor Leonard A. Kalal for his help in preparing this text.

To Colorado School of Mines Foundation Inc. goes my sincere appreciation for providing the funds for computer usage. This generous support made the completion of this study possible.

INTRODUCTION

Plane wave theory has been the guide to the interpretation of seismograms for many years. Its simplicity has given the plane wave theory a central place in the whole theory of seismic wave propagation. But one pays for this simplicity in a distrust of results which may depend on unreasonable oversimplifications. This is often shown by the lack of ties between theory and observations when waveforms, not just arrival times, are considered. This is especially true when the receiver is near the source or near the surface. It is, therefore, necessary to reconsider our theory to ensure that our course of research and development is directed toward well defined objectives. Here I consider only the effect of the sphericity of the wavefront and not the other important non-classical factors such as absorption, scattering, or hysteresis.

Frequently inferences drawn from plane wave theory are misapplied, especially near a source or a boundary. Examples of such misapplications, found in the half-space problem, are the following:

1) The radial component of P-wave displacement at the free surface is zero. This feature of cancellation of the radial direct wave by the radial reflected

P-wave is a well known implication of the plane wave theory. However, the plane wave theory does not consider the curvature of the incident wavefront and hence does not account for the existence of the surface waves, except by the use of physically unimaginable complex angles of incidence. In other words, the omission of the surface wave by the plane wave theory gives an incorrect answer here.

2) The Rayleigh wave has a distinct arrival time other than that of the P-wave. This holds true only for a surface source and receiver. When either is buried, the Rayleigh wave begins at the P-wave arrival time and develops to a maximum somewhere around the classical Rayleigh wave arrival time.

3) In a homogeneous isotropic elastic half-space the waveforms of P- and S-waves propagate without change. This is true only for the receiver being inside the critical cone and well away from the source and the boundary.

That portion of the theory of spherical wave propagation, generally regarded as the "exact ray theory," (Spencer, 1960) has evolved over the past 40 years. This exact ray theory is primarily a near field or source theory in the sense that the far simpler plane wave theory and

mode theory are also applicable in the far field. Some of the milestones in the evolution of the exact ray theory are the following:

1) From 1932 to 1937 the Russian scientists, V. Smirnov and S. Sobolev, published a series of papers dealing with problems of axially symmetric wave propagation in an elastic half-space adjoining an unbounded liquid medium, in a plane-parallel elastic layer, and later (1947) some particular cases of the problem of two adjoining half-spaces.

2) In 1939, L. Cagniard published the most detailed and general theoretical investigation of the problem which has appeared to date. His work stands today as the authoritative treatise on the subject. His approach, generally referred to as Cagniard's method, is to use the Laplace transformation, establish the solution in the transform plane and extract the explicit solution therefrom by a series of well chosen transformations. It was translated into English by Flinn and Dix (1962).

3) An independent development similar in many aspects to Cagniard's was published by C. L. Pekeris from 1940 to 1948. Pekeris and his co-workers have published many papers dealing with spherical wave propagation, several of which contain interesting numerical results.

4) Barnes and Anderson (1952) explained the phenomenon

of the so-called "tails" in the pulse propagation from a spherical source.

5) Savage (1958) showed that the case of plane waves inside of the critical cone and away from the surface is an asymptotic version of the more general case of the spherical waves.

6) Spencer (1960) generalized Cagniard's solution to the case of a multilayered half-space containing a finite source with axial symmetry. In Spencer's generalization the components of displacement (or velocity) may be expressed in terms of a classical ray path between the source and the receiver. To use the method all that is needed is an integral representation for the Laplace transform of the axially symmetric radiation field of the source. The formal solution for the responses associated with energy transmission along any generalized ray path can be obtained directly from the integral representation for the source by using generalized reflection and transmission coefficients in place of the plane wave coefficients. The beauty of the method lies in the fact that it is possible to go directly to the solution without first solving the boundary-value problem.

7) Towne (1968) pointed out that the plane wave solution does not yield the correct arrival time for critical refraction, but that the deficiency is easily corrected by

retaining higher order terms in the asymptotic expansion for the plane waves outside of the critical cone.

The exact ray theory will probably serve as a useful guide to modifications of the approximate theories. These modifications will better serve our practical needs. In this respect the work of Towne (1968) is especially interesting.

A considerable amount of work has been done on various problems in spherical wave propagation; unfortunately, most of the work is theoretical in the sense that no numerical results are given. Those works which do present numerical results, such as those of Pekeris, Alterman, Abramovici, and Jarosch (1965), Spencer (1965) and Bortfeld (1964), do not capitalize on the power of the exact ray method to analyze waves into components which are important near the source, or far from the source, or near the surface, or far from the surface. To capitalize on this feature of the method, Cagniard obtained solutions of the half-space problem in Chapters 10, 11, 12 and 13 of his book. These solutions are especially applicable to numerical study.

It is hoped that this half-space study will provide insight which will save time and money when more complicated models are critically examined.

FORMAL SOLUTION

In order to define terms used in the algorithms of the half-space problem, a statement of the mathematical concepts involved in the exact ray theory is necessary. A step-by-step development of the mathematics will not be included here, but a somewhat detailed discussion of the physical meaning of the mathematical expressions will be given. When the parentheses following an equation contain a second number, it refers to the appearence of that equation in Flinn and Dix (1962).

Statement of the Problem

A spherical source of radius R_o is centered at S(0,h) (see Figure 1). An arbitrary pressure P(t) is applied to the source to simulate an explosive charge. The problem is to determine the displacements at any point M(r,z) in the half-space (Figure 1).

As shown by Spencer (1960) the problem of elastic wave propagation can be divided into two parts, the source and the boundaries; that is, the generation of waves can be treated as a separate problem from the transmission, reflection, and propagation of the waves. This separation permits one to study the source problem first, and then use the output of the source as an input to the boundaries of

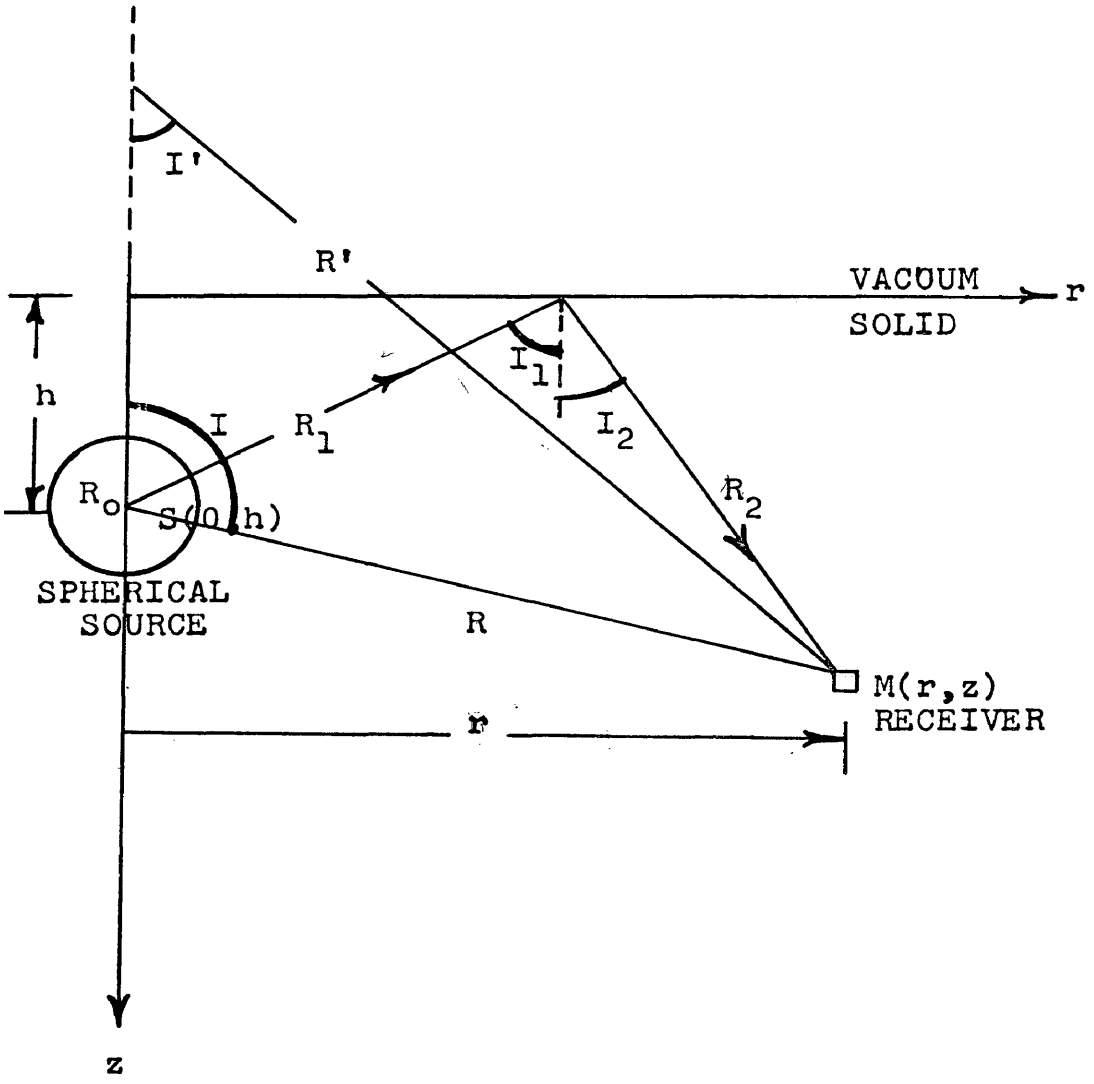

Figure 1. Geometrical configuration of the half-space problem. R_o represents the radius of the spherical source, $R = \{r^2 + (h - z)^2\}^{1/2}$, and $R' = \{ r^2 + (h + z)^2\}^{1/2}$.

Spencer's method of generalized reflection and transmission coefficients serves like a recursion formula so that a solution for one model can be used as a stepping stone to obtain solutions for more complicated models. Cagniard treated his problem in the same manner; that is, the source problem was discussed first, and then the transmission factors were obtained. The solutions and the physical meaning of the source problem and the transmission problem in a half-space will be discussed exclusively in the next few paragraphs.

In reality, the neighborhood of an explosive source is never a perfectly elastic zone. A spherical, isotropic dilatational source of radius R_o represents an imaginary spherical surface of radius R_o around the center of the source, such that the displacements on the surface are adequately represented by radial vectors of equal magnitude. Thus the source can be regarded as a linear system, whose input is the pressure $P(t)$ in a fluid filled spherical cavity and, whose output is the dilatational potential $\psi(R_o,\tau)$ at the source boundary multiplied by the radius of the cavity. In other words,

$$P(\tau) * W(\tau) = R_o\, \psi(R_o,\tau), \qquad (1)$$

where * denotes convolution with respect to the time, τ,

and $W(\tau)$ is the impulse response of the hypothetical source. To get a better physical feeling for this source system, one can visualize a situation in which an observer may have decided that his real source was adequately represented by a given radial displacement at a spherical surface represented by $l_R(R_o,\tau)$. This displacement may be written in terms of $W(\tau)$ and $P(\tau)$ as

$$l_R(R_o,\tau) = \frac{-W'(\tau)*P(\tau)}{R_o} S - \frac{W(\tau)*P(\tau)}{R_o^2} \qquad (2)$$

where $W'(\tau)$ is the derivative of the $W(\tau)$ with respect to τ. To solve for $W(\tau)*P(\tau)$ one may perform the Laplace transformation to obtain

$$L_R(R_o,s) = - \frac{S}{R_o} \left(s + \frac{1}{R_o S}\right) \bar{W}(s)\bar{P}(s), \qquad (3)$$

where S is the slowness of compressional wave, s is the transform variable, and $L_R(R_o,s)$, $\bar{W}(s)$ and $\bar{P}(s)$ are the Laplace transforms of $l_R(R_o,\tau)$, $W(\tau)$ and $P(\tau)$, respectively. Using the inverse Laplace transformation one gets,

$$P(\tau) * W(\tau) = - \left(\frac{R_o}{S} e^{-\tau/R_o S}\right)*l_R(R_o,\tau). \qquad (4)$$

Equation 4 indicates that one can obtain $P(\tau) * W(\tau)$ from a given $l_R(R_o,\tau)$ at the source boundary. Derivation of the impulse response $W(\tau)$ has been given by Sharpe (1942), Blake (1952), and many others. This impulse response, which describes the mechanical properties of the source, is

written as

$$W(\tau) = -\frac{R_o e^{-\omega_o \zeta \tau}}{\rho\gamma} \sin \gamma\tau \quad \text{for } \tau > 0, \qquad (5)$$

$$= 0 \quad \text{for } \tau \leq 0.$$

Here V_s = shear velocity

V_p = compressional velocity

$\zeta = V_s/V_p$

$\omega_o = 2\ V_s/R_o$

$\gamma = \omega_o \sqrt{1-\zeta^2}$

ρ = density of the solid medium.

Note that the $\bar{W}(s)$ is given by

$$\bar{W}(s) = -R_o/\rho\ (s^2 + 2\omega_o \zeta\ + \omega_o^2).$$

Hence $\lim_{R_o \to 0} R_o^{-3} \bar{W}(s) = 1/4\ \rho V_s^2$, that is

$\lim_{R_o \to 0} R_o^{-3} W(\tau) = 1/4\ \rho V_s^2\ \delta(\tau)$, where $\delta(\tau)$ is a Dirac impulse. This implies that the impulse response of a point source is an impulse of constant weight such that any pressure $P(\tau)$ acting in the point source will yield the dilatational potential of the same wave shape as $P(\tau)$.

The propagation of the spherical waves in a half-space are characterized by the transmission factors $A(r,z,t)$ and $B(r,z,t)$, where $t = \tau + R_o S$. These functions are called transmission factors by Cagniard because they describe the

transmission of the elastic waves in the problem. They are also the Green's functions for the problem.

Displacement Potentials

The horizontal and vertical displacements, $l_r(r,z,t)$ and $l_z(r,z,t)$, can be expressed in terms of the dilatational potential $\phi(r,z,t)$ and the shear potential $U(r,z,t)$ according to

$$l_r(r,z,t) = \frac{\partial \phi}{\partial r} \quad \frac{\partial U}{\partial z} \quad \text{and} \qquad (6,1\text{-}1)$$

$$l_z(r,z,t) = \frac{\partial \phi}{\partial z} + \frac{\partial U}{\partial r} + \frac{U}{r} \, . \qquad (7,1\text{-}1)$$

The displacement potential can be written as

$$\phi(r,z,t) = P(t) * W'(t) * A(r,z,t) \qquad (8,3\text{-}15a)$$

and $$U(r,z,t) = P(t) * W'(t) * B(r,z,t). \qquad (9,3\text{-}16)$$

Note that Eqs. (8) and (9) correspond to Eqs. (3-15a) and (3-16) in Cagniard's book. Cagniard used a step pressure and the source function F(t) and transmission factors to express the displacement potentials. But I feel that it is desirable to introduce the notation P(t) * W(t) in place of F(t) in order to give us greater physical feeling and more explicit expressions. To put it into a more explicit form one can express the problem of obtaining the potentials as

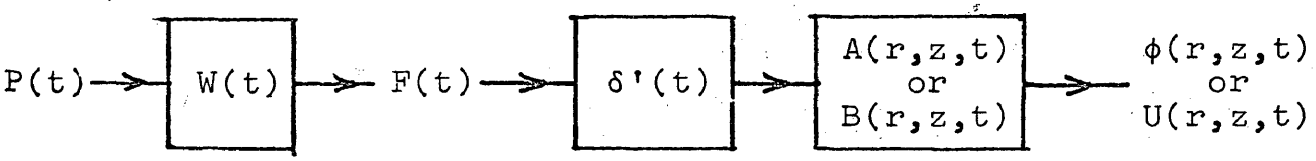

Here $\delta'(t)$ behaves as a differentiator in the system. The transmission factors may be thought of as Green's functions as described on page 11 or they may be thought of as impulse responses of the linear systems mentioned above. For example, one can visualize the $A(r,z,t)$ for an infinite medium, as a step function divided by R such that the dilatational potential is of the form $F(t)/R$.

Determination of $A(r,z,t)$ and $B(r,z,t)$

The transmission factors $A(r,z,t)$ and $B(r,z,t)$ depend only upon the mechanical character of the solid medium and source and receiver positions. The mathematical development of these Green's functions for the half-space problem has been treated by Cagniard in Chapters 10, 11, and 12 of his book as a special case of the two semi-infinite media problem treated in Chapters 1 through 9. I will outline the mathematical development only in order to give physical meaning to the mathematical symbols.

It has been shown by Cagniard in Chapter 5 of his book and by Flinn and Dix in their Appendix 5-A, that one can write the transmission factors as

$$\begin{aligned} A(r,z,t) &= 0 && \text{for } t < RS \\ &= 1/R && \text{for } RS < t < R'S \\ &= 1/R - 1/R' \\ &- \frac{i}{\pi} \int_{\Gamma EPP'} \frac{j(u)u\,du}{\{u^2r^2+(t-a(h+z))^2\}^{1/2}} && \text{for } t > R'S \end{aligned} \qquad (10,5\text{-}29')$$

and $$B(r,z,t) = 0 \qquad \text{for } t < R_1S + R_2s$$

$$= \frac{i}{\pi r} \int_{\Gamma EPP'} \frac{(t-ah-bz)f(u)u\,du}{\{u^2r^2+(t-ah-bz)^2\}^{1/2}} \cdot$$

$$\text{for } t > R_1S+R_2s \qquad (11,5\text{-}29)$$

Here s represents the slowness of the shear wave, and S represents the slowness of the compressional wave,

$$R = \{r^2 + (h - z)^2\}^{1/2},$$

$$R' = \{r^2 + (h + z)^2\}^{1/2},$$

$$a = \{u^2 + S^2\}^{1/2}$$ (with a suitable branch cut to be discussed below),

$$b = \{u^2 + s^2\}^{1/2}$$, and,

for the half-space

$$j(u) = \frac{bu^2}{(u^2 + s^2/2)^2-abu^2}$$ and

$$f(u) = \frac{u^2 + s^2/2}{(u^2 + s^2/2)^2-abu^2} \cdot$$

There are four branch cuts and two poles whose positions in the complex u-plane are independent of r,z, and t. These branch points are at $u = \pm iS$ and $\pm is$ and the poles are at $\pm iS_R$ where S_R is the classical Rayleigh wave slowness. Note that the B(r,z,t) has the same expressions as that given by Eq. (5-29) in Cagniard's book. However, there are slight differences between Eq. (10) and Cagniard's Eq. (5-29') for the expression of the A(r,z,t). This is due to the

breaking up and simplification of the k(u) in Cagniard's Eq. (5-29') and Cagniard's Eq. (10-7) for a half-space problem. The functions a and b are in general multi-valued. One point in the u-plane maps onto two points in the a-plane or b-plane. We place fixed branch cuts (Fig. 2) on the imaginary axis of the u-plane to avoid the multi-valued features of a and b. Moreover, the expressions in the denominators of Eqs. 10 and 11 are also multivalued, and to define from either of these a single valued function we place a moving branch cut in the first and fourth quadrants of the u-plane. They are called moving branch cuts because their shape is a function of time, among other things.

Cagniard's analysis of the complete elastic wave field of the half-space is in terms of equations 10 and 11. He associated the elements of his analysis with classical far-field terms as far as possible; however, since his mathematical expressions include near field components not previously expressed mathematically, the association could not be strictly one-to-one.

Using Figure 1 it can be seen that the first term of Eq. 10 does not involve the free surface, but rather is the solution to the infinite medium problem. As such, it represents the direct arrival from the isotropic dilatational source.

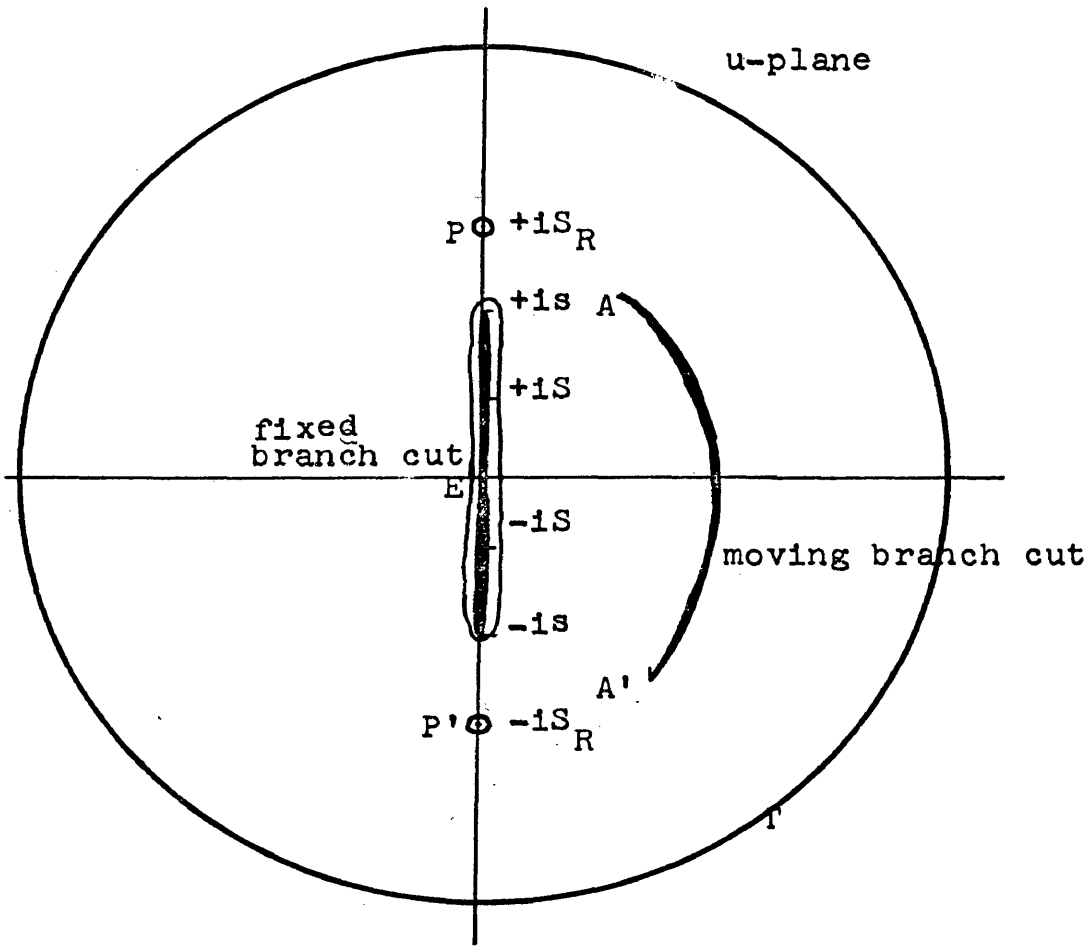

Figure 2. The contours Γ, E, P and P', and the branch cuts in the u-plane. S represents the slowness of the compressional wave, s represents the slowness of the shear wave, and S_R represents the slowness of the Rayleigh wave.

The second term of Eq. 10 is exactly the same form as the first, but for a virtual source imaged in the free surface. Thus it is part of the reflected P-wave and in the far-field near the axis of symmetry, would dominate the reflected P-wave. Further from the axis of symmetry the integral of Eq. 10 contributes to the reflected P-wave in the far-field as well as in the near-field. (See Flinn and Dix, Eq. 10-56, and Figures 10-3 and 10-4.)

The contribution of the integrals of Eqs. 10 and 11 is analyzed in terms of the contours Γ, E, P, and P' of Figure 2.

The contributions of the small circles around iS_R and $-iS_R$ can be expressed in terms of residues which exhibit the following far-field characteristics, which are suggestive of the classical Rayleigh wave:

1. For a surface source and receiver, a well defined arrival time which propagates with the classical Rayleigh velocity.

2. Primarily a surface wave. (For a surface source this wave attenuates as the three-halfs power of the receiver depth, instead exponentially as does the classical Rayleigh wave).

3. That portion of the waveform near the classical Rayleigh wave arrival time attenuates as the square root of epicentral distance.

4. Particle motion is retrograde elliptical.

Cagniard called the contribution of the contour E, around the fixed branch cut, the second surface wave because of its gross similarity to the contribution of the Rayleigh poles. This second surface wave is called by Ewing, Jardetzky and Press (1957, p. 137) the branch line integral wave. Significant differences evident for source and receiver in the far field at free surface are that second surface wave:

1. Propagates with the shear velocity.
2. Attenuates as the square of the epicentral distance.
3. Exhibits prograde elliptical particle motion.

The contribution of the Γ can be evaluated in terms of the residue at the point of infinity. Like E it cannot be associated with classical waves. It is simple in that its displacement correspondent can be expressed as a sum of nine weighted waveforms; $P(t)*W(t)$, $P(t)*W^{-1}(t)$, and $P(t)*W^{-2}(t)$, where for any function $H(t)$, $H^{-(n+1)}(t)=\int_0^t H^{-n}(\tau)d\tau$. Fortunately, these $W^{-1}(t)$ and $W^{-2}(t)$ terms cancel for late time.

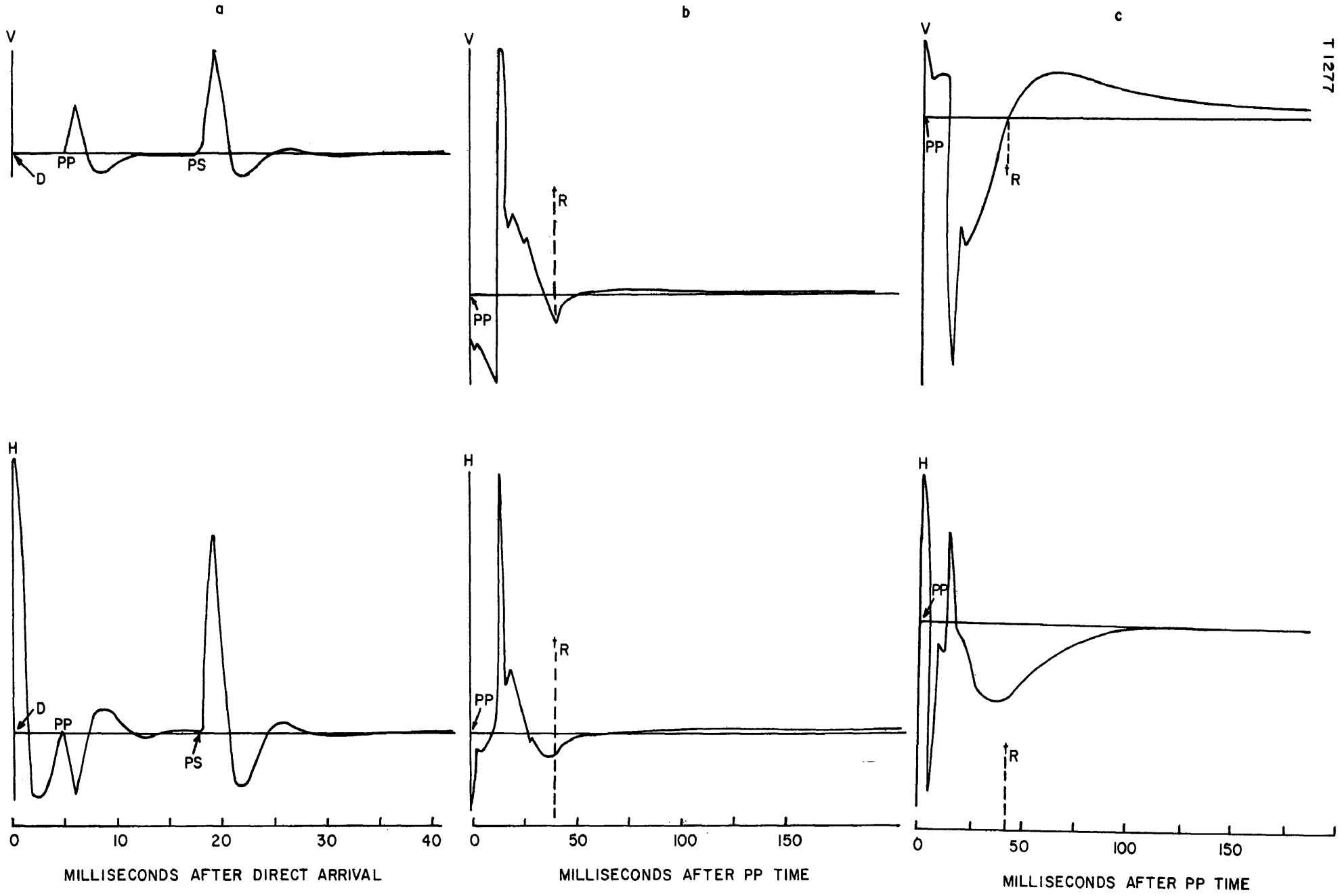

T1277

Figure 3. Synthetic seismograms of a) body wave, b) second surface wave, c) Rayleigh waves, and d) total composite seismograms at r = 300 ft, h = z = 100 ft, and for V_p = 10000 ft/sec, V_s = 5000 ft/sec, density of the solid medium = 2.4 gm/c.c. Here horizonal displacement and vertical displacement is represented by H and V, respectively. D represents direct arrival, PP represents the reflected P-wave arrival time, and PS represents the reflected S-wave arrival time, and t_R represents the classical Rayleigh wave arrival time. Impulsive pressure, radius of the cavity is 1 ft.

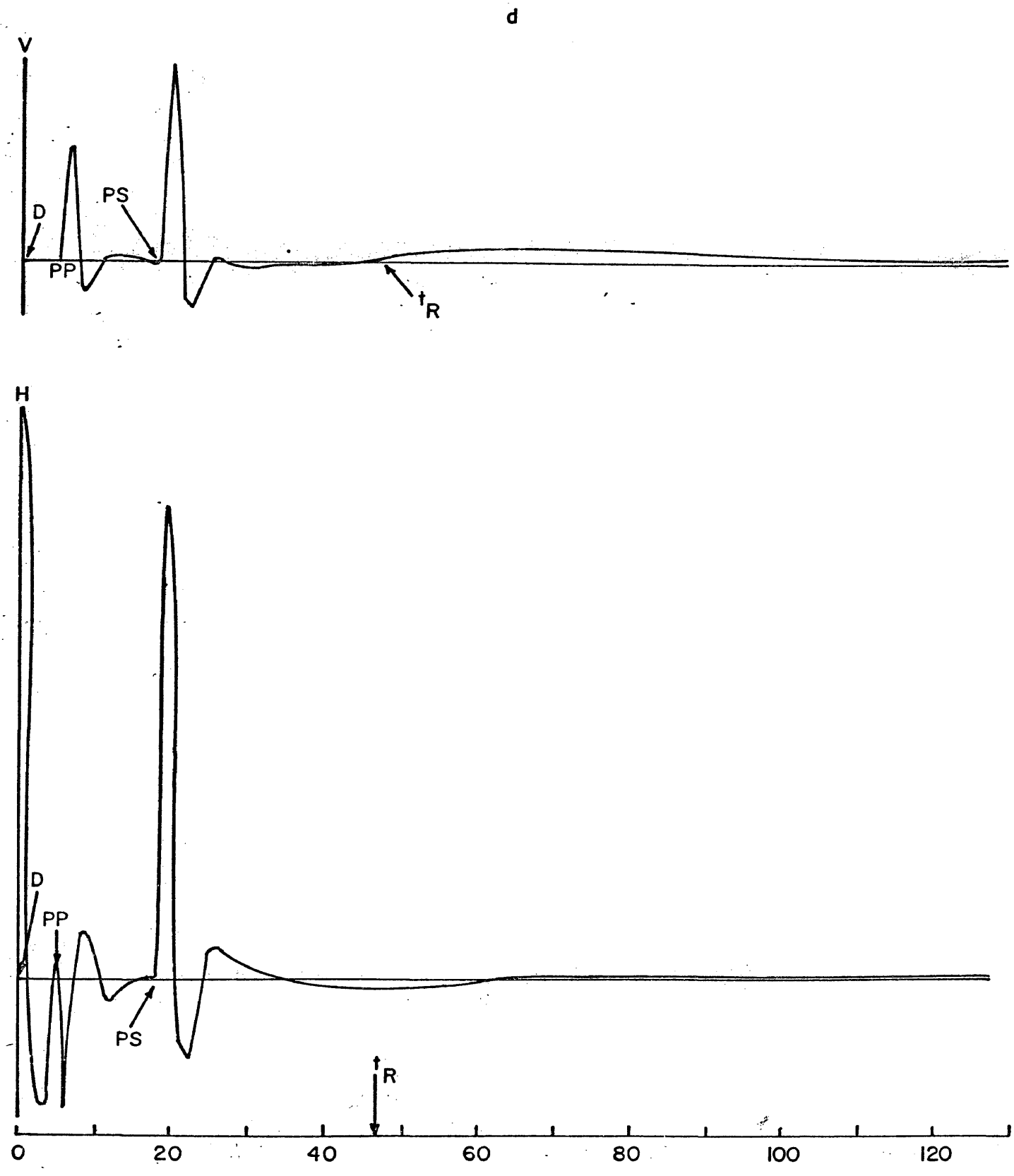
d
V
D
PP
PS
t_R
H
D
PP
PS
t_R
0
20
40
60
80
100
120
MILLISECONDS AFTER DIRECT ARRIVAL

NUMERICAL INVESTIGATION

As discussed in the previous sections, the horizontal and vertical displacements can be computed for a given pressure pulse at any point inside a half space. The necessary expressions, in terms of the transmission factors, are

$$l_r(r,z,t) = P(t)*W(t) * \left(\frac{\partial A(r,z,t)}{\partial r} - \frac{\partial B(r,z,t)}{\partial z}\right) \qquad (12)$$

and

$$l_z(r,z,t) = P(t)*W(t) * \left(\frac{\partial A(r,z,t)}{\partial z} + \frac{\partial B(r,z,t)}{\partial r} + \frac{B(r,z,t)}{r}\right) \qquad (13)$$

The transmission factors can be expressed as follows:

$$A(r,z,t) = A_1 + A_2 + A_3 \qquad (14)$$

$$B(r,z,t) = B_1 + B_2 + B_3 .$$

Here subscripts 1, 2, and 3 correspond to the body waves, the Rayleigh wave, and the second surface wave respectively. The body waves include the primary waves of the first kind, the second kind, the third kind, and the fourth kind. These transmission factors for each wave component have been checked carefully and listed in Appendix A. Accordingly, the displacements can be rewritten as

$$l_r(r,z,t) = \sum_{n=1}^{3} l_{rn} = P(t) * W(t) * \sum_{n=1}^{3} \left(\frac{\partial A_n}{\partial r} - \frac{\partial B_n}{\partial z}\right) \qquad (15)$$

and

$$l_z(r,z,t) = \sum_{n=1}^{3} l_{nz} = P(t) * W(t) * \sum_{n=1}^{3} \left(\frac{\partial A_n}{\partial z} + \frac{\partial B_n}{\partial r} + \frac{B_n}{r}\right). \qquad (16)$$

Here l_{r1}, l_{r2}, l_{r3} are the horizontal displacements of the body waves, the Rayleigh wave, and the second surface wave respectively, and l_{z1}, l_{z2}, l_{z3} are the corresponding vertical displacements.

Computer algorithms have been coded to obtain the horizontal and vertical displacements of the direct wave, reflected P-wave, reflected S-wave, Rayleigh wave, and second surface wave at any point in a half-space for arbitrary parameters. This means free choice of P-velocity and S-velocity, density of the solid medium, pressure function, and size of the source cavity. The greatest advantage of computing the waveforms by the Cagniard's method is that we are able to compute these waves piece by piece and then put them together as the composite seismograms. This enables us to study each wave separately while most other methods fail to do so. An example of the composite synthetic traces and their components is shown in Figure 3 to demonstrate this separability. Here an impulsive pressure was chosen for input pressure along with the parameters: R_o = 10 ft., ρ = 2.4 g/c.c., V_p = 10,000 ft/sec., and V_s = 5,000 ft/sec. The computations were carried out using ESSA's CDC-3800 digital computer at Boulder, Colorado.

Comparison with Finite Difference Method

Dr. Hans Leitinger (1969) has applied the finite

difference method of Alterman and Karal (1968) to compute the displacements of an isotropic source buried in a half space. He exhibited waveforms at five different epicentral distances on the surface of the half-space. His work was done using a CDC-6400 digital computer at Mobil Field Research Laboratory at Dallas, Texas.

It is quite obvious that the finite difference method has some advantages over the exact ray method. The versatility of the finite difference method is the greatest one. For example, Leitinger has demonstrated that he can compute the waveforms of the displacements for a layer-in-a-half-space almost as easily as those for a half-space. In addition, it does not require the deep involvement with mathematical analysis before the use of a computer, hence it is less time consuming. However, the finite difference method fails to provide the components of the synthetic seismogram separately and so one can only study the synthetic trace as a whole.

The process of the exact ray method, though sometimes lengthy, offers us a chance to study the synthetic seismograms in parts so that we can learn the behavior of each wave component under various circumstances, such as near a source, or at the surface of a half-space. Therefore, these two methods compliment each other in solving seismic problems. The finite difference method can better serve as a

tool to study the seismic problems using the total synthetic seismograms obtained in an easier and quicker way; and the exact ray theory is more applicable for the problems involving studies on each particular wave component.

The source function selected by Leitinger (1969) and Alterman and Karal (1968) can be expressed as a function of the type, P(t) * W(t), used by Cagniard (Eq. 5). It starts at time t = 0, causes a variation in stress during a finite time interval, and then leads to a remnant displacement for each particle. In order to have smooth second derivatives of the displacements with respect to time and distance as required for the finite difference method, the displacement potential of the source was defined by

$$\Phi_o(t) = \frac{1}{4}\{f_o(t)-4f_o(t-\Delta)+6f_o(t-2\Delta)-4f_o(t-3\Delta)+f_o(t-4\Delta)\} \quad (17)$$

$$\text{with} \quad f_o(t) = -\frac{C}{12R}\,(t-R/V_p)^4\,\delta^{-1}(t-R/V_p). \quad (18)$$

Here C is the amplification factor, and Δ is a constant measuring the sharpness of the potential pulse. Waveforms computed by Leitinger can be duplicated by letting $P(t) * \Phi_o(t) = W(t)$ in Cagniard's notations in addition to setting the same values for V_p, V_s, r, h, and z. Figures 4 to 8 show a sequence of waveforms of displacements computed by Cagniard's method at five epicentral distances -- namely, at the epicenter, and 2, 4, 6, and 8 source depths

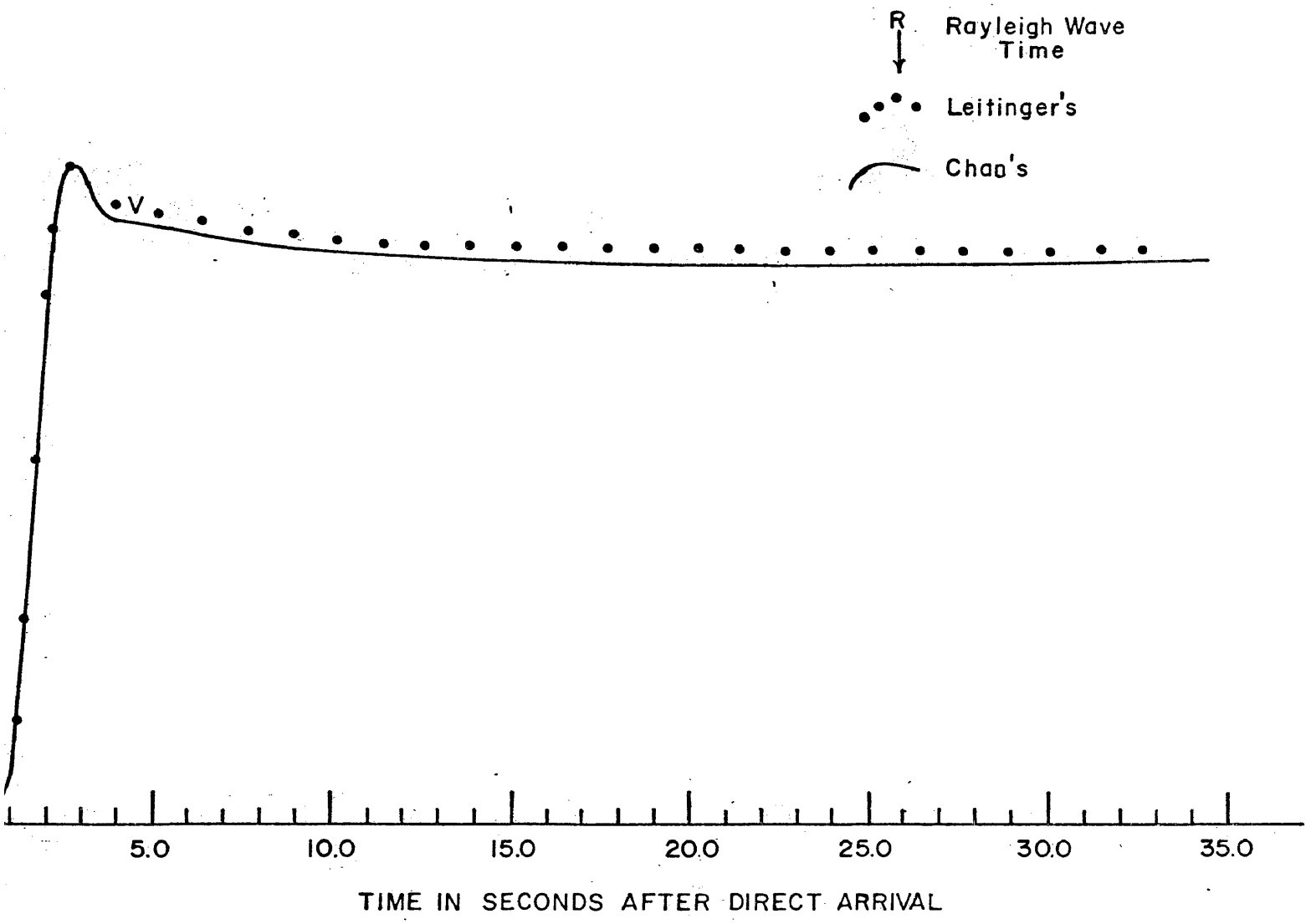

Figure 4. Comparison between waveforms of displacement at epicenter. Direct arrival time is 1.33328 seconds. r = 1 ft, h = 8 km, and z = 1 ft. V denotes vertical displacement.

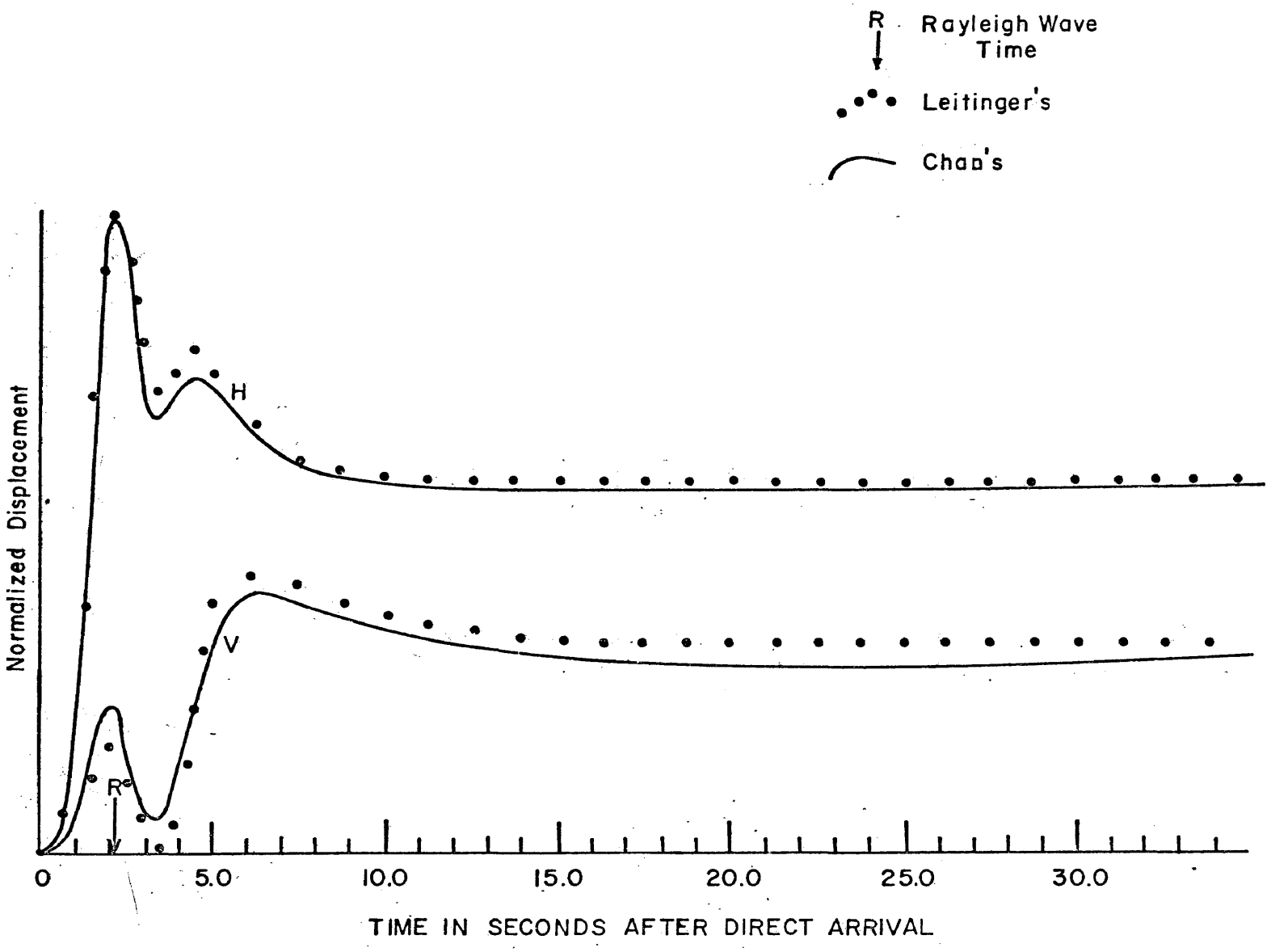

Figure 5. Comparison between waveforms of displacement at 2 source depths from epicenter. r = 16 km, h = 8 km, z = 1 ft. Direct arrival is 2.9814 seconds. Here V represents vertical displacement, H represents horizontal displacement.

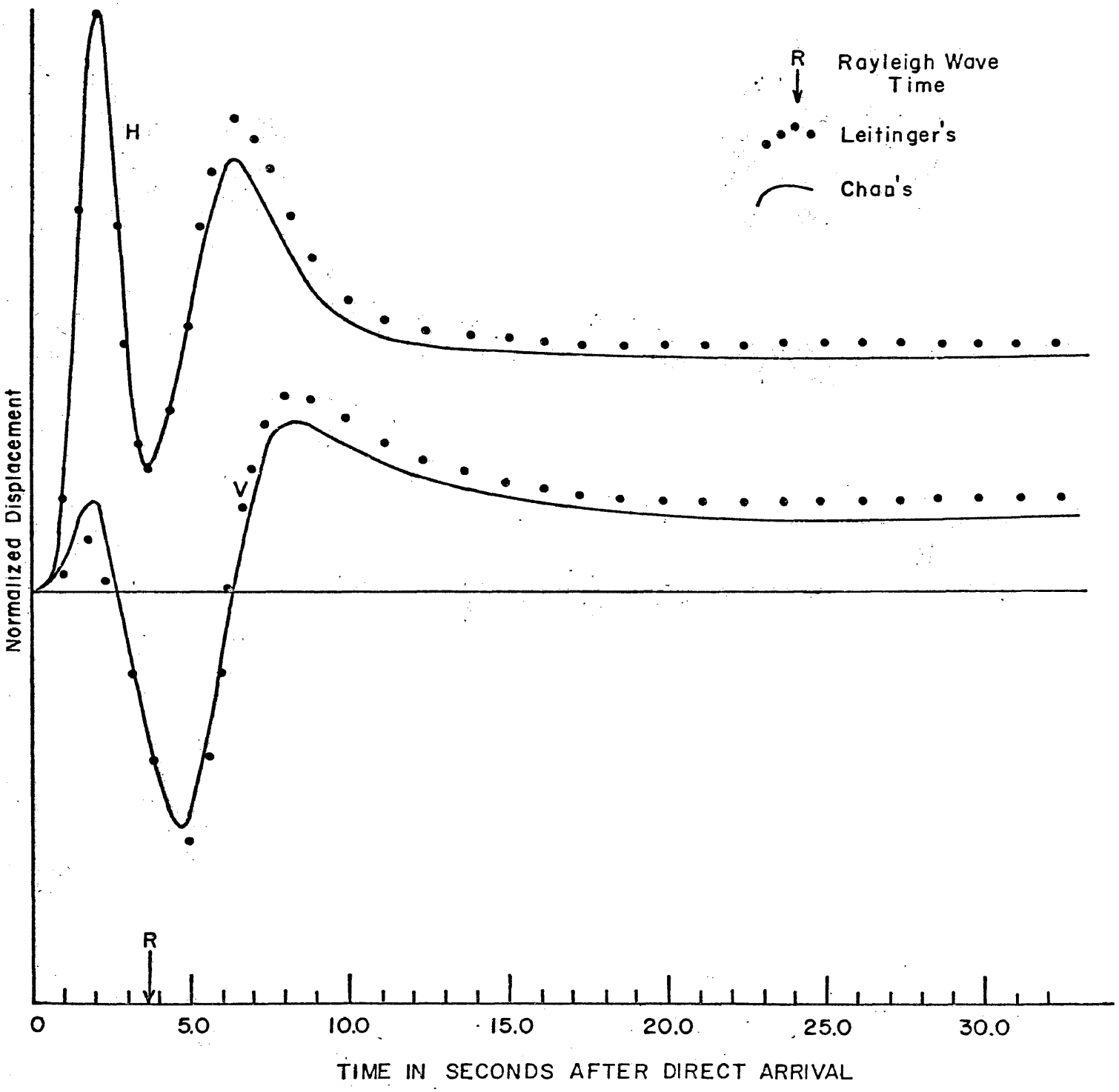

Figure 6 Comparison between waveforms of displacement at 4 source depths from epicenter. r = 32 km, h = 8 km, z = 1 ft. Direct arrival is 5.4974 seconds.

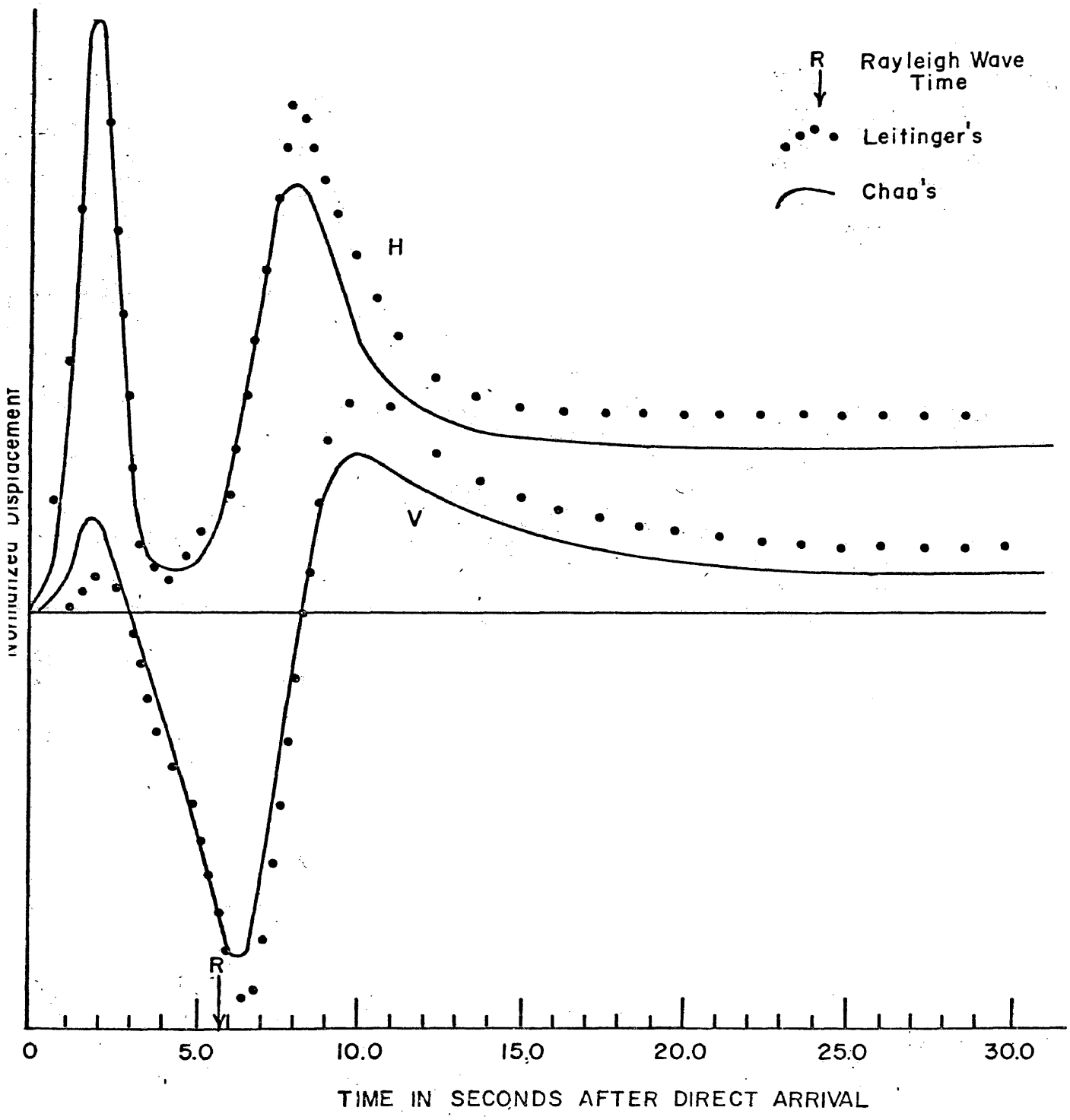

Figure 7. Comparison between waveforms of displacement at 6 source depths from epicenter. r = 48 km, h = 8 km, z = 1 ft. Direct arrival is 8.1103 seconds.

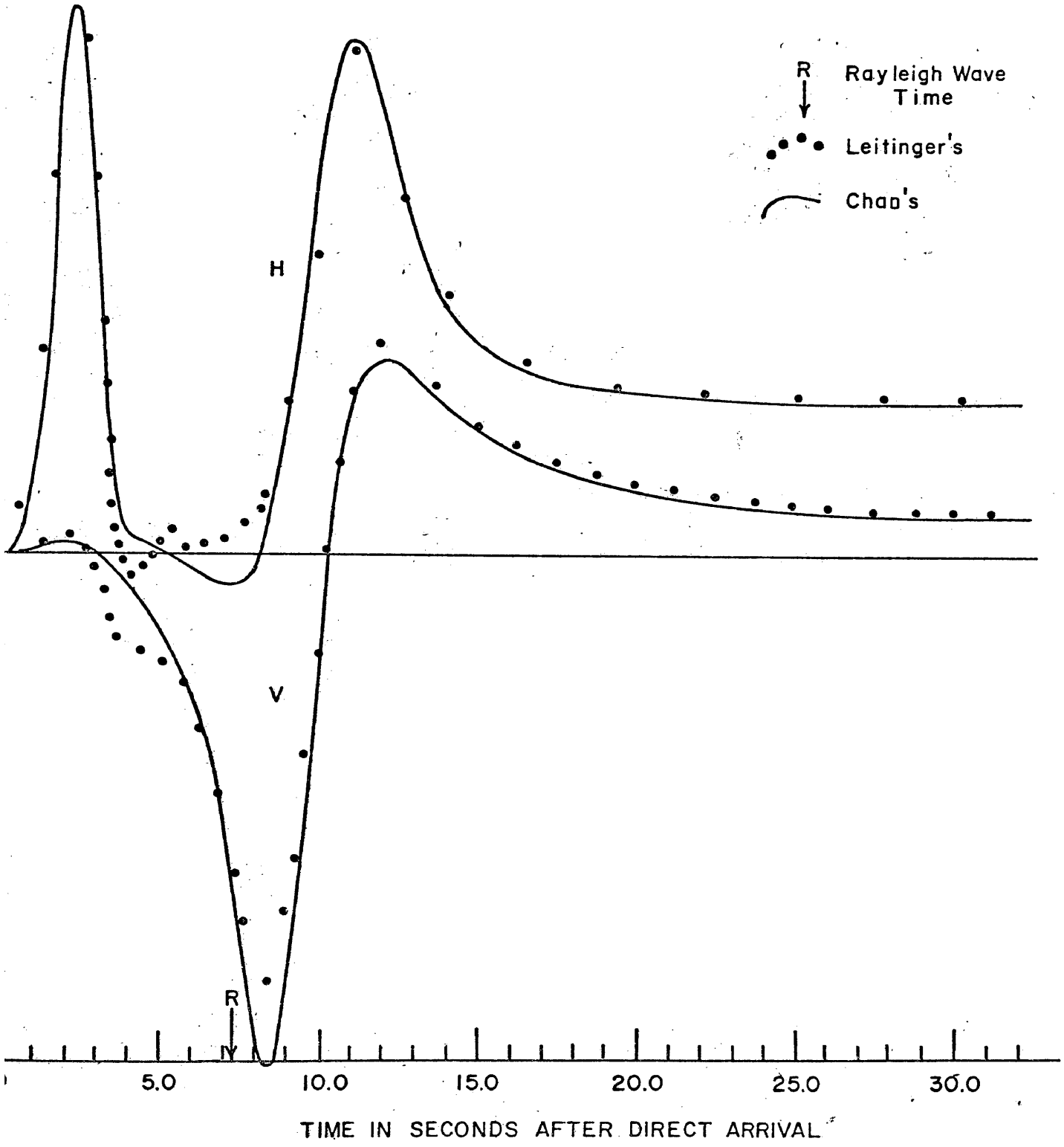

Figure 8. Comparison between waveforms of displacement at 8 source depths from epicenter. r = 64 km, h = 8 km, z = 1 ft. Direct arrival is 10.7496 seconds.

away from the epicenter. These normalized waveforms are computed for Δ = 1 second. Leitinger's corresponding waveforms, computed by the finite difference method, are also plotted in Figures 4 to 8. The Rayleigh wave time, indicated by arrow marks in Figures 4 to 8, is defined by $t_R = R'/V_R$ where V_R represents the Rayleigh velocity. The Rayleigh velocity can be obtained by finding the roots of

$$(m^2-g^2/2)^2 = m^2\{(m^2-1)(m^2-g^2)\}^{1/2} \qquad (19,11\text{-}3)$$

where $m = V_p/V_R$, $g = V_p/V_s$. Note that Eq. (19) is closely related to the classic Rayleigh equation and recall that t_R is a distinct arrival time only for both the source and the receiver at the surface.

The waveforms of displacement computed by Cagniard's and by the finite difference method show, in general, close agreement despite some minor discrepancies. The excellent agreement of the arrival times of the peaks and troughes are evident at every epicentral distance, but slight differences in amplitudes are noticeable. Note that the gradual development of the surface waves, which are characterized by the second peak in each trace, becomes evident as the observation point is moved away from the epicenter along the surface.

In conclusion, waveforms computed by the finite difference method agree in gross with those computed by the

Cagniard's method for a half-space problem. The relative amplitudes of the direct waves and the surface waves computed by the two methods are similar. There are some minor discrepancies, especially when the receiver is 8 source depths away from the epicenter. Since the finite difference method is basically an approximate method, we tend to trust the exact ray method when differences in detail occur. Figure 9 shows a similar comparison taken from Alterman and Karal (1968) for a layer on a half-space. The waveform computed by Alterman and Karal using the finite difference method is plotted to the same scale as that computed by Alterman and Abramovici (1965) using an analytic solution for the same problem. The analytic method was very similar to Cagniard's as generalized by Spencer (1960). The scales were adjusted to give the same amplitude for the peak at Ct/H = 3.25 and the same zero crossing at Ct/H = 5.75. Alterman and Karal compared the shape of the curves and stated that agreement between them is excellent; however, as shown in Figure 9, the differences are noticeable. These differences are slightly greater than the differences which are shown in Figures 4 to 8.

Quantitative Comparison of Wave Components

As our understanding of the exact ray theory has grown over the past decade we have realized that it is a near

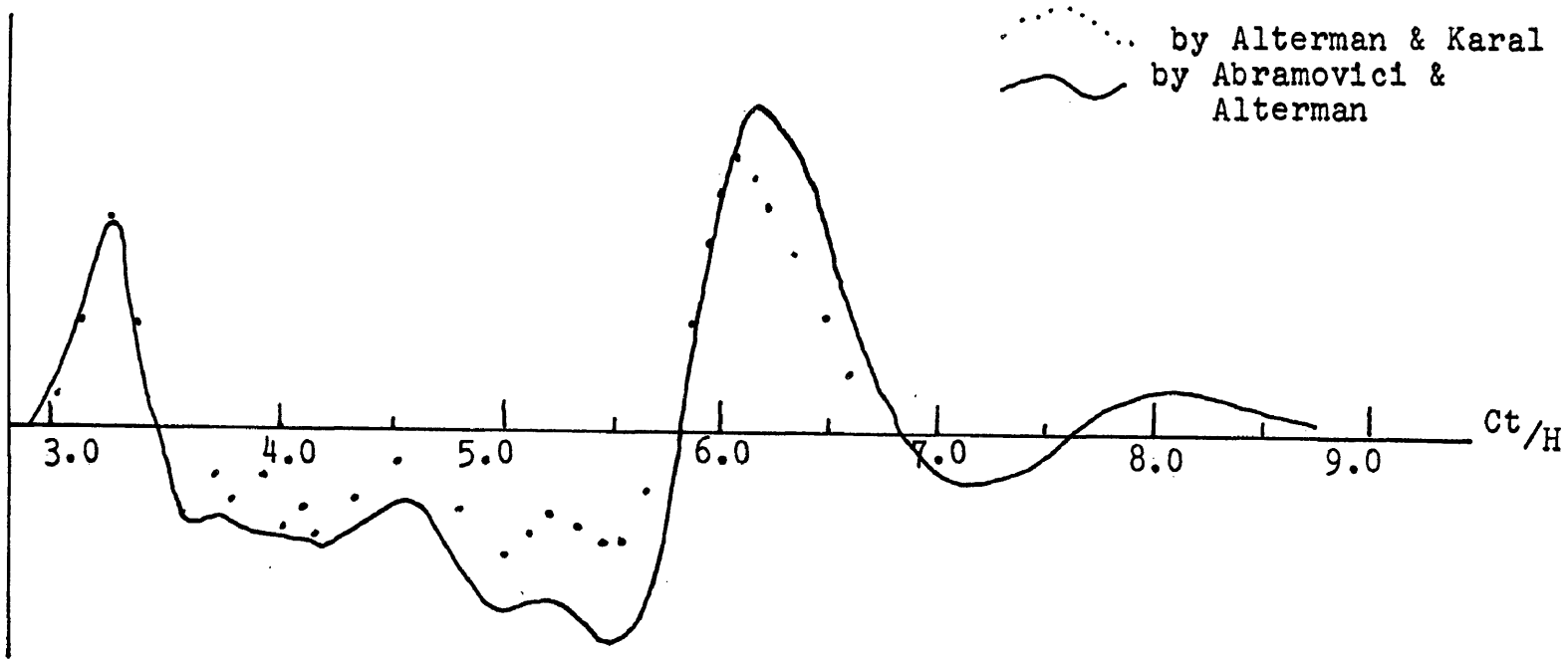

Figure 9. Comparison between vertical displacement on the surface of a layer on a half-space. Here Δ = .3 seconds, C is compressional velocity and H is thickness of the layer. The observation point is on the surface at a distance of five-layer thicknesses from the epicenter. A compressional point source is located midway between the free surface and solid-solid interface.

field or source theory which is most likely to be useful when changes in waveforms in the ill-defined near field are considered. In addition one might apply the exact ray theory to estimate changes in noise characteristics as a function of shot-receiver distances.

Since Cagniard's method provides us the opportunity of computing each component of a synthetic seismogram separately, we may make a quantitative comparison between wave components. As an example of the utility of this, we note that the second surface wave plays an important role near the surface of a half-space, near the source, but its role rapidly decreases as the receiver is moved away from this region. This wave accounts for about one-half of the computing expense of a synthetic seismogram due to the numerical integration required in the computation of the transmission factors; therefore, one would like to avoid computing second surface waves whenever their contribution is negligible.

As briefly discussed on page 20, according to the classification in Cagniard's book, the particle displacements of a spherical isotropic source in a half-space are made of a sum of:

I. Body waves -- a term used synonymously with "primary waves."

a. Primary waves of the first kind -
These are the waves which make up the observed transient elastic field far from the source and the boundary. Their geometric attenuation is as the reciprocal of the ray path distance from the source and their wave shape is given by F'(t) (see Cagniard; p. 167), or P(t) * W'(t) in my notation.

b. Primary waves of the second kind -
These components determine that portion of the field remaining after all transients have died away (see Cagniard; p. 138). The geometric attenuation of primary waves of the second kind is as the reciprocal of the square of the raypath distance from the source and their wave shape is given by W(t) * P(t) (see Cagniard; p. 168).

c. Primary waves of the third kind -
The geometric attenuation of these waves is as the reciprocal of the cube of the raypath distance from the source and their wave shape is given by $W^{-1}(t) * P(t)$. These components do not appear in the remnant field because of the complete mutual cancellation of compressional and shear components for very late times (see Cagniard; p. 169).

d. Primary waves of the fourth kind -
The geometric attenuation of these waves is as the reciprocal of the fourth power of the raypath distance from the source and their wave shape is given by $W^{-2}(t) * P(t)$. These components, like the primary waves of the third kind, are not in the remnant field because of the complete mutual cancellation of compressional and shear components (see Cagniard; p. 169).

II. Surface Waves

a. Rayleigh wave - The mathematical expression of these waves is in terms of residues of two simple conjugate poles. The residues are functions of time which when convolved with $W'(t) * P(t)$ express a waveform which evolves through propagation into the classical Rayleigh wave. If there exists more than one boundary then a denumerable infinity of pairs of poles appear, each pair representing a normal mode of the far-field mode theory (Ewing, Jardetzky and Press; 1957, p. 138). Near the surface and far from a surface source the pattern of the particle motions for the Rayleigh wave is elliptical retrograde, and the amplitude of the displacement of the Rayleigh wave varies inversely as the square root of the radial distance.

b. Second surface wave - called branch line integral wave by Ewing, Jardetzky, and Press (1957, p. 137). This wave resembles the Rayleigh enough to be called a surface wave; i.e., near the surface and far from a surface source it is more-or-less confined to surface and its particle trajectories are elliptical. However, in the far field near the shear wave arrival time, the second surface wave amplitude diminishes as the square of the epicentral distance. Its particle trajectories are prograde instead of retrograde.

For the purpose of this quantitative comparison, it is desirable to regroup these components as follows:

I. Classical ray components -- primary waves of the first kind. According to the plane wave classical ray theory, the reflected P- and S-waves possess the same waveforms as the incident wave in a half-space inside of the critical angle (see, for example, White, 1965). Since the incident wave and the primary wave of the first kind have the common wave form, W'(t) * P(t), and since these waves dominate the far field we elected to call the primary wave of the first kind the classical ray (CR) component.

II. Non-classical ray components -- primary (or body) waves of the second, the third, and the fourth kind plus the surface waves. These components are not considered in the plane wave theories in which the causality constraint is imposed.(NCR).

III. Surface waves -- Rayleigh waves and the second surface wave.(SW).

IV. Second surface wave -- as in the original classification of Cagniard.(SSW).

The quantitative comparison of these wave component amplitudes was done in the frequency domain to facilitate interpretation in terms of various source spectra.

Closed-form transforms (i.e., explicit equations without integrals) could be used for the body waves. Unfortunately, it is very difficult to derive closed-form transforms for the surface waves because of their mathematical complexity. In fact, the expressions of the SSW are in terms of elliptical integrals such that the derivation of closed-form transforms appears to be impossible. Hence it is necessary to apply the numerical Fourier transformation to obtain amplitude spectra for the surface waves. Fortunately, the NCR, the SW, and the SSW are all of low frequency and converge rapidly for the impulsive pressure I have used, so that truncation and aliasing problems are not difficult.

Since the CR is characterized by W'(t) multiplied by time-independent factors, they can be transformed mathematically into their closed-form expressions. Since the impulse response, W(t), is a damped sine function, one can write its closed-form transform as

$$W(t) \longleftrightarrow \tilde{W}(\omega) = \frac{R_o/\rho}{(\omega^2-\omega_o^2)^2-2i\omega_o\zeta\omega} \quad , \qquad (15)$$

where ω denotes frequency in radians per second, $i = \sqrt{-1}$ and the other symbols are defined on page 10. To test my numerical Fourier program I have computed the amplitude spectrum of the impulse response W(t) by my numerical method and by the closed-form expression. Figure 10 shows the agreement between these spectra.

Six examples are given to show the amplitude spectra of the vertical displacement of the CR, the NCR, the SW, and the SSW of an impulsive pressure source in a half-space. Elastic parameters of the solid medium are: ρ = 2.4 gm/c.c., V_p = 8,000 ft/sec, V_s = 4,500 ft/sec. The source is a sphere 1 ft in radius whose center is 3 ft below the surface. Figures 11 to 13 show the plots of amplitude spectra of the CR and NCR at the surface (r = 12 ft, z = 1/4 ft), at the same depth as the source (r = z = 3 ft), and at greater epicentral distance and depth (r = z = 6 ft). Note that oscillations appear on the amplitude spectra of the CR,

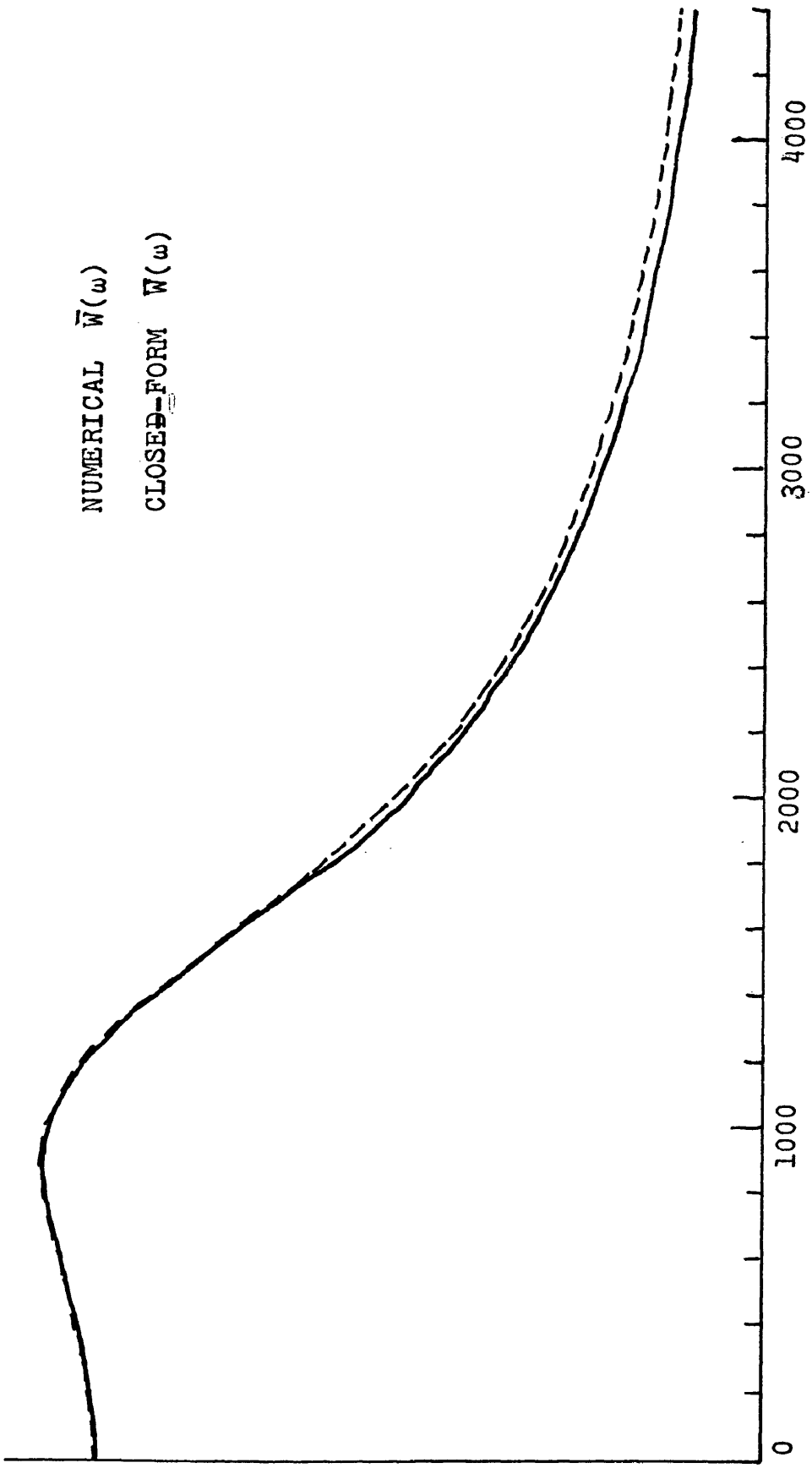

Figure 10. Comparison between the a-plitude spectra of the numerically transformed $\bar{W}(\omega)$ and the closed-form $W(\omega)$. Sampling interval is 50 microseconds, V_p = 8000 ft/sec, and V_s = 4500 ft/sec.

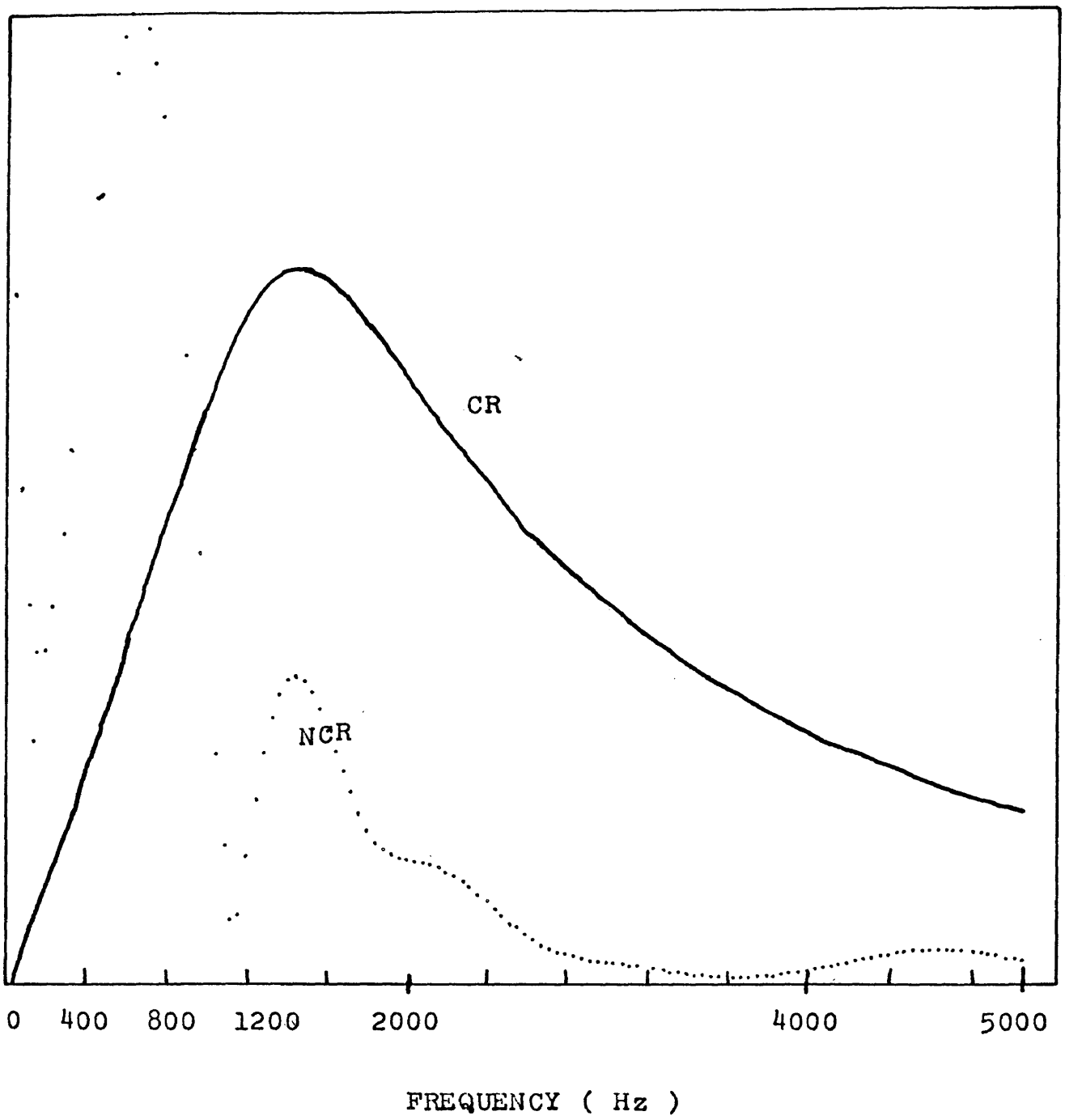

Figure 11. Amplitude spectra of the vertical displacement of CR and the NCR at r = 12 ft, h = 3 ft, and z = 1/4 ft.

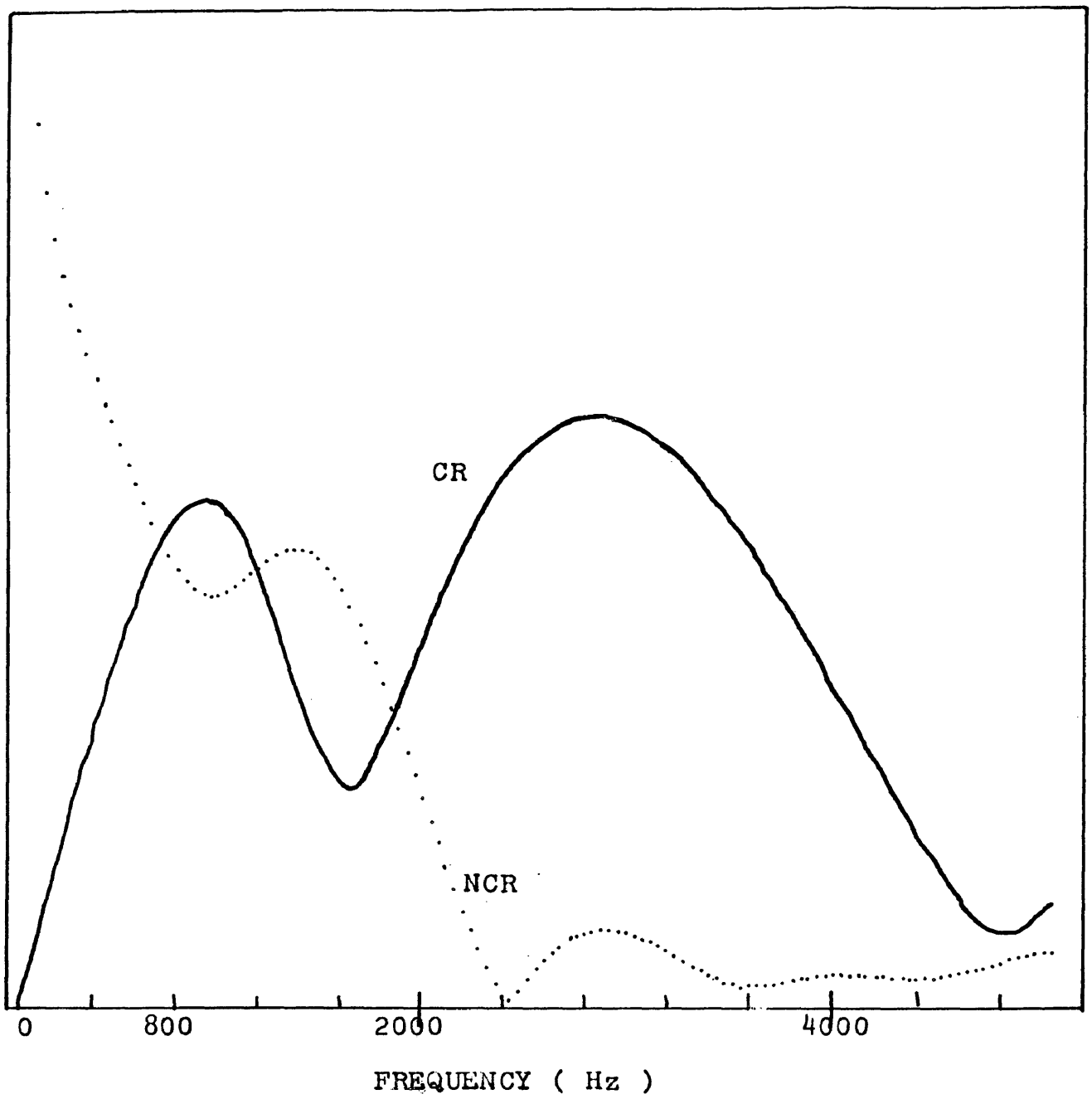

Figure 12. Amplitude spectra of the vertical displacement of the CR and the NCR at r = h = z = 3 ft.

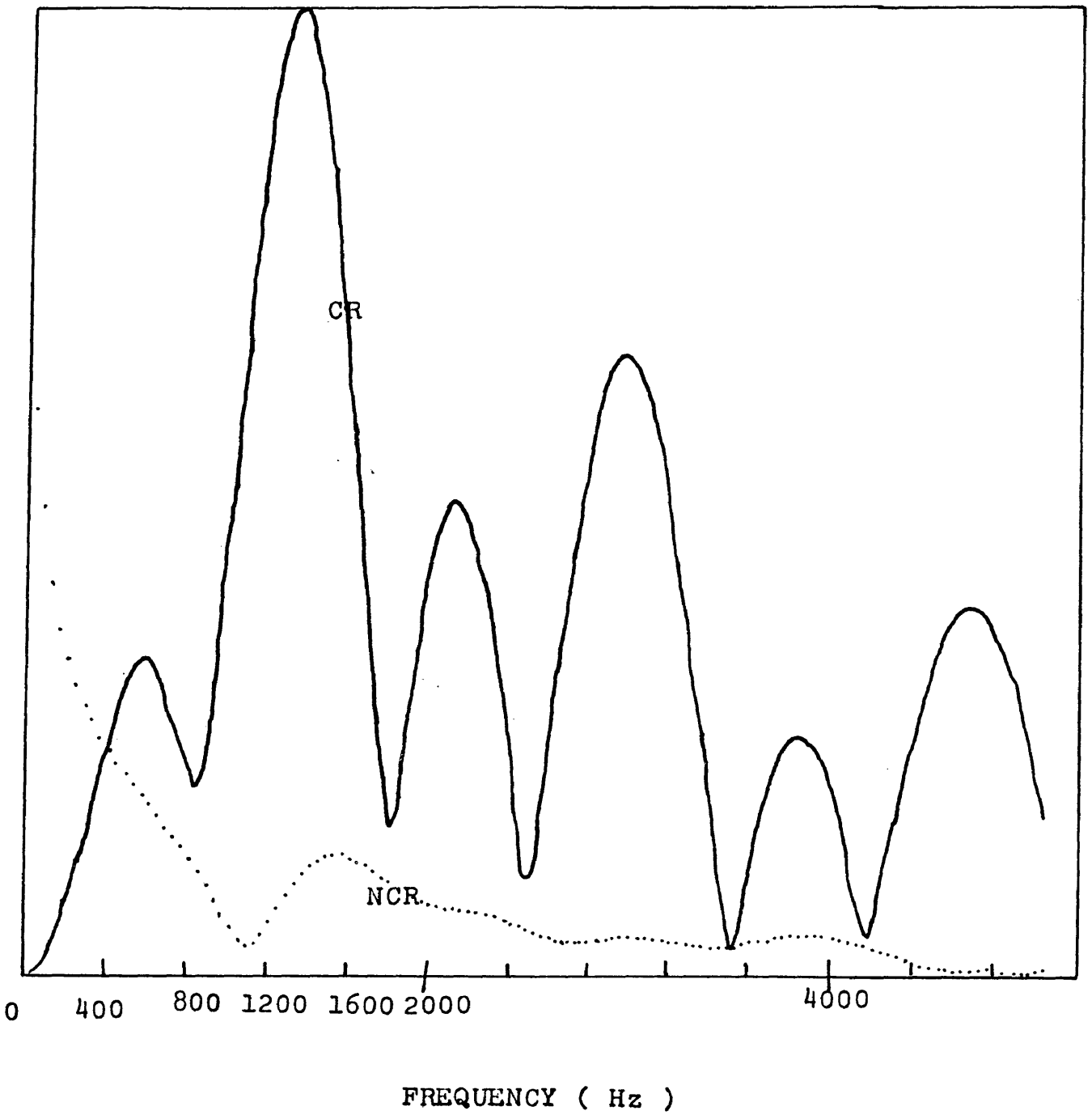

Figure 13. Amplitude spectra of the vertical displacement of the CR and the NCR at r = 6 ft, h = 3 ft, and z = 6 ft.

shown in Figures 12 to 13, when the observation point is at greater depths. The oscillations are due to the interference of spectral components of the 3 transient arrivals -- the direct wave, the reflected P-wave and the reflected S-wave -- which arrive at different times, but have the same waveforms. This phenomenon does not appear when the observation point is at the surface, and all three waves arrive at the same time (see Figure 11). Figure 12 also shows less severe interference because there is no vertical component of the direct wave at r = z = 3 ft. This interference will affect the quantitative comparison of wave components. The effect will be illustrated in the next section where a quantitative comparison of the CR and the NCR is made in the r-z plane.

Figures 14 to 16 show the relative amplitude spectra of the NCR, the SW, and the SSW at three observation points. Sixty-four graphs of this type have been plotted by the CDC-6400 through the CDC-280 graphics system. These were used to plot Figures 27 to 36 which provide quantitative comparisons in the r-z plane.

Figures 17 to 26 show the amplitude variations of the vertical displacements along the surface for each wave component. Each graph is for a different frequency. Precisely, the graphs have been plotted for 10 frequencies from the

amplitude spectra of the vertical displacement at some points of observation just below the surface. These points were selected at z = 1/4 ft, and r = 2, 3, 8, 12, 20, 50, 100, 200 (500 and 1000 ft for the CR only) feet.

Among these graphs only the amplitude variations for the CR have been plotted out to 500 and 1000 ft. For these values of r the SSW became excessively expensive. The reasons for this are discussed in detail in Appendix B.

From Figures 17 to 26, the amplitude variation curves for the CR show a steady decrease as r increases, for all frequencies. At large epicentral distances the rate of change of the amplitude of the vertical displacement for the CR is, as expected, as $1/r^2$ (but as 1/r for the horizontal displacement).

The amplitudes of the NCR appear in a complicated pattern for r being less than 50 ft for all frequencies; for 80 Hz the pattern is still complicated at 150 ft. Within this range, called the complex range, one can make few generalizations concerning the NCR components. However, outside of the complex range all wave components of the NCR have approached asymptotes. In this asymptotic range the surface waves become predominant over the other components of the NCR. In the asymptotic range the amplitudes of the Rayleigh wave vary as

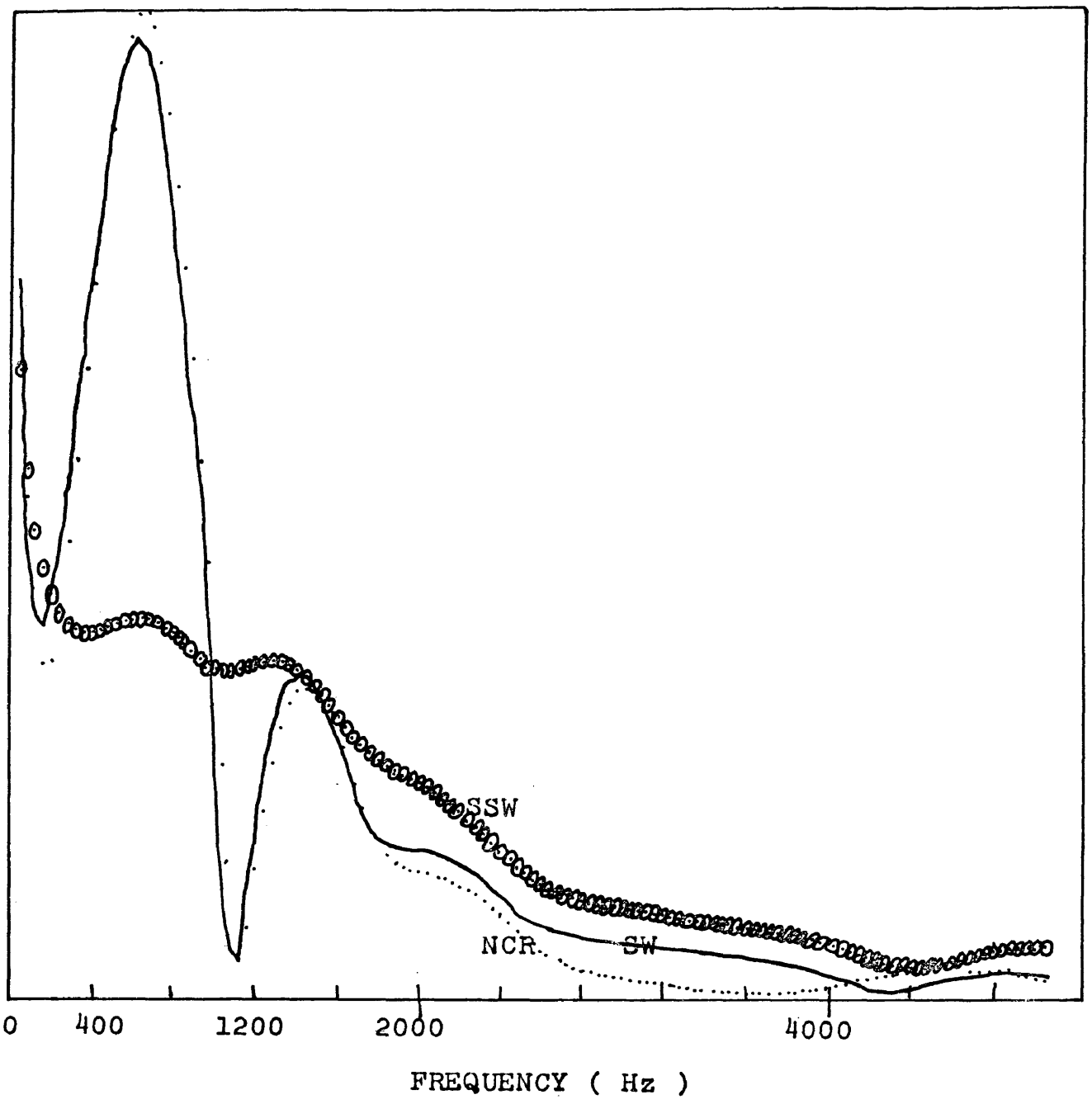

Figure 14. Amplitude spectra of the vertical displacements of the NCR, the SW, and the SSW at r = 12 ft, h = 3 ft, and z = 1/4 ft.

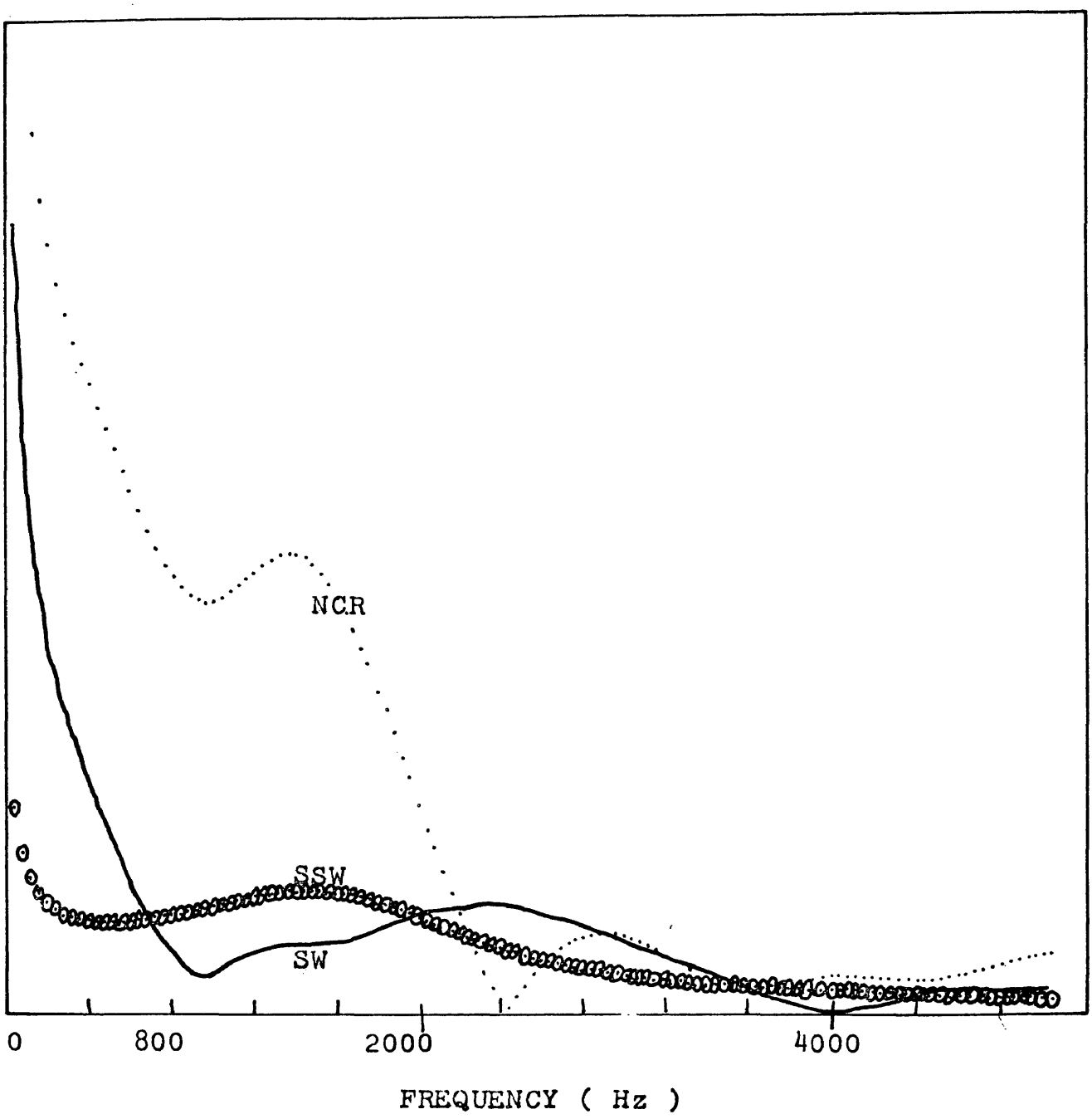

Figure 15. Amplitude spectra of the vertical displacements of the NCR, the SW, and the SSW at r = h = z = 3 ft.

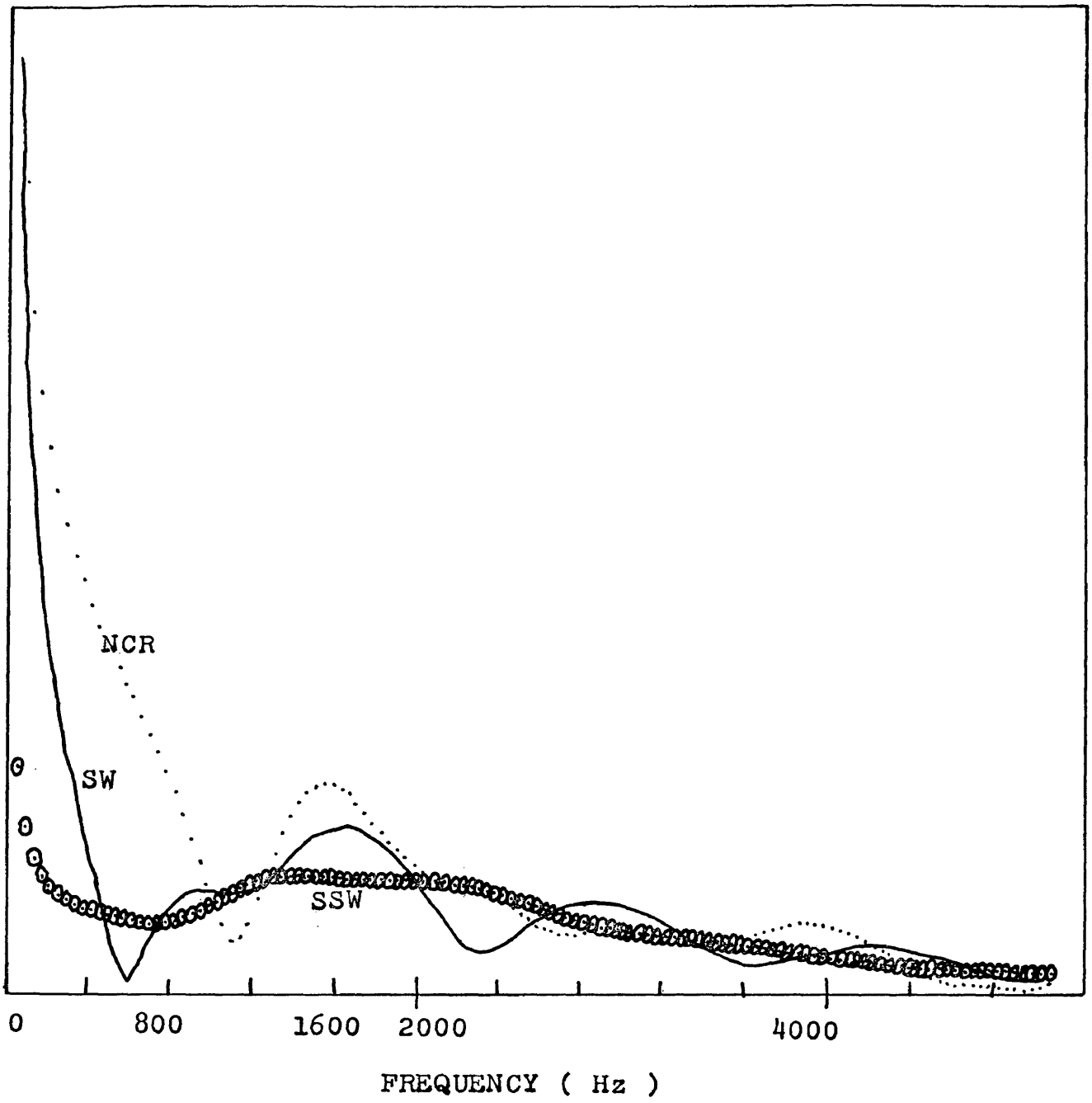

Figure 16. Amplitude spectra of the vertical displacements of the NCR, the SW, and the SSW at r = 6 ft, h = 3 ft, and z = 6 ft.

$1/\sqrt{r}$ (see Figures 17 to 26) and it may be seen to dominate the NCR for compressional wavelengths, λ_p, longer than about three source depths. This geometric attenuation agrees with classical Reyleigh wave theory (see Ewing, Jardetzky, and Press, 1957) and the theory of the Rayleigh wave kinematic discontinuity as presented by Cagniard for a surface source and receiver (see Cagniard, p. 174). The idea of the kinematic discontinuity was introduced by Cagniard to describe and explain step and logarithmic discontinuities in the transmission factors or their derivatives.

The amplitudes of the SSW vary as $1/r^2$ for the wavelengths exceeding approximately 3 source depths. This is consistent with the theoretical prediction by Cagniard (p. 207) for far field analysis near t = SR'; however, the rate of decay in amplitude appears to change from $1/r^2$, for wavelengths greater than 3 source depths, to $1/\sqrt{r}$, for wavelengths smaller than 3 source depths. This was attributed to inadequacies of a numerical integration (see Appendix B).

Comparisons of the amplitudes among wave components can be made, according to the above analysis, in terms of frequency, or wavelength, along the surface of the half-space. One sees, from these figures, that the wave components vary in a complicated pattern for $r < 17h$ or $r < 1.5\ \lambda_p$, where h is the source depth and λ_p represents

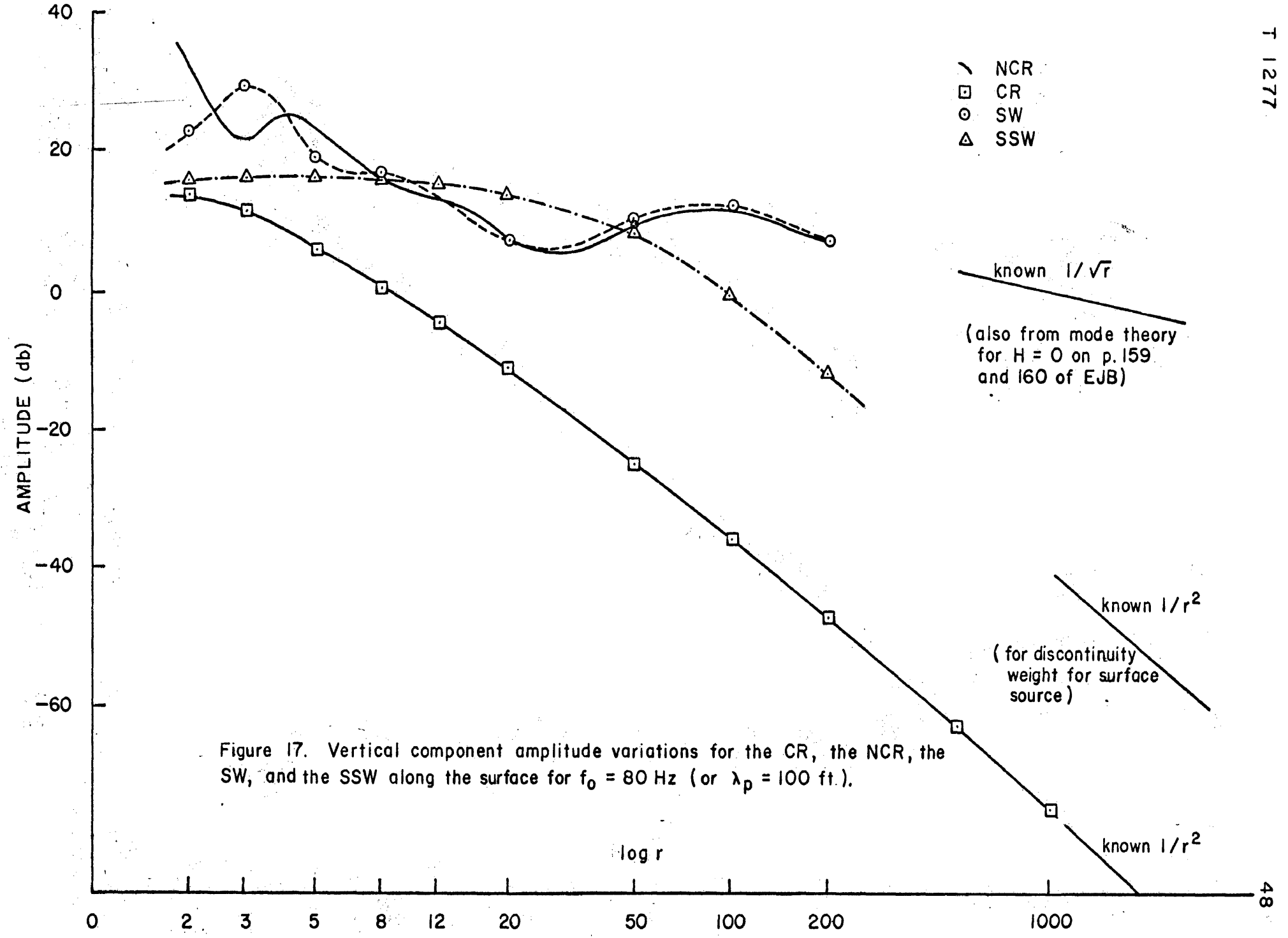

Figure 17. Vertical component amplitude variations for the CR, the NCR, the SW, and the SSW along the surface for f_0 = 80 Hz (or λ_p = 100 ft.).

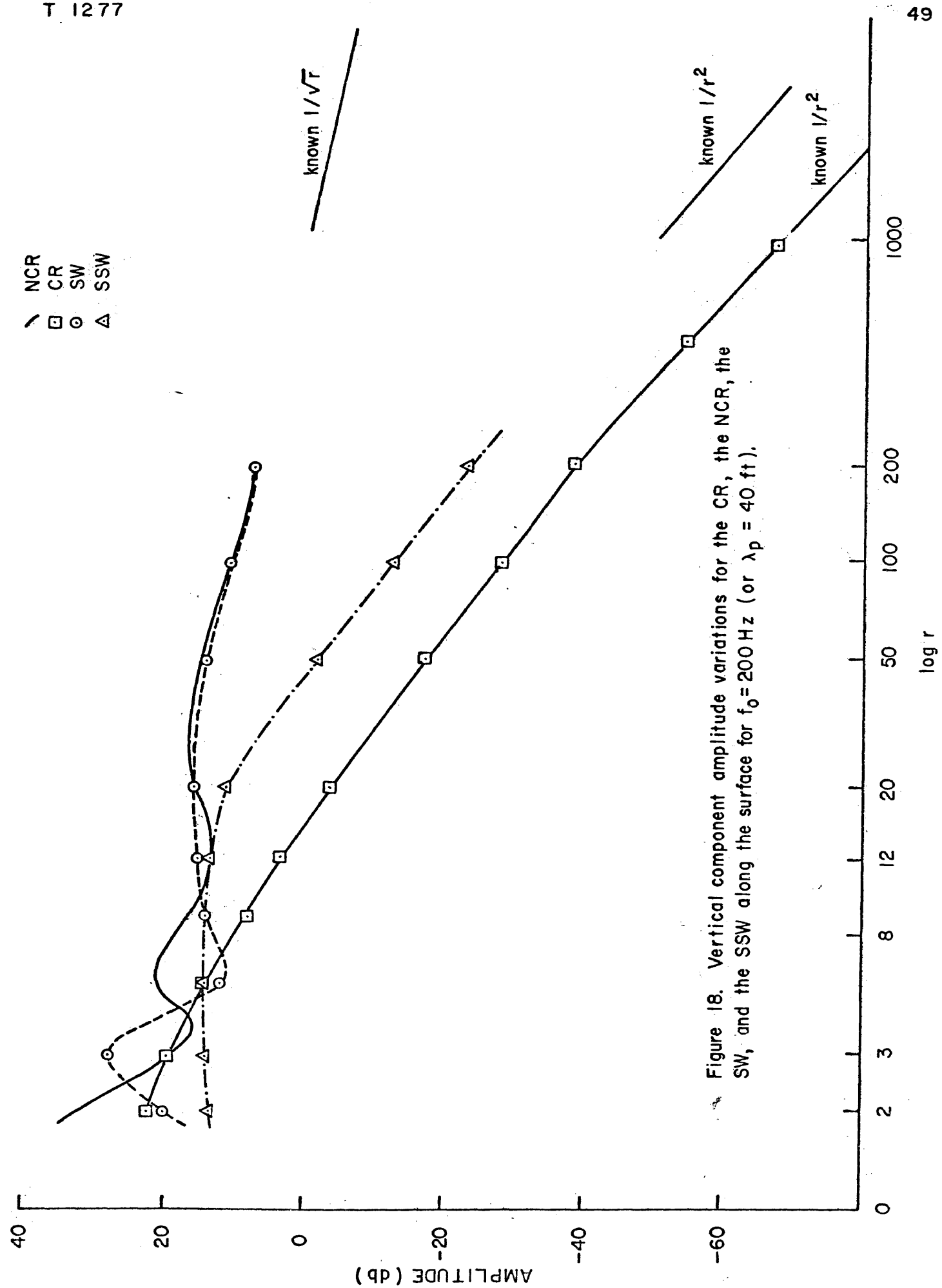

Figure 18. Vertical component amplitude variations for the CR, the NCR, the SW, and the SSW along the surface for $f_o = 200$ Hz (or $\lambda_p = 40$ ft).

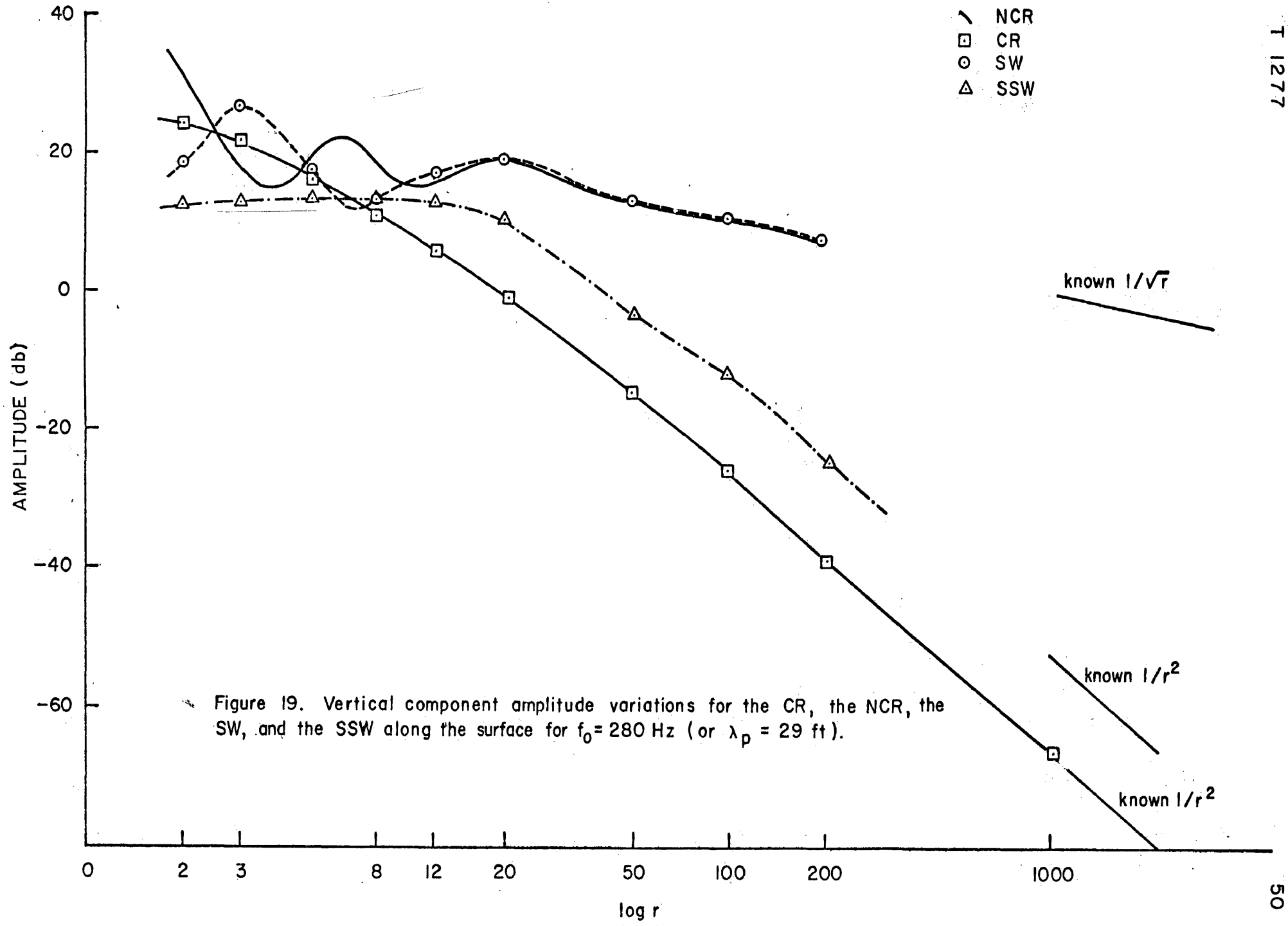

Figure 19. Vertical component amplitude variations for the CR, the NCR, the SW, and the SSW along the surface for $f_0 = 280$ Hz (or $\lambda_p = 29$ ft).

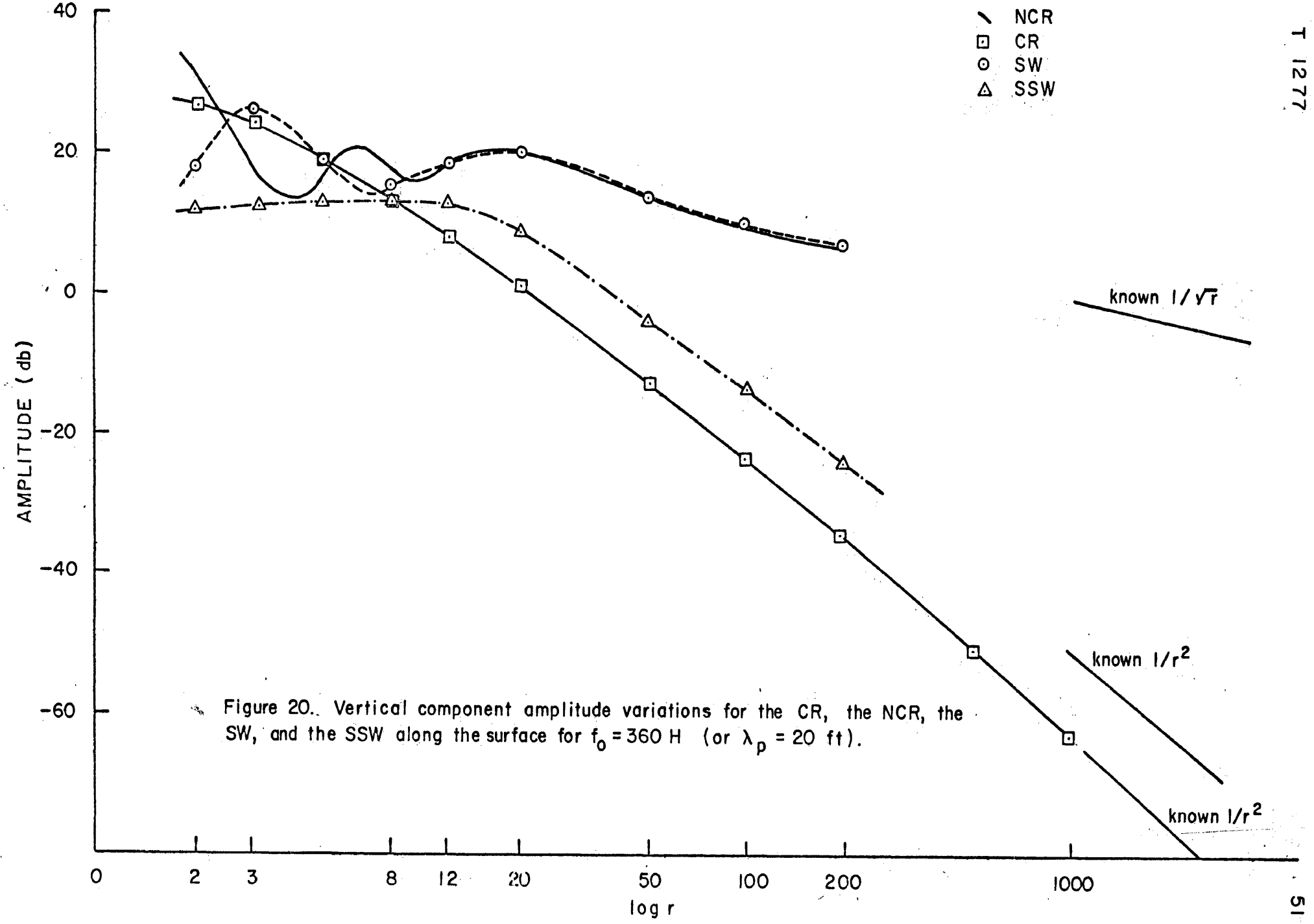

Figure 20. Vertical component amplitude variations for the CR, the NCR, the SW, and the SSW along the surface for $f_0 = 360$ H (or $\lambda_p = 20$ ft).

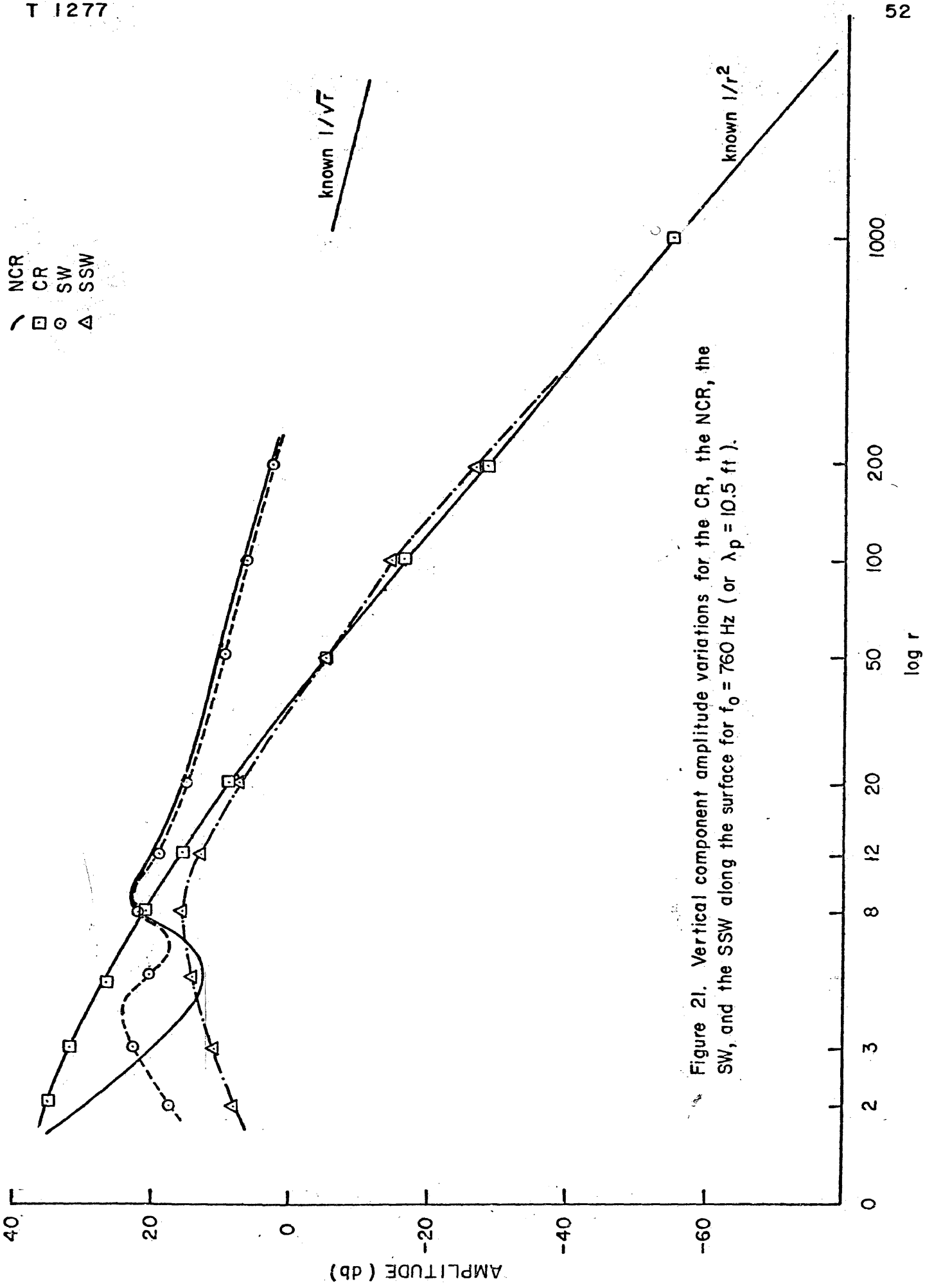

Figure 21. Vertical component amplitude variations for the CR, the NCR, the SW, and the SSW along the surface for f_0 = 760 Hz (or λ_p = 10.5 ft).

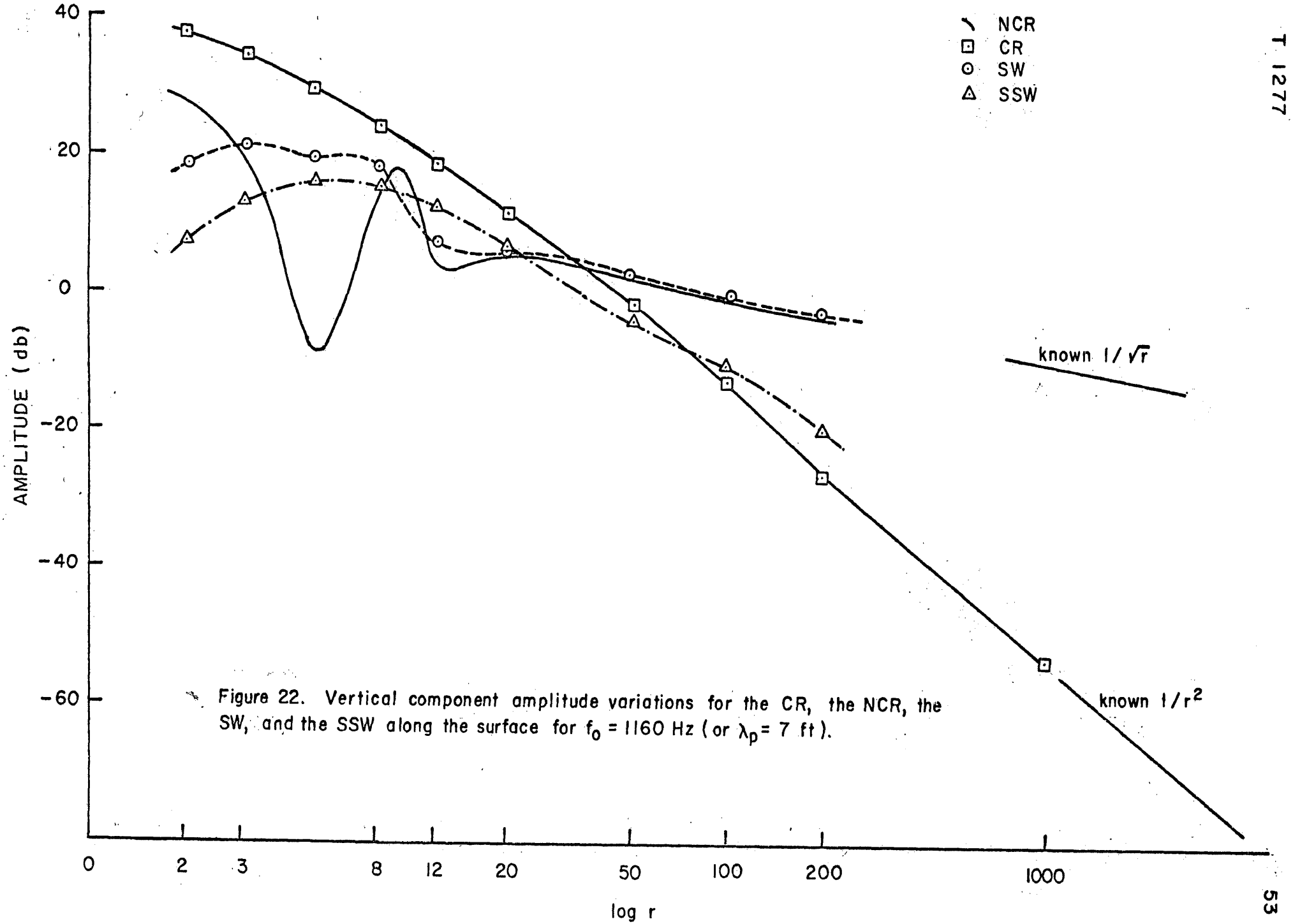

Figure 22. Vertical component amplitude variations for the CR, the NCR, the SW, and the SSW along the surface for f_0 = 1160 Hz (or λ_p = 7 ft).

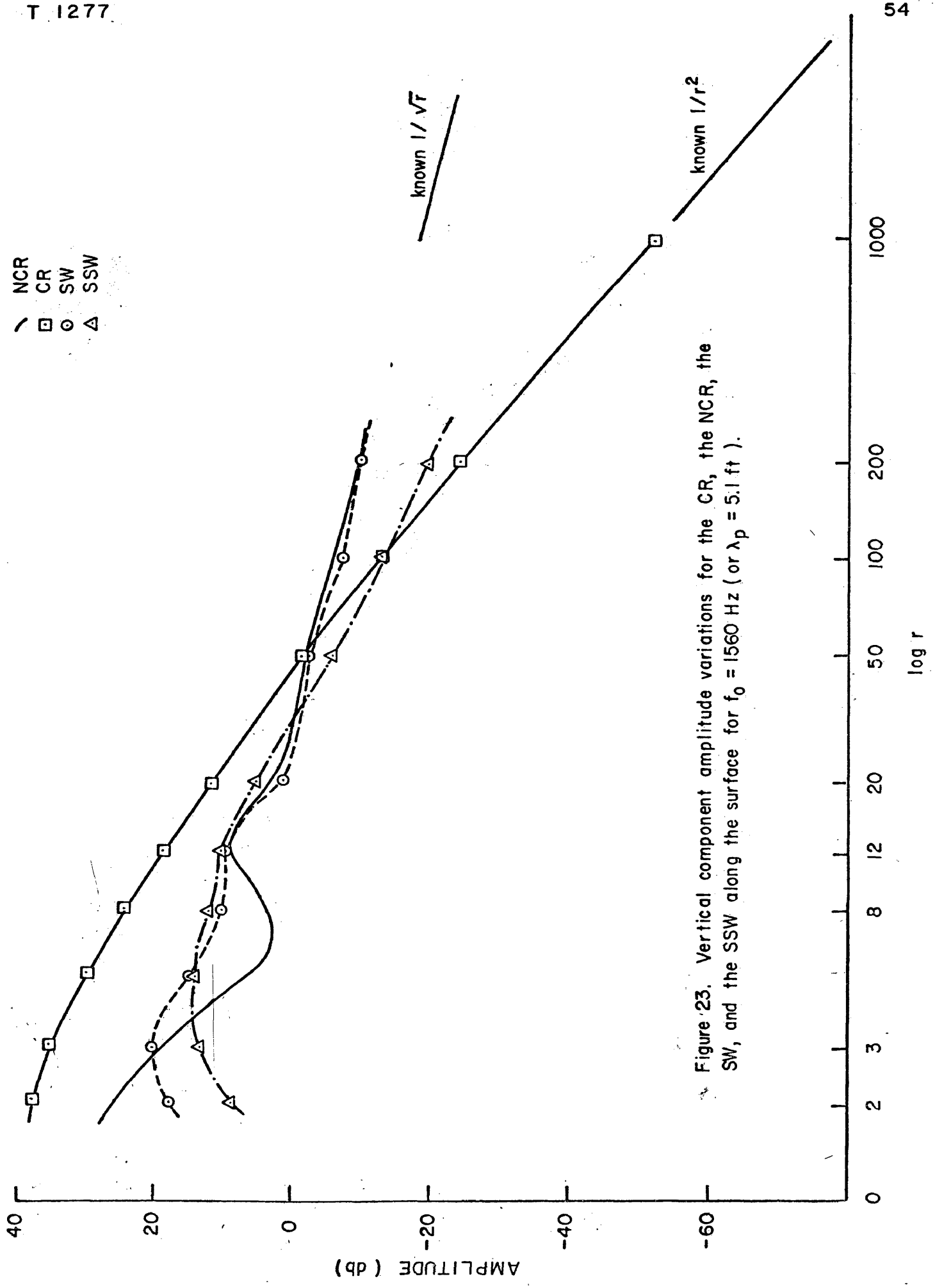

Figure 23. Vertical component amplitude variations for the CR, the NCR, the SW, and the SSW along the surface for f_0 = 1560 Hz (or λ_p = 5.1 ft).

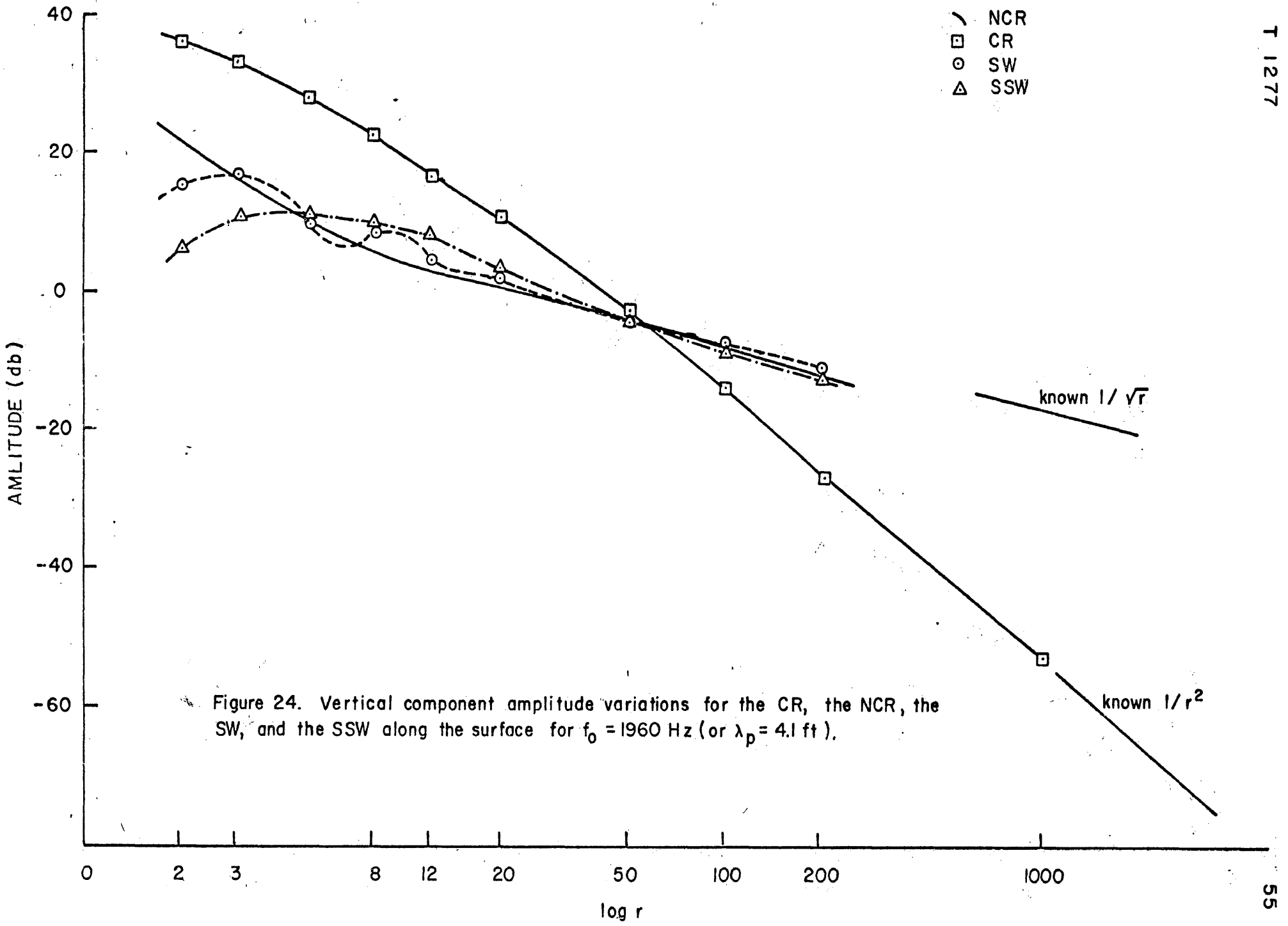

Figure 24. Vertical component amplitude variations for the CR, the NCR, the SW, and the SSW along the surface for f_0 = 1960 Hz (or λ_p = 4.1 ft).

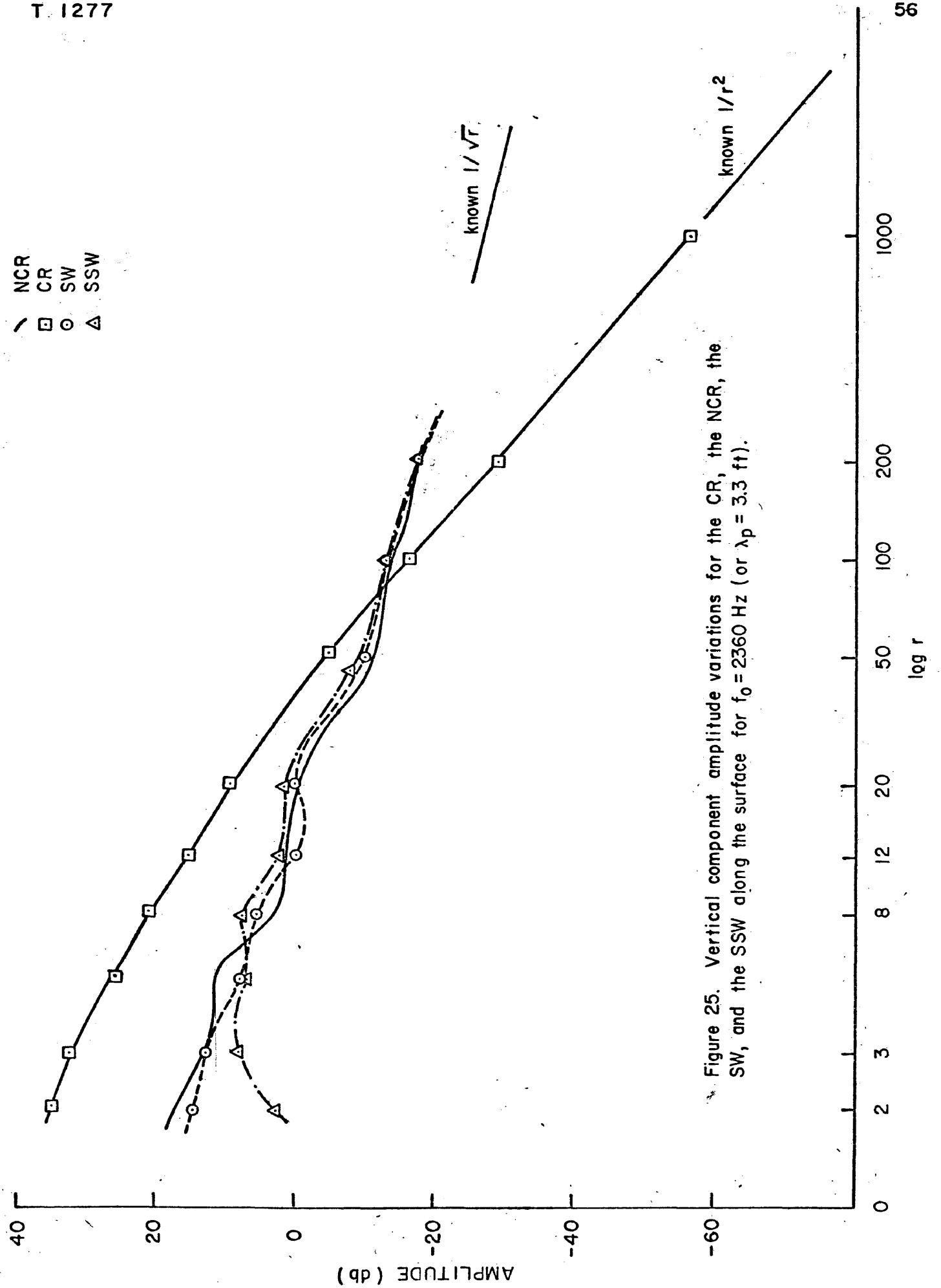

Figure 25. Vertical component amplitude variations for the CR, the NCR, the SW, and the SSW along the surface for $f_0 = 2360$ Hz (or $\lambda_p = 3.3$ ft).

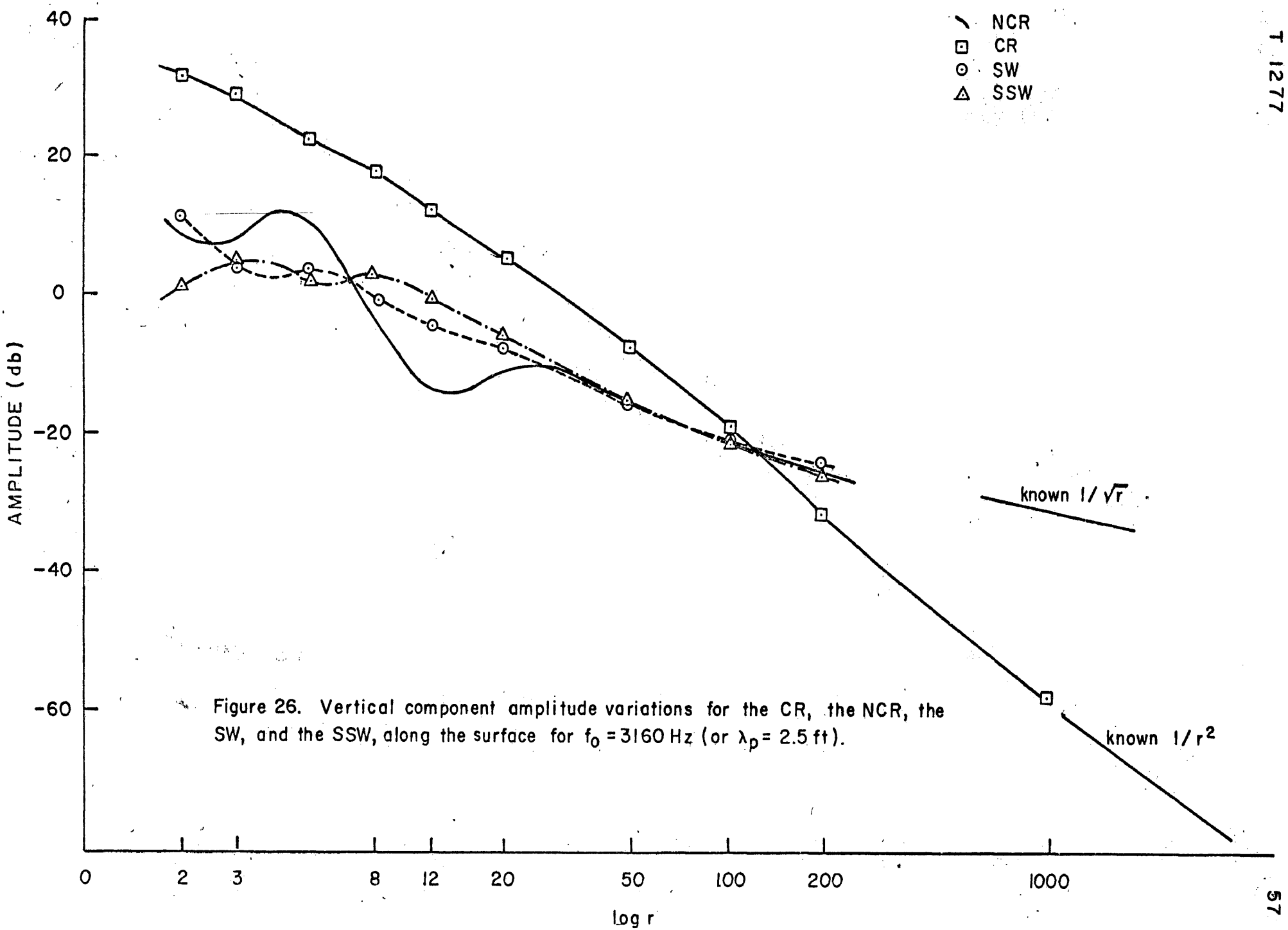

Figure 26. Vertical component amplitude variations for the CR, the NCR, the SW, and the SSW, along the surface for $f_0 = 3160$ Hz (or $\lambda_p = 2.5$ ft).

wavelengths of the compressional waves. For $r > 17h$ or $r > 1.5\ \lambda_p$, the geometric attenuation of the wave components is described by asymptotes which are consistent with available predictions of inexact theory. Within ten source depths of the epicenter the CR dominate when the wavelengths are smaller than approximately one source depth.

The quantitative comparisons of this section will now be used to divide the half-space into portions such that in each portion one of the wave components dominates to a specific degree. These portions, or elastic fields, can be named after the dominating wave. For instance, the region where the CR dominates is called the CR field; space outside of this region is called the NCR field. In the same manner, we can have the SW field and the SSW field. All these fields will be defined in terms of frequencies.

Quantitative Definition of the Elastic Fields

Since the vertical displacements are more interesting to the exploration seismologists and our computer funds are limited, the boundaries of the elastic fields are to be drawn in terms of vertical displacements and inside of a frame ranging from 0 to 20 ft horizontally and from 0 to 10 ft vertically. From Figures 17 to 26 we have seen that the amplitude of each wave component varies a great deal for r less than 20 ft on the surface. Hence it is especially

worthwhile to investigate the elastic fields within this horizontal range.

Definition of these elastic fields inside the previously mentioned frame is in terms of ratios of spectral amplitudes. More specifically, the shape and size of the elastic fields were determined from the ratios of any spectral wave amplitude to the spectral NCR wave amplitude at each point of observation inside of the frame. Hence, one can define these elastic fields in terms of three factors: type, level, and frequency. The term type refers to the sort of waveform that was compared with the NCR waveform, and level refers to the minimum ratio of the spectral wave amplitude necessary for the point of observation to be in one of those elastic fields. Frequency refers to the specific frequency of investigation. For example, the CR field at level 100 and frequency 100 Hz would be a region of the half-space in which the amplitude of the CR is 100 times greater than the amplitude of the NCR at a frequency f_o = 100 Hz. This is, in other words, a region of the half-space in which one may compute waveforms assuming, to an uncertainty less than one percent and for the frequencies near 100 Hz, that the waveforms do not change as they propagate along the classical ray paths.

For this study the spherical source is located three

feet below the surface and given a radius of 1 foot. The elastic parameters of the solid medium are: ρ = 2.4 gm/c.c., V_p = 8000 ft/sec, and V_s = 4500 ft/sec. Amplitude spectra of the CR, the NCR, the SW, and the SSW were computed and plotted for 32 carefully selected points of observation in the 20 x 10 ft frame. All computations were carried out on CU's digital computer, CDC-6400, at Boulder, Colorado.

The method used to plot the various fields is shown in Figure 27. The binary information, concerning the inside or outside of a certain elastic field, was determined by comparing the relative amplitudes, as presented in graphs like Figures 11 through 16. In this study, the levels were put at 1.0, 0.5, and 0.5 for the CR field, the SW field, and the SSW field, respectively. In Figure 27 the CR field at level 1.0 and frequency f_o = 360 Hz is represented by the region cross-hatched down to the left, the SW field at level 0.5 and frequency f_o = 360 Hz is represented by the region cross-hatched down to the right, the SSW field at level 0.5 and frequency f_o = 360 Hz is represented by the dotted region. As plotted in Figure 27, the CR field is far away; i.e., more than a quarter wavelength, from the source and the surface. The region complimentary to the CR field, in which the NCR dominates, is called the NCR field of level 1.0 and frequency f_o = 360 Hz. The NCR field occupies the regions surrounding the source and close to the surface. The SW field is a flat region lying just under the surface and extending to

infinity; the SSW field develops to a loop-like region which terminates near r = 12 ft at the surface. The implication of such plot will be discussed later. In the same manner, plots of the elastic fields at the same levels have been sketched in Figures 28 through 37 for another ten frequencies. These frequencies are chosen to be 40 Hz, 120 Hz, 200 Hz, 280 Hz, 760 Hz, 1160 Hz, 1560 Hz, 1960 Hz, 2360 Hz, and 3160 Hz. Since the surface waves are a part of the NCR component, the SW field as well as the SSW field were not drawn inside of the CR field.

Several observations have been made from the numerical examples of the elastic fields at the chosen eleven frequencies. They are stated as follows:

1. At lower frequencies, or longer wavelengths, the entire 20 x 10 ft rectangular area is outside of the CR field. This dominance of the NCR fields at 40 Hz, 120 Hz, 200 Hz, and 280 Hz is illustrated in Figures 28, 29, 30, and 31, respectively. The SW fields and the SSW fields occupy most of the NCR field for these frequencies.

2. At higher frequencies, or shorter wavelengths, almost the entire 20 x 10 ft frame is the CR field at level 1.0 except for small portions near the source. These are shown in Figures 33, 34, 35, 36, and 37, for frequency f_o = 1160 Hz, 1560 Hz, 1960 Hz, 2360 Hz, and 3160 Hz,

respectively. In Figures 33 and 37, small traps of the NCR field appear in the CR fields. This feature is due to the previously-mentioned destructive interference of the CR. One should note from Figures 27 through 32 that a SW region, dominated by the Rayleigh wave, will always dominate the surface in the far field. This might be called the Rayleigh wave plate.

3. At an intermediate frequency range, such as f_o = 360 Hz, or 760 Hz, the elastic fields are all present in the 20 x 10 ft area, shown in Figures 27 and 32.

4. As shown in Figure 38, the size of the portion of the SW field in the 20 x 10 ft frame decreases as the frequency increases from almost the entire area to the loop-like regions to the flat regions lying just under the surface. Note that the SW fields do not develop in a region above the source.

5. The shape and size of the SSW fields varies as the frequency increases in the manner shown in Figure 39. Note that the boundaries of the SSW fields intersect the surface to form closed loops. The closed loops of the SSW fields, unlike the SW fields, enable one to compute the synthetic seismograms at some epicentral distance without computing the SSW on the surface of a half-space, at least for these frequencies.

6. Figure 40 shows the distribution of the CR fields at level 1.0 and frequencies exceeding 360 Hz.

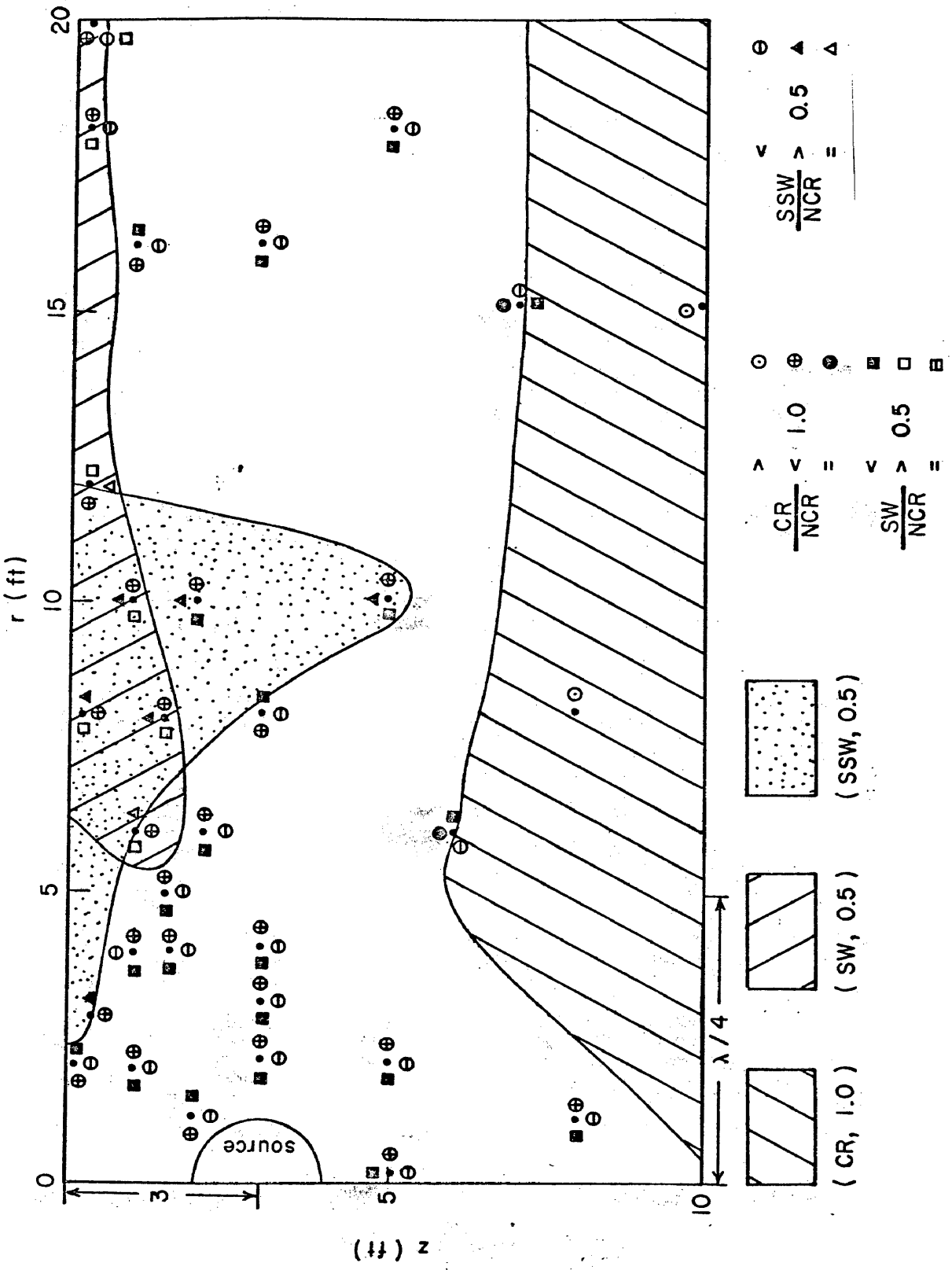

Figure 27. Distribution of elastic fields for f_o = 360 Hz. Here λ denotes compressional wavelength.

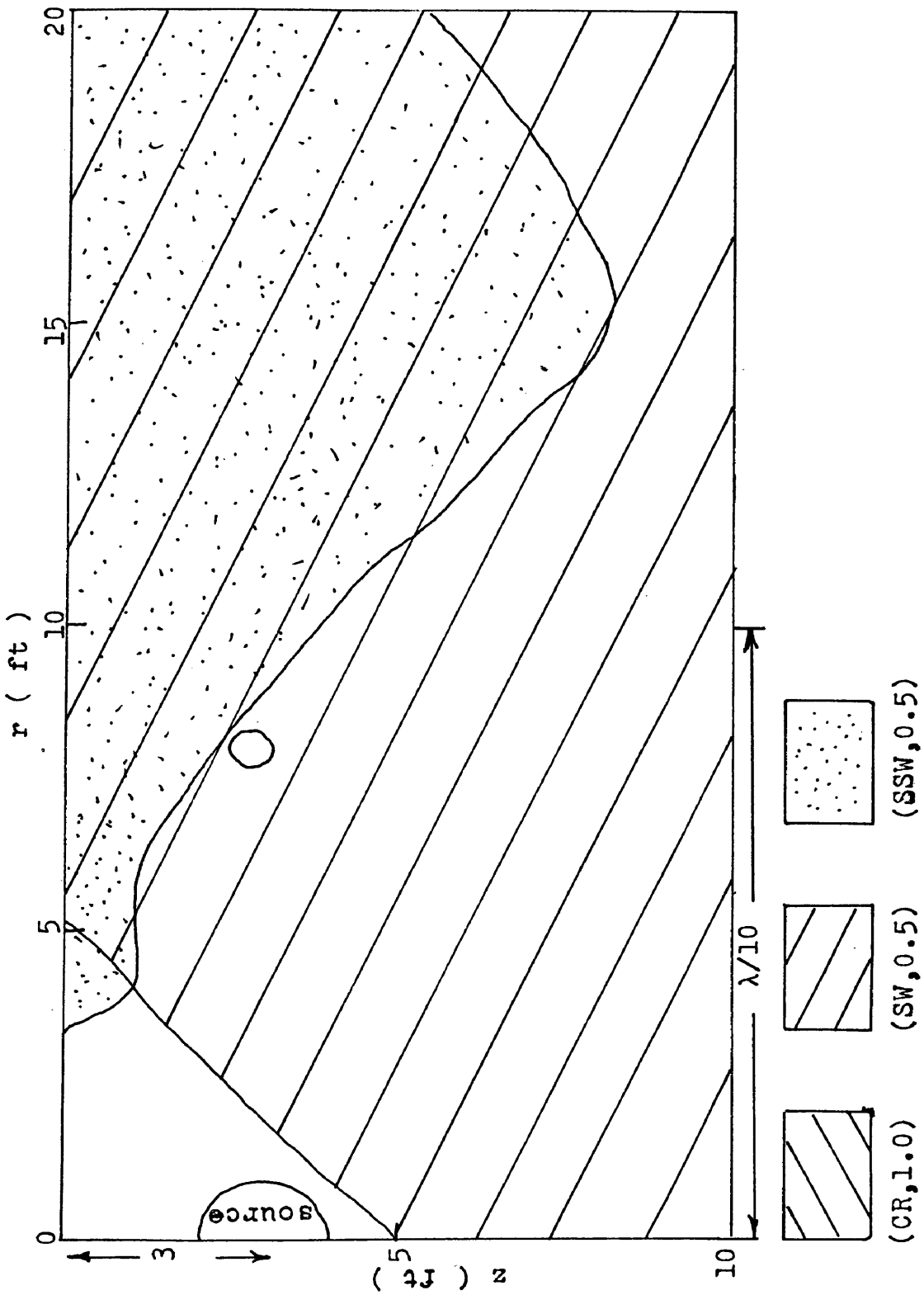

Figure 28. Distribution of the elastic fields for f_o = 40 Hz. Here λ denotes compressional wavelength.

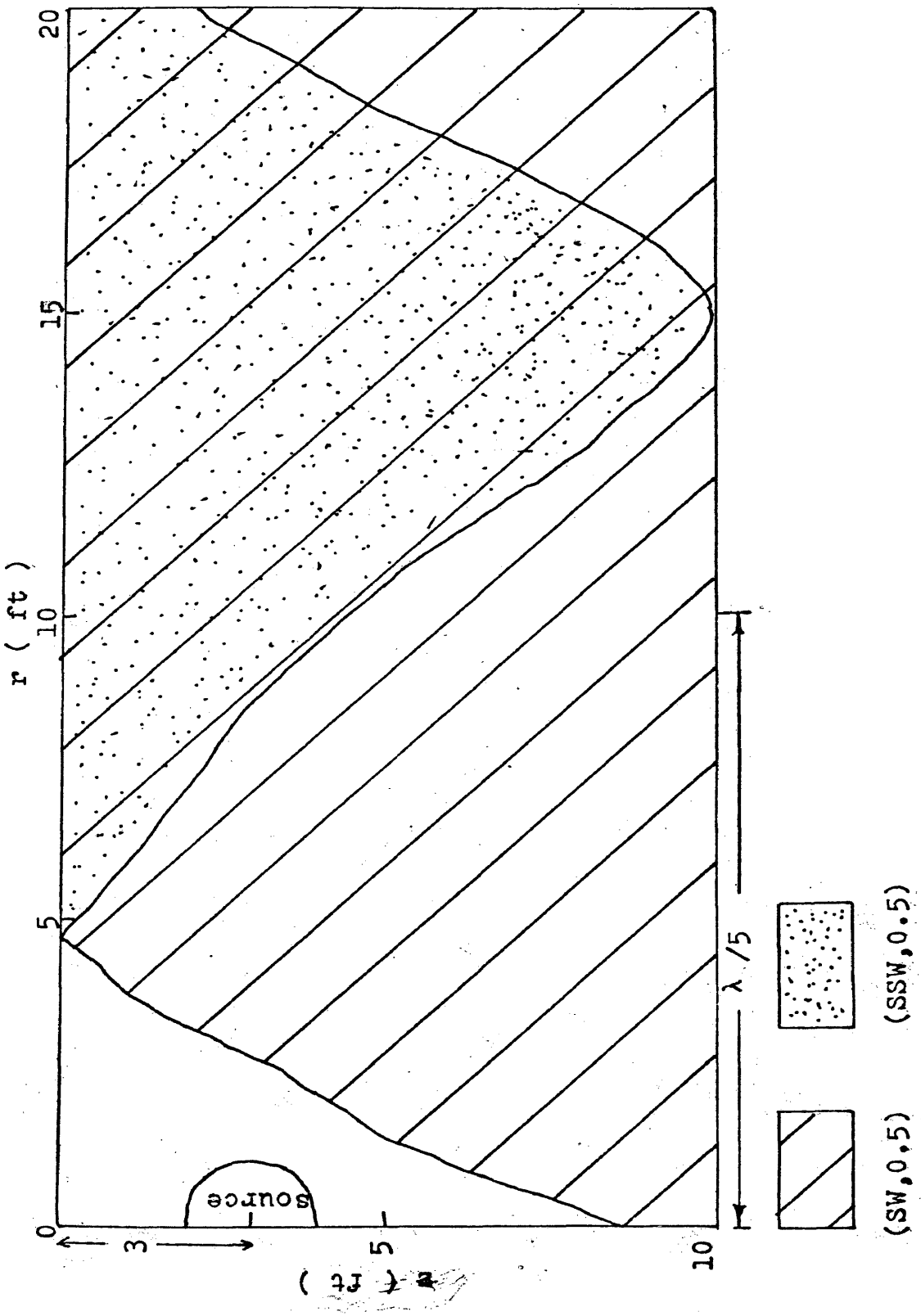

Figure 29. Distribution of the elastic fields for f_o = 120 Hz. Here λ denotes compressional wavelength.

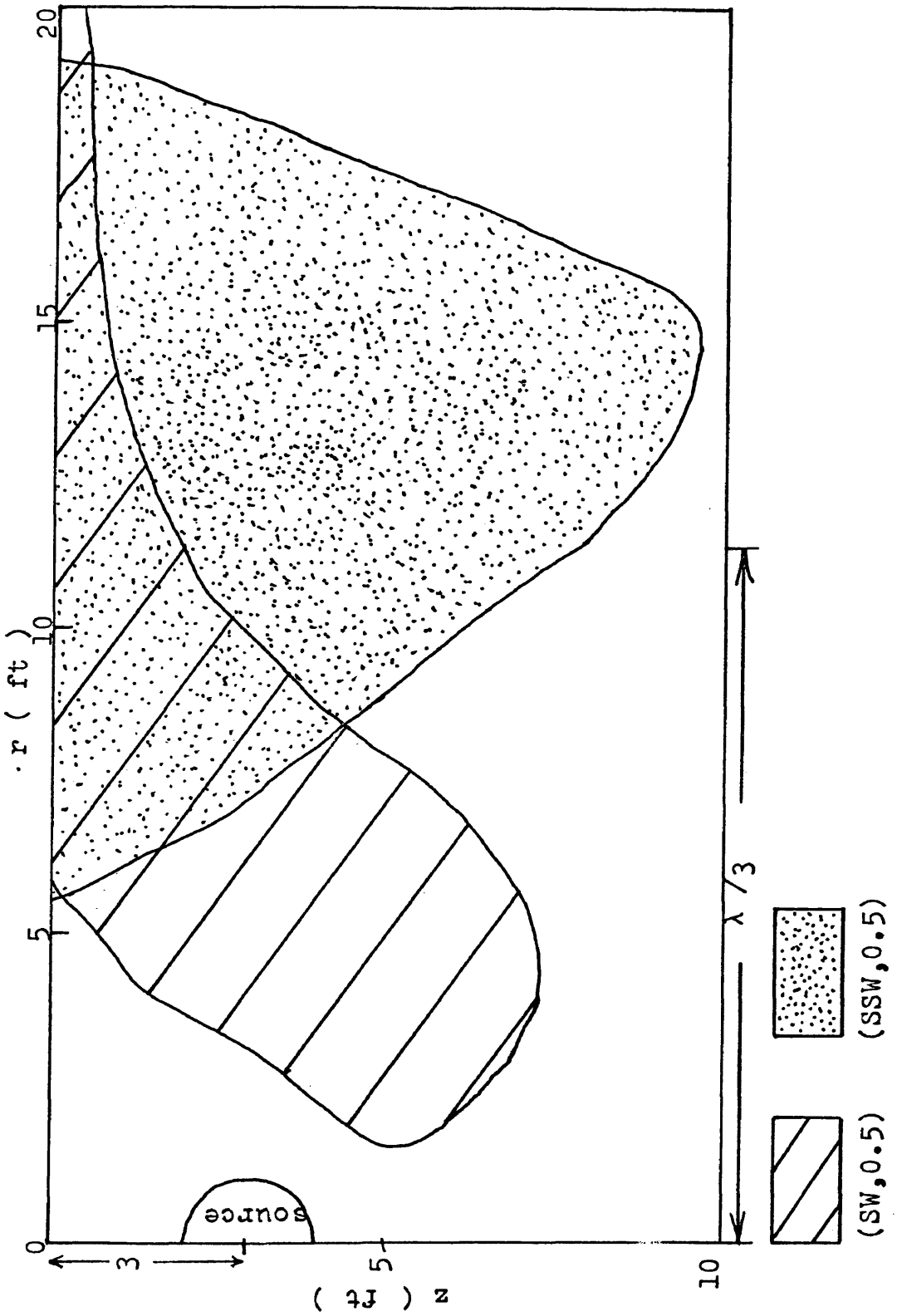

Figure 30. Distribution of elastic fields for f_o = 200 Hz. Here λ denotes compressional wavelength.

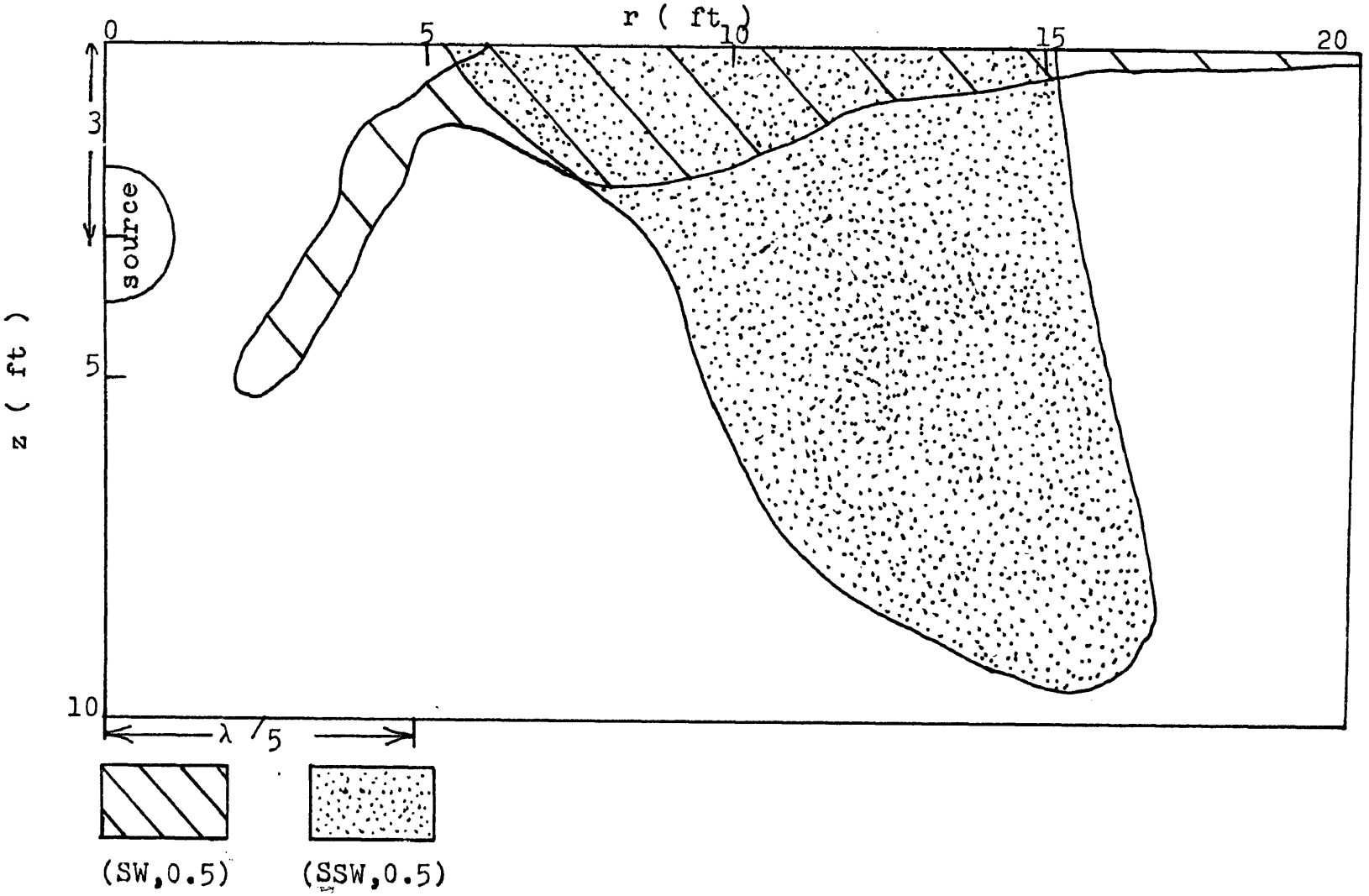

Figure 31. Distribution of elastic fields for f_o = 280 Hz. Here λ denotes compressional wavelength.

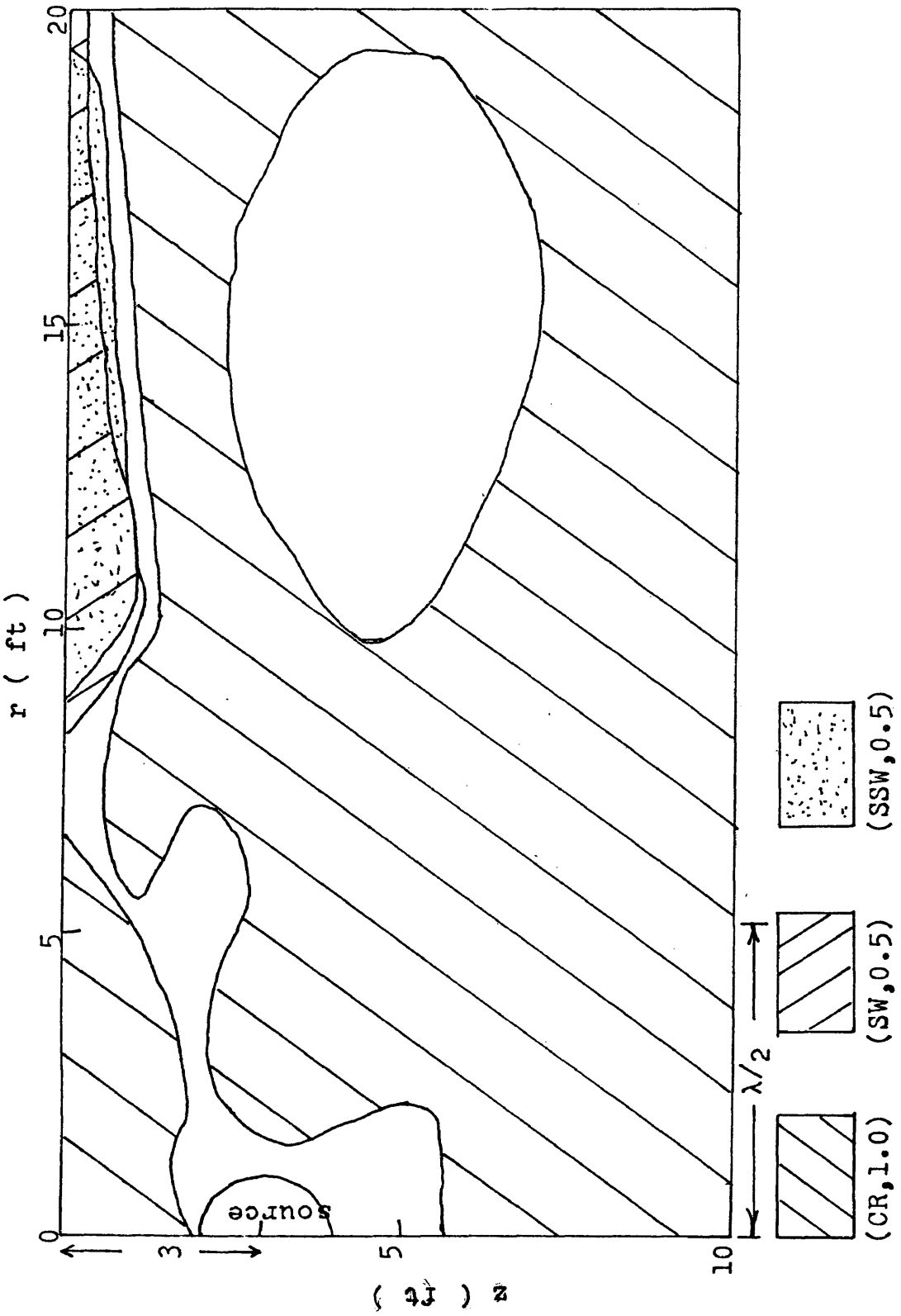

Figure 32. Distribution of elastic fields for f_o = 760 Hz. Here λ denotes compressional wavelength.

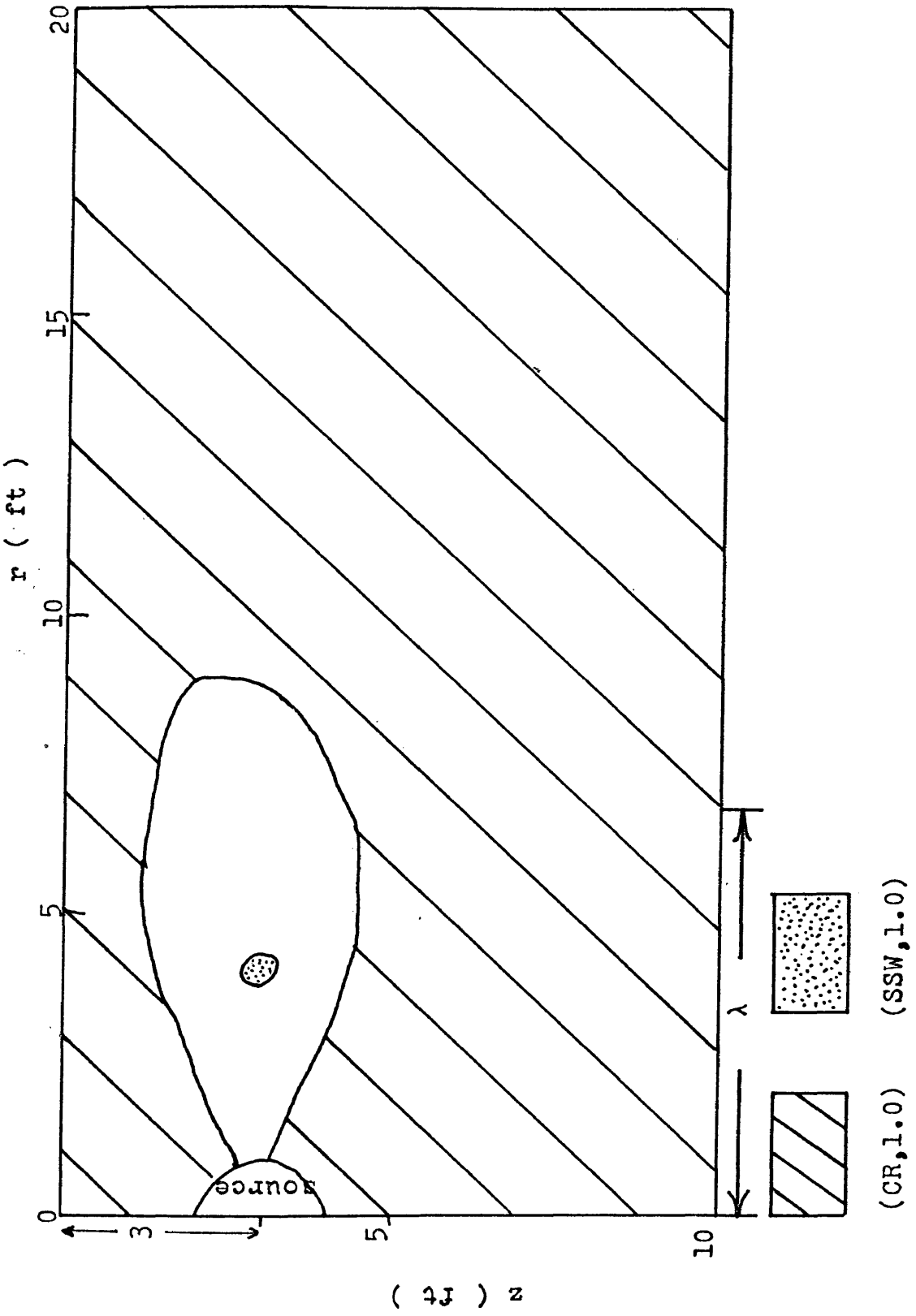

Figure 33. Distribution of elastic fields for f_o = 1160 Hz. Here λ denotes compressional wavelength.

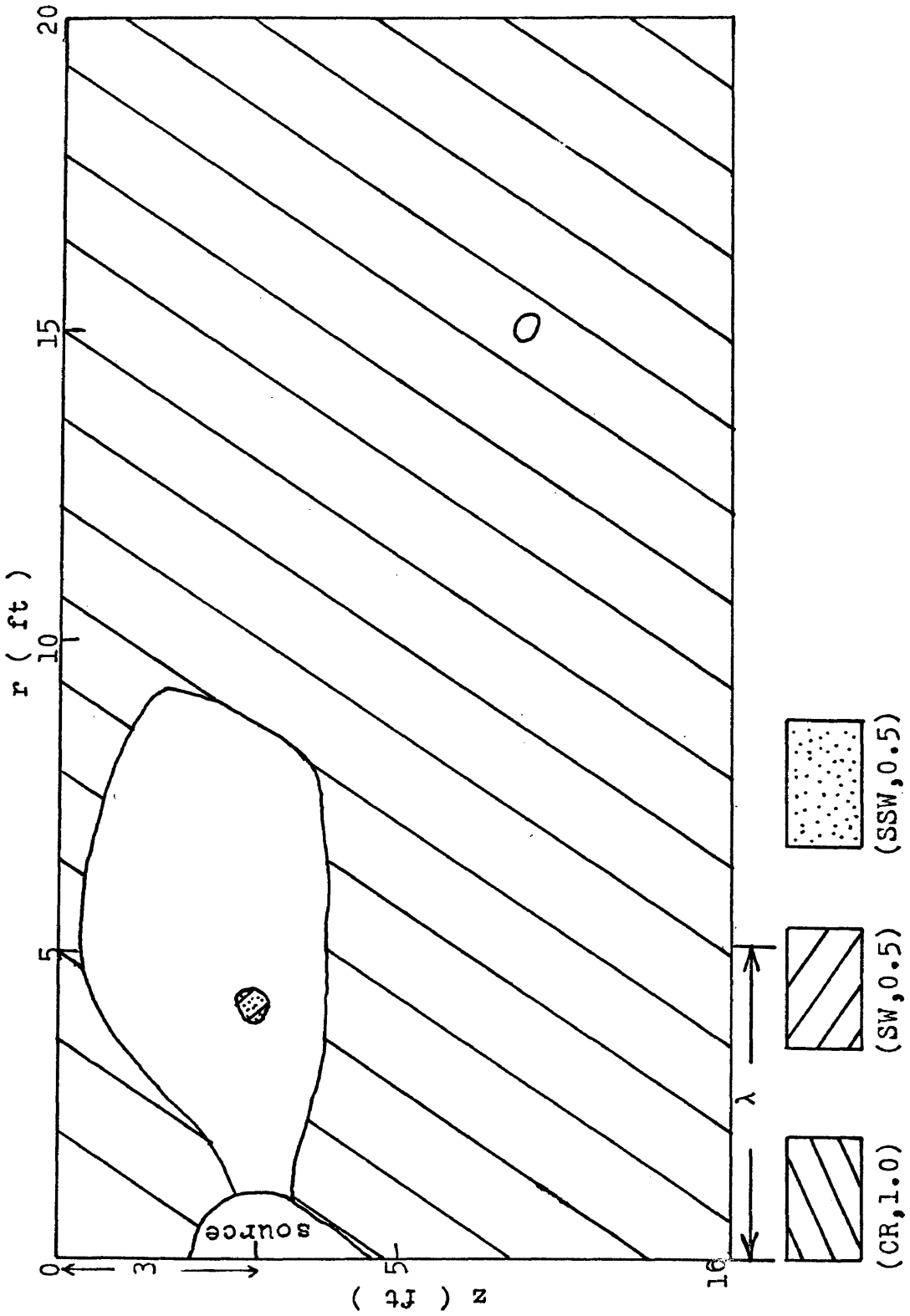

Figure 34. Distribution of elastic fields for f_o = 1560 Hz. Here λ denotes compressional wavelength.

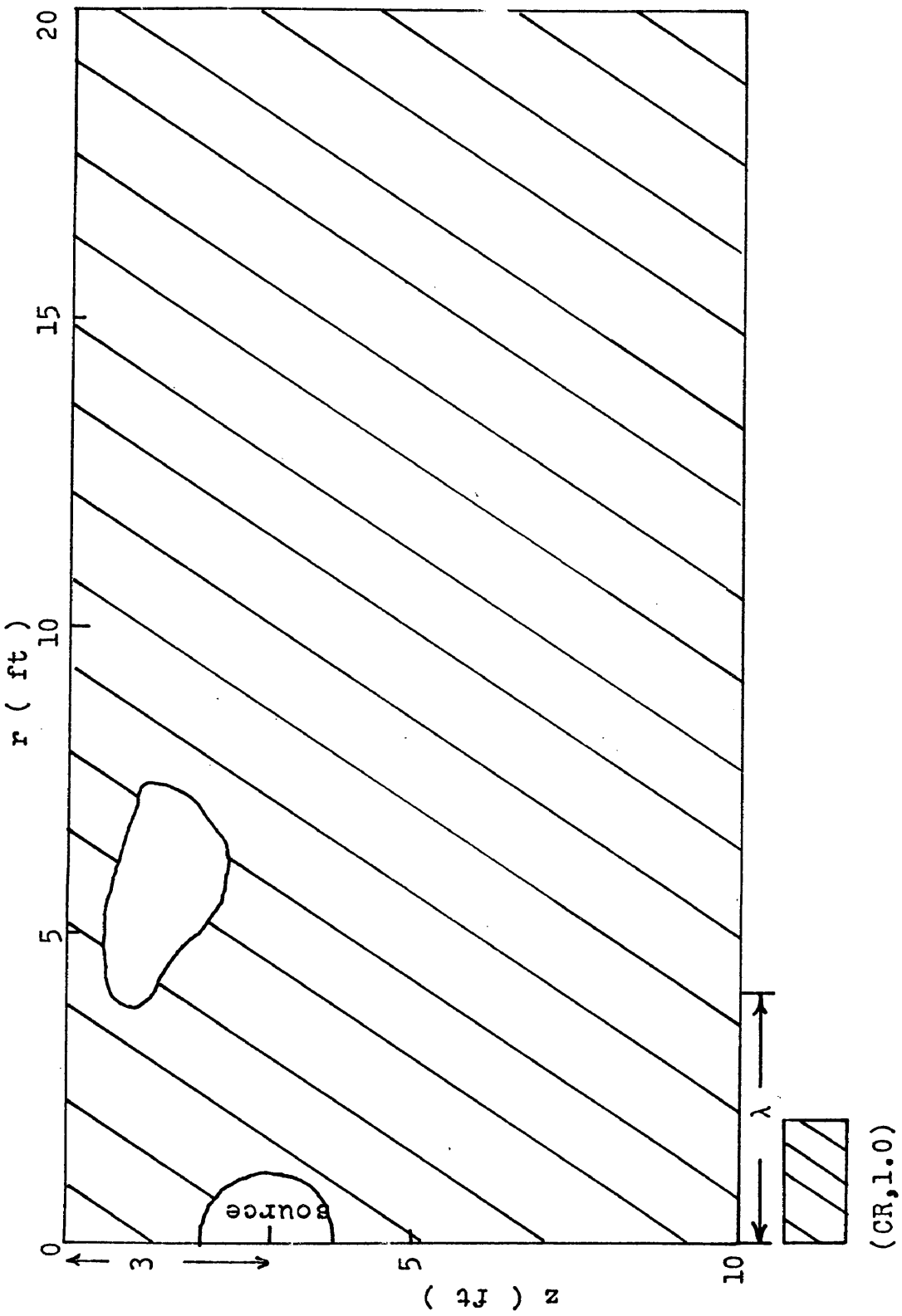

Figure 35. Distribution of elastic fields for f_o = 1960 Hz. Here λ denotes compressional wavelength.

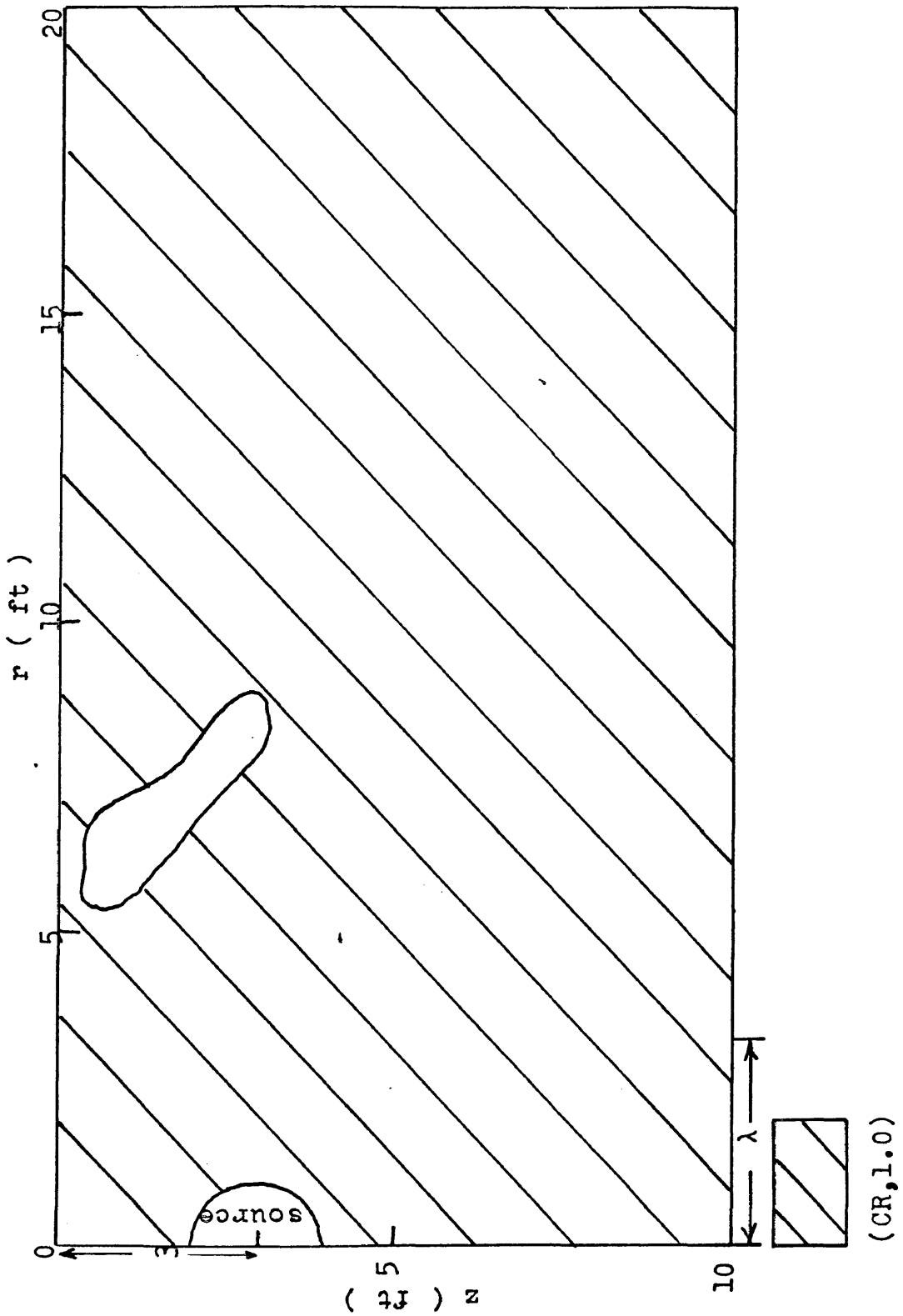

Figure 36. Distribution of the elastic fields for f_o = 2360 Hz. Here λ denotes compressional wavelength.

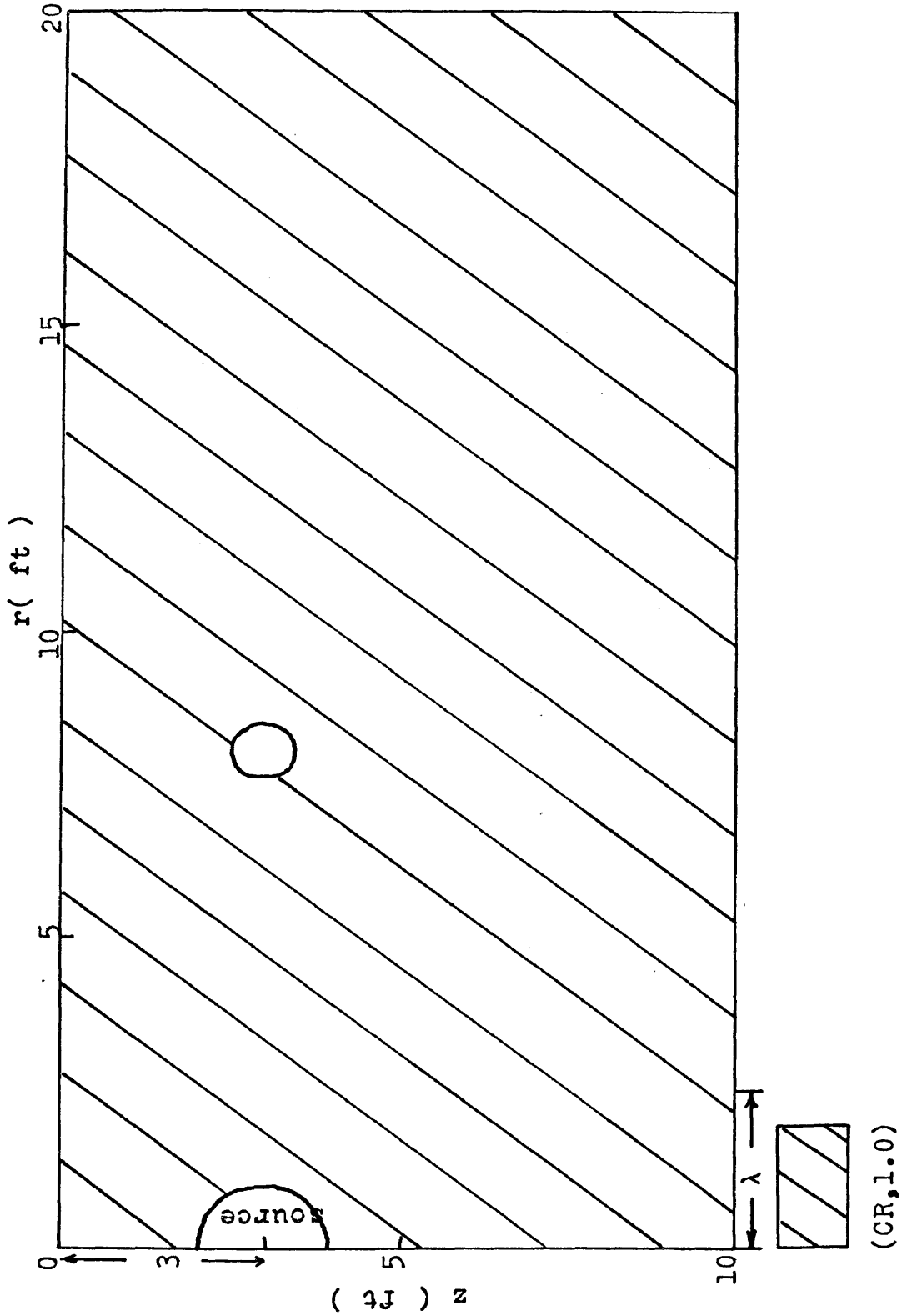

Figure 37. Distribution of elastic fields for f_o = 3160 Hz. Here λ denotes compressional wavelength.

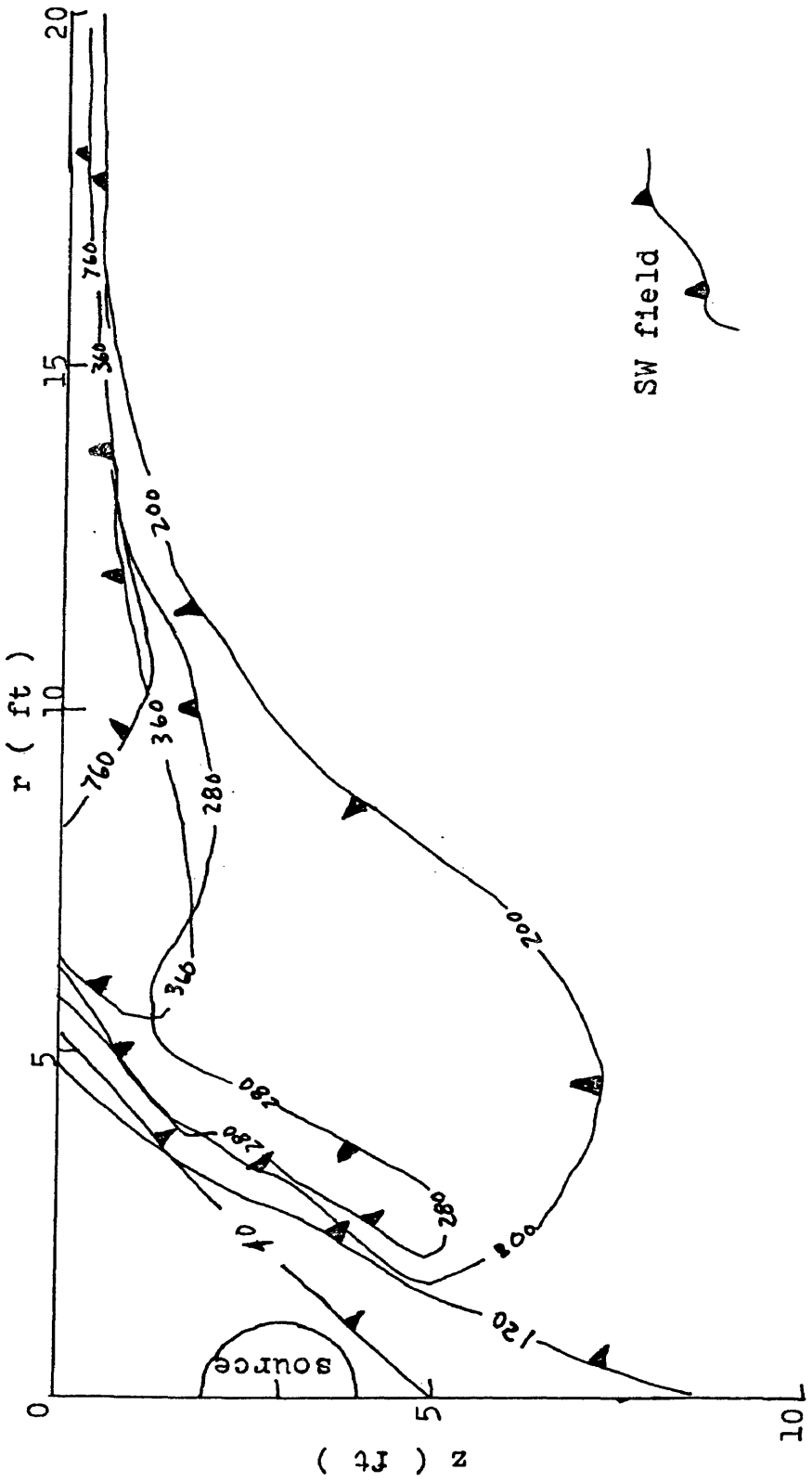

Figure 38. Distribution of the SW fields at level 0.5 and for f_o less than 760 Hz.

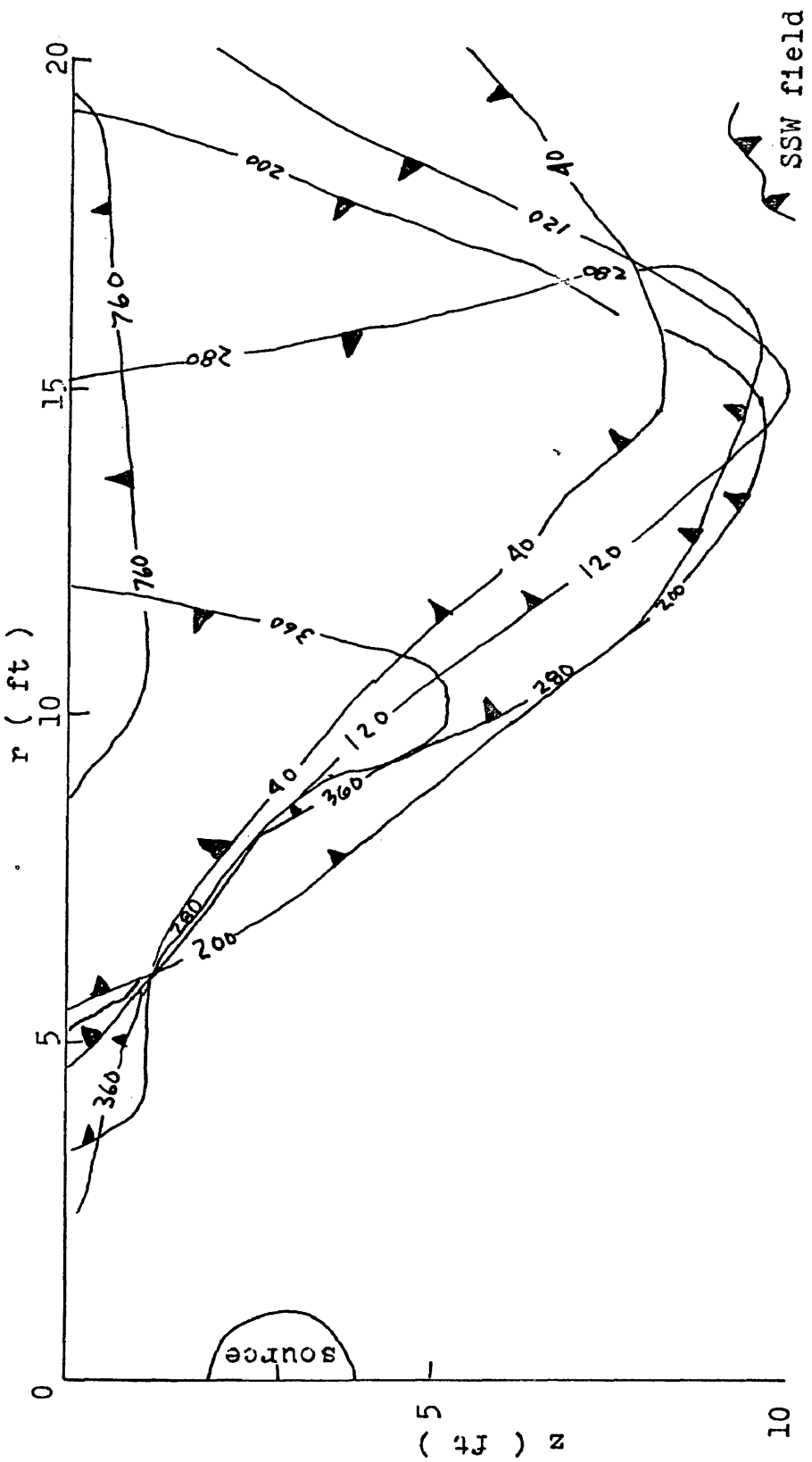

Figure 39. Distribution of the SSW fields at level 0.5 and for frequencies less than 760 Hz.

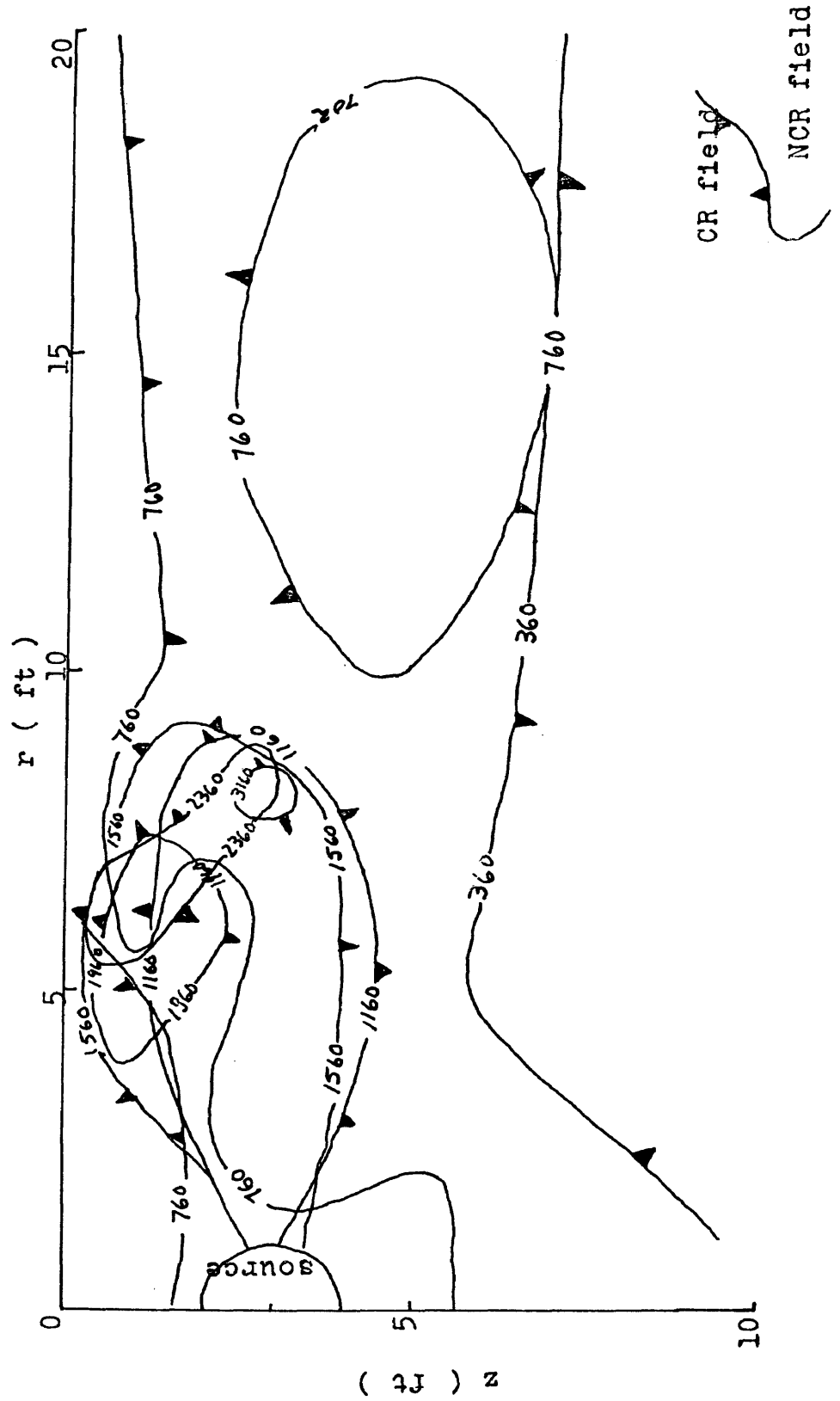

Figure 40. Distribution of the CR fields and the NCR fields at level 1.0 and for frequencies greater than 360 Hz.

CONCLUSIONS

The mathematical analysis of Cagniard's method yields equations which can be used to compute a complete synthetic seismogram as four components of body waves and two components of surface waves. These wave components are in terms of particle displacements for a given source and given parameters of the solid semi-infinite medium.

Comparisons made between seismograms computed by the finite difference method and the exact ray method indicate that there are some minor discrepancies between the results of two completely different approaches but that the waveforms are so similar that they appear to be nearly identical until they are superimposed. These minor discrepancies were attributed to the approximations used in the finite difference method.

Cagniard's analysis enables us to study the behavior of each wave component under different circumstances; such as near the source, far from the source, near the surface, and far from the surface.

Quantitative comparisons of the amplitudes of the vertical displacement of the classical ray components, the surface waves, the second surface waves, and the nonclassical ray components indicate that:

1. At the surface, the non-classical ray components dominate in the synthetic seismograms for large distance from the epicenter for all frequencies; but, the classical ray components dominate at high frequencies near the epicenter.

2. Except near the epicenter, the surface waves dominate the surface seismograms as expected, especially at long epicentral distances. The Rayleigh wave, whose amplitude varies only as the reciprocal of the square root of the radial distance at large epicentral distances, dominates as the point of observation is moved farther away from the source.

3. At high frequencies the classical ray components dominate almost the entire 10 x 20 ft frame. Exceptions are explainable as small pockets of destructive interference. At intermediate frequencies, the classical ray components dominate in the region far away from the source and below the surface. The surface waves reach deeper and farther and the primary waves of the second, the third, and the fourth kind prevail in the neighborhood of the source. At lower frequencies, the non-classical ray components are pronounced in the entire observed field. The surface wave fields penetrated still deeper into the half-space.

4. In general, the second surface waves penetrate deeper into the half-space than the Rayleigh waves near the source. Far from the source the Rayleigh waves dominate.

RECOMMENDATIONS

Mathematical analysis of the liquid-to-solid and solid-to-solid cases have been treated in Cagniard's book and should now be investigated and the results compared with those of this study.

Asymptotic approaches to the solid-to-solid problem have been given by Sommerfeld (1909), Muskat (1933), and van d. Waerden (1947). Muskat's solutions involve an approximation, which supposes that $\omega r/V_p$ is of the order of 1 or greater, where ω is angular frequency and V_p is the compressional velocity of the solid medium. The approach I used requires r to be small so that instability will not occur in the numerical integration by Romberg quadrature. Hence Muskat fields should be investigated at selected levels and frequencies.

Although Cagniard's theory is exceptionally rigorous it is still necessary to have experimental confirmation of the theoretical results. Thus suitable models should be constructed.

REFERENCES

Alterman, Z., and Karal, F. C., 1968, Propagation of elastic waves in layered media by finite difference methods: Seismol. Soc. America Bull., v. 58, no. 1, p. 367-397.

Barnes, C. and Anderson, D. V., 1952, The sound field from a pulsating sphere and the development of a tail in pulse propagation: Jour. Acoustical Soc. America, v. 24, p. 229.

Blake, F. G., 1952, Spherical wave propagation in solid media: Jour. Acoustical Soc. America, v. 24, p. 211-215.

Bortfeld, R., 1964, Examples of synthetic refraction arrivals and wide-angle reflections: Geophys. Prosp., v. 12, no. 1, p. 100-114.

Cagniard, L., 1939, Reflection et Refraction Des Ondes Progressives Seismoques: Gauther-Villars, Paris (Transl. by E. A. Flinn and C. H. Dix, New York, McGraw-Hill, 1962).

Ewing, M. W. and Jardetzky, W. S. and Press, F., 1957, Elastic waves in layered media: New York, McGraw-Hill.

Gray, R. L., 1968, Numerical investigation of reflection and transmission of spherical compressional waves: Colorado School of Mines Doctoral Thesis.

Leitinger, H., 1969, Investigation of displacement steps in a layered half-space by the finite difference method, Colorado School of Mines Doctoral Thesis.

Muskat, M., 1933, Theory of refraction shooting: Physics, v. 4.

Pekeris, C. L., 1940, A pathological case in the numerical solution of integral equation: U.S. Natl. Acad. Sci. Proc., v. 26, p. 433-437.

_____ 1941, The propagation of an SH pulse in a layered medium: Am. Geophys. Union Trans., v. 22, p. 27.

Pekeris, C. L., 1948, Theory of propagation of explosive sound in shallow water: Geol. Soc. America Mem. 27.

_____ 1955, The seismic surface pulses: U.S. Natl. Acad. Sci. Proc., v. 41, p. 469-480.

_____ 1955, The seismic buried pulse: U.S. Natl. Acad. Sci. Proc., v. 41, p. 629-639.

_____ 1960, Propagation of seismic pulses in layered liquids and solids: Internatl. Symp. on stress wave propagation in materials, Interscience, New York.

Pekeris, C. L., Alterman, Z., Abramovici, F., and Jarosch, H., 1965, Propagation of a compressional pulse in a layered solid: Review of Geophys., v. 3, no. 1, p. 25-47.

Pekeris, C. L., and Lifson, H., 1957, Motion of the surface of a uniform elastic half-space produced by a buried pulse: Jour. Acoustical Soc. America, v. 29, p. 1233-1238.

Pekeris, C. L. and Longman, I. M., 1958, The motion of the surface of a uniform elastic half-space produced by a buried torque-pulse: Geophys. Jour., v. 1, p. 146-153.

Pekeris, C. L. and Longman, I. M., 1958, Ray-theory solution of the problem of propagation of explosive sound in a layered liquid: Jour. Acoustical Soc. America, v. 30, p. 323-328.

Pekeris, C. L., Longman, I. M., and Lifson, H., 1959, Application of ray-theory to the problem of long-range propagation of explosive sound in layered liquid: Seismol. Soc. America Bull., v. 47, p. 247-250.

Savage, J. C., 1958, Reflection from a liquid of higher sound velocity: Jour. Acoustical Soc. America, v. 30, p. 974-978.

Sharpe, J. A., 1942, The production of elastic wares by explosion pressures, Part I and II: Geophysics, v. 7, p. 144-154; 311-321.

Smirnov, V. and Sobolev, S., 1932, On a new method in the problem of elastic vibrations: Trudy Inst. Seism. Akad. Nauk U.S.S.R., No. 20.

Smirnov, V. and Sobolev, S., 1932, Sur Le Problem Plan Des Vibrations Elastiques: Acad. sci Paris Comptes rendus, v. 194, p. 1437-1439.

Smirnov, V. and Sobolev, S., 1932, Sur quelques problems des vibrations elastiques: Acad. sci Paris Comptes rendus, v. 194, p. 1797-1799.

Smirnov, V. and Sobolev, S., 1933, On the application of a new method of investigation of the elastic vibrations in space with axial symmetry: Trudy Inst. Seism. Akad. Nauk U.S.S.R., no. 39.

Sobolev, S., 1932, Application de la theorie des ondes planes a la solution du probleme de H. Lamb: Trudy Inst. Seism. Akad. Nauk U.S.S.R., no. 18.

_____ 1933, Sur les vibrations d'un demiplan et d'une couce a conditions initiatees arbitraires: Sbornik Mat. (Moscow), v. 40.

_____ 1937, Some aspects of the theory of propagation and vibration: In P. Frank and R. von Mises, Differential and integral equations of mathematical physics, pt. 2, (only in Russian edition).

Sommerfeld, A., 1909, Uber die ausbreitung der wellen in der drahtlosen telegraphie: Ann. Physik, v. 28, p. 665.

Spencer, T. W., 1960, The method of generalized reflection and transmission coefficients: Geophysics, v. 25, no. 3, p. 625-641.

_____ 1965, Long-time response predicted by exact ray theory: Geophysics, v. 30, no. 3, p. 363-368.

_____ 1965, Refraction along a layer: Geophysics, v. 30, no. 3, p. 369-388.

Towne, D. H., 1967, Wave phenomena: Reading, Mass., Addison-Wesley Pub. Co., 482 p.

_____ 1968, Pulse shape of spherical waves reflected and refracted at a plane interface separating two homogeneous fluids: Jour. Acoust. Soc. America, v. 44, no. 1, p. 65-76.

Towne, D. H., 1968, Pulse shape of totally reflected plane waves as a limiting case of the Cagniard solution for spherical waves: Jour. Acoust. Soc. America, v. 44, no. 1, p. 77-83.

van d. Waerden, B. L., 1947, Reflection and refraction of seismic waves: Reprinted by Shell Development Co. in 1957.

White, J. E., 1965, Seismic waves: radiation, transmission, and attenuation: McGraw-Hill, New York.

APPENDIX A

EXPRESSIONS FOR THE DISPLACEMENTS OF THE BODY WAVES AND THE TRANSMISSION FACTORS FOR THE RAYLEIGH WAVE AND THE SECOND SURFACE WAVE

The numbers contained in the parenthesis, following the equations refer to the appearance of the same equations in Flinn and Dix (1962). Angles I, I', I_1 and I_2 have been defined in Figure 1 on page 7.

I. Primary terms of the first kind

1. For the direct wave

a. For l_r (radial displacement):

$$-\frac{S \sin I}{R} W'(t-RS) \qquad (10\text{-}55)$$

b. For l_z (vertical displacement):

$$\frac{S \cos I}{R} W'(t-RS)$$

2. For the reflected P-wave

a. For l_r

$$S \sin I' \left\{\frac{1}{R} - A_3(R'S + 0)\right\}W'(t-R'S) \qquad (10\text{-}56)$$

b. For l_z

$$S \cos I' \left\{\frac{1}{R'} - A_3(R'S+0)\right\}W'(t-R'S)$$

where

$$A_3(R'S+0) = \frac{2}{R'}\{1 + \frac{\{(g^2/2) - \sin^2 I'\}^2}{\sin^2 I' \cos I' (g^2 - \sin^2 I')^{1/2}}\}^{-1}$$

3. For the reflected S-wave

a. For l_r: $s\cos I_2 B(R_1S+R_2s+0)W\{t-(R_1S+R_2s)\}$

b. For l_z: $-s\sin I_2 B(R_1S+R_2s+0)W\{t-(R_1S+R_2s)\}$ (10-57)

where

$$B(R_1S+R_2s+0) = -\frac{4\sin^2 I_1 \cos^2 I_2}{g^2\cos^2 2I_2 + \sin 2I_2 \sin 2I_1}$$

$$r^{-1/2}\left(\frac{h \sin I_1}{\cos^3 I_1} + \frac{z \sin I_2}{\cos^3 I_2}\right)^{-1/2}$$

II. Primary terms of the second kind.

1. For the direct wave

a. For l_r: $-\frac{\sin I}{R^2} W(t-RS)$

b. For l_z: $\frac{\cos I}{R^2} W(t-RS)$ (10-59)

2. For the reflected P-wave

a. For l_r: $\frac{2 \sin I'}{(g^2-1\ R'^2}\{12(g^2-1)\cos' I' - 4g^2+3\}W(t-R'S)$

b. For l_z: $\frac{2\cos I'}{(g^2-1)^2 R'^2}\{12(g^2-1)\cos^2 I' - 8g^2+7\}W(t-RS)$ (10-60)

3. For the reflected S-wave

a. For l_r:

$$\left\{\frac{g^2 \sin I'}{(g^2-1)R'^2}\left(6\cos^2 I' + \frac{2g^2+1-g^4}{g^2(g^2-1)}\right) - \frac{3h}{R'^3}\sin 2I'\right.$$

$$\left. - \frac{6}{(g^2-1)R'^4 S^2}\sin I'(5\cos^2 I'-1)(R_1 S+R_2 s)^2\right\}$$

$$W(t-(R_1 S + R_2 s)) \qquad (10\text{-}61)$$

b. For l_z:

$$\left\{\frac{g^2 \cos I'}{(g^2-1)R'^2}\left(6\cos^2 I' + \frac{2g^2+1-g^4}{g^2(g^2-1)}\right) - \frac{2h}{R'^3}(3\cos^2 I'-1)\right.$$

$$\left. - \frac{6}{(g^2-1)R'^4 S^2}\sin I'(5\cos I' - 3)(R_1 S+R_2 s)^2\right\}$$

$$W\{t - (R_1 S + R_2 s)\}$$

III. Primary terms of the third kind

1. For the reflected P-wave

a. For l_r:

$$\frac{12}{(g^2-1)R'^3 S}\sin I'(5\cos^2 I'-1)\, W^{-1}(t-R'S) \qquad (10\text{-}63)$$

b. For l_z:

$$\frac{12}{(g^2-1)R'^3 S}\cos I'(5\cos^2 I'-3)\, W^{-1}(t-R'S)$$

2. For the reflected S-wave

a. For l_r:

$$\frac{-12}{(g^2-1)S^2}\frac{R_1S+R_2s}{R'^4}\sin I'(5\cos^2 I'-1)\ x$$

$$W^{-1}\{t-(R_1S+R_2s)\} \qquad (10\text{-}64)$$

b. For l_z:

$$-\frac{12}{(g^2-1)S^2}\frac{R_1S+R_2s}{R'^4}\cos I'(5\cos^2 I'-3)$$

$$W^{-1}\{t-(R_1S+R_2s)\}$$

IV. Primary terms of the fourth kind

1. For the reflected P-wave

a. For l_r:

$$\frac{12}{(g^2-1)R'^4S^2}\sin I'(5\cos^2 I'-1)W^{-2}(t-R'S) \qquad (10\text{-}65)$$

b. For l_z:

$$\frac{12}{(g^2-1)R'^4S^2}\cos I'(5\cos^2 I'-3)W^{-2}(t-R'S)$$

2. For the reflected S-wave

a. For l_r

$$\frac{-12}{(g^2-1)R'^4S^2}\sin I'(5\cos^2 I'-1)W^{-2}(t-(R_1S+R_2s)) \qquad (10\text{-}66)$$

b. For l_z: (10-66)

$$- \frac{12}{(g^2-1)R'^4S^2} \cos I'(5\cos^2 I'-3)W^{-2}\{t-(R_1S+R_2s)\}$$

Expressions for the transmission factors of the Rayleigh wave are obtained by calculation of the residue at P and P' (see Figure 2). They are expressed by M_r^P, M_z^P, N_r^P, and N_z^P in Chapter 11 of Cagniard's book. We first write the definitions as follows:

$$M_r^P = \frac{-2\delta m^4(m^2-g^2)^{1/2}}{R'^2} M_1(\tau_*)^{-3/4} \sin\frac{3\theta_1(\tau_*)}{2} \sin I'$$

$$M_z^P = \frac{-2\delta\{m^2-(g^2/2)\}^2}{R'^2} M_1(\tau_*)^{-3/4} M_2(\tau_*)^{1/2} \cos\{\theta_2(\tau_*)-\frac{3\theta_1}{2}(\tau_*)\}$$

(11-12)

$$N_r^P = \frac{2\delta m^2(m^2-g^2/2)(m^2-g^2)^{1/2}}{R'^2} N_1^{-3/4}(\tau_*)\sin\frac{3\phi_1(\tau_*)}{2} \sin I'$$

$$N_z^P = \frac{2\delta m^2(m^2-g^2/2)}{R'^2} N_1(\tau_*)^{-3/4} N_2(\tau_*)^{1/2} \cos\{\phi_2(\tau_*) - \frac{3\phi_1(\tau_*)}{2}\}$$

where

$$\tau_* = \frac{\tau}{R'_1 S}$$

$$M_1(\tau_*) = (\tau_*^2-m^2+\cos^2 I')^2 + 4\tau_*^2 \cos^2 I'(m^2-1)$$

$$\tan\theta_1(\tau_*) = \frac{2\tau_* \cos I'(m^2-1)^{1/2}}{\tau_*^2 - m^2 + \cos^2 I'} \qquad 0<\theta_1<\pi$$

$$M_2(\tau_*) = \tau_*^2 + (m^2-1)\cos^2 I'$$

$$\tan\theta_2(\tau_*) = \frac{(m^2-1)^{1/2}\cos I'}{\tau_*} \qquad 0<\theta_2<\frac{\pi}{2}$$

$$N_1(\tau_*) = (\tau_*^2 - m^2\sin^2 I' - (\frac{h}{R'}\{(m^2-1)^{1/2}-(m^2-g^2)^{1/2}\}$$

$$+ \cos I'\,(m^2-g^2)^{1/2})^2 + 4\tau_*^2(\frac{h}{R'}\{(m^2-1)^{1/2}-(m^2-g^2)^{1/2}\}$$

$$+ \cos I'\,(m^2-g^2)^{1/2}\}^2$$

$$\tan\phi_1(\tau_*) = \frac{2\tau_*\{\frac{h}{R'}\{(m^2-1)^{1/2}-(m^2-g^2)^{1/2}\}+\cos I'(m^2-g^2)^{1/2}\}^2}{\tau_*^2-m^2\sin^2 I'-\{\frac{h}{R'}\{(m^2-1)^{1/2}-(m^2-g^2)^{1/2}\}+\cos I'(m^2-g^2)^{1/2}\}^2} \qquad 0<\phi_1<\pi \qquad (11\text{-}10)$$

$$N_2(\tau_*) = \tau_*^2 + \{\frac{h}{R'}\{(m^2-1)^{1/2}-(m^2-g^2)^{1/2}\}+\cos I'(m^2-g^2)^{1/2}\}^2$$

$$\tan\phi_2(\tau_*) = \frac{1}{\tau_*}\{\frac{h}{R'}\{(m^2-1)^{1/2}-(m^2-g^2)^{1/2}\}+\cos I'(m^2-g^2)^{1/2}\} \qquad 0<\phi_1<\frac{\pi}{2}$$

and

$$\delta = \frac{2(m^2-g^2/2)^2}{3m^4(g^2-1)-m^2g^2(3g^2-2)+g^6/2} \qquad (11\text{-}11)$$

The transmission factors of the second surface wave are presented in integral forms. Integration along the

path E in the u-plane has been transformed onto path K in the λ-plane, where $\lambda = \frac{ia}{S}$. Path K designates a clockwise half-loop around the positive real axis between 0 and $|\sqrt{g^2-1}|$ starting and ending on the imaginary axis (see Cagniard, p. 190).

The mathematical expressions of the transmission factors of the second surface wave are written as follows:

$$M_r^E = -\frac{2\sin I'}{\pi R'^2 S} \operatorname{Im} \int_K Q^{-3/2}\{u^2 j(u)\}\lambda d\lambda$$

$$M_z^E = -\frac{2S}{\pi R'^2} \operatorname{Re} \int_K Q^{-3/2}(\tau_* + i\lambda\cos I')j(u)\lambda^2 d\lambda$$

(12-6)

$$N_r^E = -\frac{2\sin I'}{\pi R'^2} \operatorname{Im} \int_K P^{-3/2}\{u^2 f(u)\}\frac{b}{S}\lambda d\lambda$$

$$N_z^E = \frac{2}{\pi R'^2} \operatorname{Im} \int_K P^{-3/2}(\tau_* - \frac{b}{S}\frac{z}{R'} + i\lambda\frac{h}{R'})\{u^2 f(u)\}\lambda d\lambda$$

where $P = -\sin^2 I'(\lambda^2+1)+(\tau_*+i\lambda\frac{h}{R'}-\frac{b}{S}\frac{z}{R'})^2$

$$Q = \tau_*^2 - \lambda^2 - \sin^2 I' + 2i\lambda\tau_*\cos I' .$$

APPENDIX B

THE MOVEMENT OF THE MOVING BRANCH CUT AS A FUNCTION OF TIME AND RADIAL DISTANCE

In Chapter 12 of his book Cagniard treated the problem of obtaining the transmission factors for the second surface wave by integrating along the path E (see Figure 2) in the u-plane. As shown in Figure 2, there is a fixed branch cut and a moving branch cut in the u-plane. The fixed branch cut accounts for the multivalued feature of the radicals a and b and is denoted by the heavy line on the imaginary axis of the u-plane; the moving branch cut accounts for the multivalued feature of the radical $\{u^2r^2 + (t - ah - bz)^2\}^{1/2}$ and is represented by two branch points A and A' and the curve connecting them. The positions of the two branch points depend upon the time t and the locations of the source and receiver.

There is no contribution to the integral between $u = -iS$ and $+iS$ on the path E, hence integration which begins at $u = \pm iS$ on the right side of the fixed branch cut and ends on the left side of the fixed branch cut at $u = \pm iS$ by going around $u = \pm$ is will be all that is needed here. The integrals of the transmission factors of the second surface wave are bounded along the path if the receiver is at a

finite distance from the source. It will remain bounded as the receiver is moved arbitrarily far away from the source, provided that neither A nor A' approaches u = ± is. When the receiver is far away from the source at the surface, i.e., r ≈ R ≈ R', and t approaches to sR' the integrands become unbounded. This is due to the fact that the branch points A and A' have fallen on the fixed branch cut between u = ± iS and ± is and are arbitrarily close to u = ± is under these conditions (see Cagniard, p. 192 and p. 209). When t is greater than $R_1S + R_2s$, the branch points move away from the fixed branch cut so that the integrands remain bounded.

The Romberg quadrature numerical integration program used in this study was first acquired from the IBM Share File No. 7090-1481 by Mr. R. L. Gray. It is coded in such a way that integration along a given path is performed in minimal time if the integrand is bounded. When the integrand is unbounded, in or near the range of integration, the integration by this method requires much more computer time, provides less accurate results and becomes unstable. This shortcoming of the algorithm prevented us from computing waveforms of the second surface wave at the free surface for the epicentral distances exceeding 200 ft.